TÉCNICO LISBOA

Development of personalised musculoskeletal models based on current clinical evaluation data in children with Cerebral Palsy

Vasilisa Đalović

Biomedical Engineering

Supervisors: Prof. António Prieto Veloso
Prof. Carlos Miguel Fernandes Quental

Examination Committee

Chairperson: Prof. João Orlando Marques Gameiro Folgado
Members of the Committee: Prof. António Prieto Veloso
Prof. Miguel Pedro Tavares da Silva
Prof. Rita Noélia Silva Fernandes

May 2025

Declaration

I declare that this document is an original work of my own authorship and that it fulfills all the requirements of the Code of Conduct and Good Practices of the Universidade de Lisboa. This thesis is part of the research project entitled “Development of a simulation platform based on musculoskeletal models to predict recovery of gait following orthopedic interventions in cerebral palsy children”, referenced as PTDC/EMD-EMD/5804/2020.

Acknowledgments

This thesis marks the end of my academic journey across five different countries, and I am deeply grateful to everyone who shaped my path and helped me grow.

Firstly, I would like to thank Professor António Veloso for inviting me to join the project ”Development of a simulation platform based on musculoskeletal models to predict recovery of gait following orthopaedic interventions in children with cerebral palsy” (PTDC/EMD-EMD/5804/2020, [1]), for providing the necessary conditions, and for all the support he gave throughout. Secondly, I would like to thank Professor Carlos Quental for the availability and attention he always showed and for all the constructive critiques that significantly improved this work.

A very special thank you to Dr. Basilio Gonçalves for the help he provided during the final stages of the journey. His guidance was crucial for the completion of this thesis. I am truly grateful for his constant support, kind words, and positive energy that kept me motivated when I needed it. I am also thankful to his team in Vienna, who warmly welcomed me and made me feel part of the group during my time there.

High school in England was the starting point of this beautiful journey, and I want to thank my physics teacher, Mr. King, for making me fall in love with his subject. His passion and everyday examples turned complex equations into simple ideas and made me see the world with different eyes.

The two years spent at Instituto Superior Técnico were a wonderful experience, and my final academic thanks go to all the professors for guiding me and helping shape my professional trajectory and to all my Portuguese colleagues who helped me adapt to the dynamics of the university.

I would like to thank all my friends for their constant presence and support throughout this journey. To my friends from Italy, Jovana and Milica, for the countless hours we spent in the study rooms preparing for exams and for all the beautiful moments we shared outside of the university. Even after leaving Italy, your support remained unwavering through my master’s. To Nikola and Kristijan, who made my time in

Vienna even more memorable. To all my friends in Lisbon, with whom I had the honor of experiencing the beauty and energy of that city. And to all my friends in Montenegro, thank you for always being there.

Finally, my deepest gratitude goes to my family and to my boyfriend, Milos, for your unconditional love, constant support, and presence through all the ups and downs of this journey. Thank you for always believing in me. I would like to dedicate this thesis to my parents and my paternal grandfather, who gave me wings to fly.

Resumo

A marcha agachada, comum em crianças com paralisia cerebral (PC), continua a ser um desafio para uma avaliação precisa e um tratamento eficaz, devido às suas causas múltiplas e inter-relacionadas. Modelos neuromusculoesqueléticos podem fornecer informações relevantes, mas, ao dependerem de rotinas de otimização, podem não captar as coativações típicas nestas crianças. Os objetivos desta dissertação foram comparar o desempenho de um modelo informado por EMG com a otimização estática tradicional e investigar a biomecânica da marcha em crianças com PC com marcha agachada e em crianças tipicamente desenvolvidas (TD) que simularam esse padrão de marcha anormal, com o intuito de distinguir as alterações primárias causadas pela doença neurológica das adaptações secundárias induzidas pela postura agachada. Participaram quatro crianças com PC (GMFCS I–III) e seis crianças TD. Os parâmetros cruciais foram estimados através de simulações musculoesqueléticas usando o software OpenSim e o plugin CEINMS. O modelo informado por EMG produziu estimativas mais realistas e precisas de ativações musculares, mantendo uma boa correspondência com os momentos articulares medidos experimentalmente. As crianças TD conseguiram simular a marcha agachada, demonstrando desafios biomecânicos como maior força no quadríceps. No entanto, as crianças com PC geraram forças musculares substancialmente mais elevadas e apresentaram ativações prolongadas e quase constantes em grupos musculares-chave, refletindo défices neuromusculares primários. Estas diferenças claras em magnitude e duração das forças permitem distinguir as deficiências primárias do sistema neuromuscular das adaptações secundárias relacionadas com a postura agachada.

Palavras Chave

Marcha em flexão, Paralisia cerebral, Modelação musculoesquelética, Modelação musculoesquelética informada por EMG, CEINMS

Abstract

Crouch gait, common among children with Cerebral Palsy (CP), remains a challenge for accurate assessment and effective treatment due to its multiple, interacting underlying causes. Neuromusculoskeletal models can provide insights but may miss co-contractions in these children when using optimisation routines. The aims of this dissertation were to compare performance of EMG-informed model with traditional static optimisation, and to investigate the biomechanics of gait in CP children exhibiting crouch gait, and healthy children simulating this abnormal gait pattern in order to distinguish between the primary deviations caused by the neurological disease and secondary deviations caused by the crouched gait. Four children with CP (GMFCS I-III) and six typically developing (TD) children were included in this study. Parameters crucial to the study were estimated through musculoskeletal simulations using OpenSim software and CEINMS plug-in tool. The EMG-informed model produced better and more accurate estimates of muscle activations while still closely reproducing experimentally measured joint moments. The TD children successfully simulated crouch gait by demonstrating the same biomechanical challenges, such as increased quadriceps forces. However, CP children generated substantially higher muscle forces and showed prolonged, near-constant activation in key muscle groups, reflecting their primary neuromuscular deficits, whereas TD children when asked to walk in a crouch posture produced lower overall forces and their muscle activation patterns resembled those seen in normal gait. These clear contrasts in force magnitude and timing therefore allow to separate the primary impairments of the neuromuscular system (excessive force, sustained activation) from the secondary, posture-driven adaptations observed in crouch walking.

Keywords

Crouch gait, Cerebral palsy, Musculoskeletal modelling, EMG-informed musculoskeletal modelling, CEINMS

Contents

List of Figures

List of Tables

Acronyms

AFO	Ankle-foot orthoses
BoNT-A	Botulinum Neurotoxin-A
CNS	Central Nervous System
CFCS	Communication Function Classification System
CP	Cerebral Palsy
DOF	Degrees of Freedom
EDACS	Eating and Drinking Ability Classification System
EMG	Electromyography
GMFCS	Gross Motor Function Classification System
GRAFO	Ground Response Foot Orthosis
GRF	Ground Reaction Forces
NMSK	Neuromusculoskeletal
ICF	International Classification of Functioning, Disability and Health
IK	Inverse Kinematics
SO	Static Optimization
MACS	Manual Abilities Classification System
SD	Standard Deviation
ID	Inverse Dynamics
OFL	Optimal Fiber Length
TSL	Tendon Slack Length
RMSE	Root Mean Square Error
R^2	coefficient of determination
MTU	Musculotendon unit
MVC	Maximum Voluntary Contraction
PVL	Periventricular Leukomalacia
QTM	Qualisys Track Manager
PVHI	Periventricular Hemorrhagic Infarction
SCPE	Surveillance for Cerebral Palsy in Europe
TD	Typically Developing
CEINMS	Calibrated EMG-Informed NMS Modelling Toolbox

1

Introduction

Contents

1.1 Motivation and objectives

Walking is one of the fundamental activities in everyday life, as it is crucial for social interactions and for performing daily tasks. Considering the higher level of physical activity in children compared to adults, the effects of walking on them are even more significant. This is due to its crucial role in their overall development and well-being [16]. When nerves stimulate muscles, they produce forces. These forces are transmitted to the skeletal structure, resulting in the generation of angular movements at the joints. Smooth, purposeful movement results from the neural system's appropriate coordination of the activation of multiple muscles. However, the presence of neurological abnormalities, such as Cerebral Palsy (CP), leads to irregular movements [13].

CP is the most prevalent neurological condition in children and is caused by non-progressive disruptions that take place in the developing fetus or infant brain. Studies have shown that in around 90% of cases, CP is caused by harmful processes that damage the normal brain rather than by defects in brain development. Cerebral Palsy is primarily distinguished by neurological impairments resulting from brain malformations and secondarily by muscular and skeletal deformities [17]. The rate of CP is about 2 to 3 per 1000 live births. When children are born very early or with a deficient birth weight, this rate goes up to 40–100 per 1000 live births. The disabling condition is permanent during the life of the affected children [18].

Although the Central Nervous System (CNS) is initially injured in cases of CP, the peripheral neuromuscular system, especially the skeletal muscles, is where clinical symptoms first appear. Muscle contractures, which restrict joint movement due to high passive muscle force, are frequently a consequence of CP [6]. Therefore, the primary symptoms of CP are a lack of motor control and muscle spasticity. As a result, secondary problems such as bone abnormalities and reduced gait efficiency frequently appear.

One of the most common pathological gaits in CP is the crouch gait. The crouch is defined by an excessively flexed knee at the stance phase of gait. In a crouch, the muscles' ability to extend the knee and hip is diminished, resulting in the production of higher-than-normal muscular forces while walking. Furthermore, there is a marked decrease in efficiency. Increased joint reaction forces result from increased muscle forces, potentially contributing to the progressive development of degenerative arthritis and joint discomfort. If not appropriately treated, children diagnosed with CP will gradually develop impaired gait, which will ultimately result in more severe functional disabilities [19].

To improve motor performance or avoid further decreases, several therapies are available. However, finding the best therapy is difficult, and results may not fulfill expectations. Three-dimensional gait analysis has emerged as a valuable tool, contributing to a reduction in treatment failures that necessitate additional interventions. Gait analysis involves assessing the biomechanics of walking, typically using specialized technology to capture and analyze movement patterns. Specifically, it has demonstrated its effectiveness in improving treatment outcomes by providing detailed insights into a patient's gait mechanics [20]. By employing computational models and simulations, it becomes possible to adapt therapies more precisely to individual needs. Especially for neurological impairments, these instruments allow comparison of therapy approaches' results. Furthermore, for clinical purposes, evaluating the representativeness of a model by comparing the pre-operative data with the post-operative status is highly relevant [21].

Static Optimization (SO) has traditionally been used to estimate muscle forces during gait under the assumption that the CNS minimizes some measure of effort. However, SO cannot reproduce key features of pathological gait—most notably muscle co-contractions [22]. EMG-informed Neuromusculoskeletal (NMSK) modeling instead incorporates recorded Electromyography (EMG) signals. Frameworks like Calibrated EMG-Informed NMS Modelling Toolbox (CEINMS) [23] and the EMG-driven model of Lloyd [24] use experimental EMG data to improve activation predictions, while hybrid approaches [25] combine EMG constraints with optimization for muscles lacking EMG signals, yielding more accurate joint-moment and muscle-force estimates.

Despite this promise, there are virtually no studies validating EMG-informed muscle-force predictions against a gold standard in children with CP, and SO still fails to capture co-contraction patterns in pathological gaits [25]. Moreover, almost no work has healthy children simulate crouch gait to disentangle primary neurological impairments from secondary compensations, limiting our ability to pinpoint the true origin of specific deviations.

The most common method for identifying gait deviations in children with CP is to compare kinematics and muscle contributions against unimpaired gait data from healthy peers. While the primary crouched posture reflects the neurological disorder, many other deviations arise secondarily through muscle or postural compensation.

This dissertation pursued two main goals. The first goal was to evaluate whether an EMG-informed neuromusculoskeletal model could outperform traditional SO in predicting individual muscle activations and joint moments. The second goal was to apply these tools to compare the gait biomechanics and muscle function of CP children with crouch gait with that of healthy children simulating this atypical gait

pattern. This approach can improve the differentiation between primary gait deviations associated with neurological disorders and secondary deviations resulting from compensatory body mechanisms. To complete these goals, OpenSim and CEINMS were used.

The specific objectives within this scope can be outlined as:

1. Comparing the accuracy and efficacy of SO and CEINMS in estimating muscle activations and joint moments.

2. Using the optimization method that yielded the best accuracy, compare muscle forces between Typically Developing (TD) children walking normally, TD children simulating crouch gait, and CP children walking in crouch gait to differentiate between the primary and secondary deviations.

1.2 Document outline

This document is divided into six main chapters. Chapter 1 provides a concise overview of the motivations behind initiating this dissertation, outlines the set objectives, and discusses the contributions it makes to the scientific domain. Chapter 2 provides a summary of the most relevant and crucial existing research that aligns with the focus of this work. Chapter 3 clarifies the relevant theory and analytical concepts crucial for comprehending and developing the research. Chapter 4 describes the subjects and all the details on how data acquisition was performed. Additionally, a brief explanation of the use of Visual 3D, OpenSim, and CEINMS is provided. Chapter 5 presents the expected results and their critical interpretation. Lastly, Chapter 6 brings together the main insights of this dissertation, its limitations, proposes improvements, and offers recommendations for future exploration.

2

Literature Review

The study of human motion plays an important role in many fields, including biomechanics, sports science, clinical diagnosis, and rehabilitation. Understanding how the body moves is highly useful for improving athletic performance, deciding on rehabilitation strategies, and developing assistive devices. Moreover, it can help identify abnormalities and dysfunctions caused by different neurological disorders. Gait analysis helps diagnose and monitor many neuromuscular and musculoskeletal conditions, including multiple sclerosis, stroke, and CP. Some of the gait abnormalities are subtle, and therefore, may not always be detectable through visual observation alone [26].

In the 19th century, brothers Weber showed how step length and cadence vary with walking speed. After that, in the late 19th century, Eadweard Muybridge employed multiple synchronized cameras to capture motion frame by frame. This research gave a foundation for the visual analysis of gait [27]. As video camera systems were developing, the gait analysis process was becoming quicker and more effective. Today, gait analysis uses high-speed multi-camera setups which track reflective markers in the three-dimensional space. This is often combined with surface EMG and force-plate measurements of ground reaction forces [28]. Today, thanks to gait analysis, researchers can compute detailed kinematic and kinetic parameters.

Modeling and simulation are increasingly used to study movement because they offer a clear view of how the nervous system and muscles work together to coordinate motion. Although motion capture data provides a detailed analysis of the kinematics and dynamics of body-segmental movement, it does not fully explain the coordinated actions of muscles in generating a synchronized gait pattern. The extensive use of computational musculoskeletal modeling has been a common practice to gain additional understanding of muscle forces, joint reaction forces, and muscle-induced accelerations [29].

Although musculoskeletal modeling has demonstrated its potential, its incorporation into routine clinical examinations has yet to become popular. Ursula Trinler's systematic review [30] aimed to assess the practical suitability of existing methods for estimating muscle forces in clinical settings. The study revealed a widespread consensus among the analyzed models in accurately predicting the activation timing of specific muscles throughout the normal gait cycle. Nevertheless, an immense difference in the force magnitude and peak timing of the impact has been observed across the methods used. The root reason of these variations remains unknown, which presents a problem in finding the most accurate model.

Musculoskeletal models may not be widely used in clinical practice, but researchers are still analyzing abnormal gait patterns associated with neurological pathologies such as CP. The most common gait pattern in children with CP is frequently recognized as crouch gait. As a result, it is urgent to investigate the complexities of muscle forces and their influence on motion in order to identify the fundamental factors contributing to this abnormal gait. Moreover, understanding these motions becomes crucial for deciding about appropriate treatments.

Hicks et al. [31] investigated how crouching postures impact hip and knee extension during single-limb stance gait phase. They divided the individuals into three groups based on crouch gait severity to compare extension capability to each representative crouched posture. In this investigation, they determined muscular extension ability based purely on body segment orientation and inertial characteristics, not activation or force-generating capacity. All crouch severity levels showed decreased joint extension. These groups revealed significant decreases in joint accelerations generated for important stance-phase muscles and increases in the joints' accelerations induced by gravity. Based on the results, Hicks and colleagues came to the conclusion that an individual in a crouch gait must generate more energy to maintain that posture. They also created a musculoskeletal model that can handle different tibial torsion angles by using a method developed before to simulate torsional bone deformities. This investigation revealed that an escalation in the deformity angle corresponded to a decrease in hip and knee extension accelerations. These results suggest that minor interventions, such as correcting a patient's tibial alignment, have the potential to significantly enhance the efficiency of the patient's gait.

One of the main causes of crouch gait in individuals with CP is muscle weakness. Studies that investigated the effects of strength training have inconsistent results [19]. Steele et al. [32] examined, using musculoskeletal models, how much muscle groups could be weakened before crouch gait become impossible. Knowing how much muscle strength is needed to walk in a crouch gait, compared with normal gait, can show how muscle weakness leads to crouch walking. Furthermore, it can help design more effective strength-training programs. Steele and colleagues developed a musculoskeletal model for three typically developing children and six children with CP who walked with varying degrees of crouch severity. The muscular weakening was induced by progressively decreasing the maximal isometric force of each muscle group until the simulation could no longer replicate the gait of each individual. The obtained results indicate that moderate crouch gait needed considerably higher knee extensor strength than unimpaired gait. However, compared to unimpaired gait, moderate crouch gait required less hip abductor strength, while mild crouch gait required less ankle plantarflexor strength. The lower strength required from hip abductors and ankle plantarflexors during crouch gait implies that these muscle groups may be weak and might be targeted for strength training.

Although musculoskeletal modeling could offer clear benefits, its use in CP clinical management is still uncertain because modeling assumptions can distort how results are interpreted. This uncertainty is due to the potential distortion of clinical interpretation caused by modeling assumptions. For example, most models derive muscle activations via static optimization by minimizing total activation or metabolic cost, yet these cost functions ignore the co-contraction and atypical activation patterns present in CP. On the other hand, anomalies in muscle activation can be captured via calibrated EMG-informed approaches within computational modeling software, which may allow for more accurate estimates of joint and muscle contact forces. Moreover, the most commonly used musculoskeletal models scale an individual's anatomy using general healthy adult models, which may oversimplify the complexity of the anatomy, particularly in children and especially in children with CP, who have unique morphology, muscle composition, and bone anatomy.

Davico et al. [33] explored the utility of calibrated electromyography (EMG)-informed models in OpenSim and CEINMS, a plug-in tool for OpenSim that integrates EMG data into musculoskeletal simulations, for personalized treatment planning. The study involved 13-year-old identical twin brothers, one with unilateral CP and the other typically developing. The results showed that these models, which use EMG data and joint-specific parameters, perform better than generic models that use static optimization technique. These models achieved lower Root Mean Square Error (RMSE) and higher coefficient of determination (R^2) when reproducing the recorded EMG activation patterns and inverse-dynamics joint moments compared to static optimization. This study reveals the potential of EMG-informed models for improving the management of CP by capturing pathology-related muscle activation abnormalities, thereby improving the fidelity of neuromusculoskeletal simulations. However, this proof-of-concept investigation is limited by its reliance on a single CP subject (and his twin), which restricts the generalizability of the findings.

Veerkamp et al. [22] employed subject-specific neuro-musculoskeletal models - extending the conventional musculoskeletal framework with a representation of CNS control in order to explore muscle function during walking in children with CP and TD children. Concentrating on personalised model optimization, the study evaluated four different approaches that calculate muscle activations and muscle forces - SO that minimised summed-excitation squared, SO with maximum isometric muscle forces scaled to body mass, an EMG-assisted approach using optimization to minimize summed-excitation squared while reducing tracking errors of experimental EMG-linear envelopes and joint moments, and EMG-assisted with calibrated musculotendon model parameters. The results highlighted the limitations of SO, especially when it comes to explaining CP patients' impaired motor function and muscular weakness. EMG-assisted methods performed much better in estimating muscle activations and muscle joints, particularly when musculotendon model parameters were customised.

In order to better understand crouch gait, most of the researchers typically rely on known values from unimpaired gait and compare them with this pathological gait [32]. However, extending this comparison to healthy children walking in a crouched posture can contribute to the research, by providing additional insights into the biomechanics of this gait. While such studies have been valuable, they have generally been limited by small sample sizes and by examining only natural walking or single crouch conditions. In particular, few investigations have asked healthy children to simulate a true crouch gait, which would help separate deviations caused by neuromuscular impairment from those arising purely through compensatory posture. This type of analysis could possibly distinguish between primary deviations caused by the neurological issues and secondary deviations caused by the crouched gait.

The biomechanics of crouch gait in healthy subjects were examined in the study of Matjačić and Olenšek [34]. They investigated how hamstring and iliopsoas contractures affect gait mechanics by using an exoskeleton with artificial muscles. In their experiments, subjects walked normally, with isolated hamstring contraction, with isolated iliopsoas contraction, and with the combination of both. They measured joint angles and moments at hip,knee, and ankle, throughout the gait cycle, and showed that each walking combination produced different kinematic and kinetic results. This work suggested that these differences may be clinically relevant and may suggest targeted intervetions.

Balzar et al. research [35] investigated compensating foot motion during gait in healthy children with an experimentally produced bilateral knee flexion contracture. Three-dimensional Oxford Foot model kinematic and kinetic data was used to analyze hindfoot and forefoot kinematics in various planes during stance. The findings indicated that the foot tended to compensate for the artificial knee flexion contracture with increased dorsiflexion, eversion, and external rotation of the hindfoot, influencing motion in other foot segments. These findings are valuable as they suggest that surgical treatment, aiming to improve knee extension, can also reduce the risk of possible compensation mechanisms around the foot.

However, these pioneering induced-crouch experiments remain constrained by very small cohorts and by testing only a single contracture or posture in isolation. Neither Matjačić and Olenšek nor Balzar et al. included children with CP for direct comparison, and both focused solely on external kinematics and foot/segment kinetics-without recording muscle activity or employing neuromusculoskeletal modeling to estimate internal forces. Consequently, it is still unclear which deviations arise purely from the crouched posture versus those driven by pathological muscle activation. By contrast, the present work assembles a sample of typically developing children (including those simulating crouch gait) and children with CP, and uses EMG-informed CEINMS modeling alongside recorded EMG and inverse-dynamics

joint moments to validate muscle activations and force estimates. This comprehensive approach bridges the gap between posture-driven biomechanics and neuromuscular pathology.

3

Theoretical Concepts

Contents

This chapter is structured into five sections, each presenting fundamental theoretical concepts crucial for comprehending and developing the research. The chapter opens with an exploration of the structural framework of the lower extremity: its bones, joints, and the muscle-tendon unit, illustrating how contractile fibers and elastic tendons cooperate to generate and transmit force. Following this biomechanical foundation, a brief explanation of all phases of a normal gait cycle and which muscles drive the movement. The subsequent section explains cerebral palsy, the specific disease of focus, covering its etiology, classification schemes and gait deviations, and current clinical intervention strategies. Next section gives a brief explanation of EMG and its contribution to gait analysis. The chapter concludes with an overview of musculoskeletal modelling approaches, firstly explaining computational modelling techniques used to represent muscle activity and then software used for this study.

3.1 Anatomy of the Lower Limb

The human lower limbs are highly specialised for weight-bearing support, stability, and locomotion. Through an integrated system of bones, joints, and muscles, the legs enable upright walking, which is an orchestrated series of coordinated movements involving multiple joints and muscle groups. Figure 3.1 illustrates the anatomy of the lower limb.

3.1.1 Major Bones of the Lower Limb

The lower limb contains 30 bones in total. The single femur (thigh bone) is the longest and strongest bone in the body, forming the upper leg and contributing roughly one-quarter of a person's height. Proximally, the rounded head of the femur articulates with the hip bone (pelvic acetabulum) at the hip joint. Distally, the femur meets the tibia at the knee [36]. The tibia (shin bone) is the larger, medial bone of the lower leg and bears most of the body's weight, whereas the thinner fibula runs laterally and serves mainly for muscle attachment and ankle stability. At the knee, the patella (kneecap), the largest sesamoid bone, is embedded in the quadriceps tendon and articulates with the distal femur. The patella protects the tendon from friction and increases the leverage of the quadriceps muscle across the knee, thereby improving the efficiency of knee extension. Distal to the leg are the bones of the foot: seven tarsals (including the talus and calcaneus), five metatarsals, and 14 phalanges (toe bones). The talus of the ankle receives the weight from the tibia, transferring it to the calcaneus (heel bone) and other tarsals, while the arrangement of metatarsals and phalanges forms the forefoot and toes that support gait and balance.

3.1.2 Key Joints of the Lower Limb

The major joints of the lower extremity include the hip, knee, and ankle (along with the smaller joints of the foot).

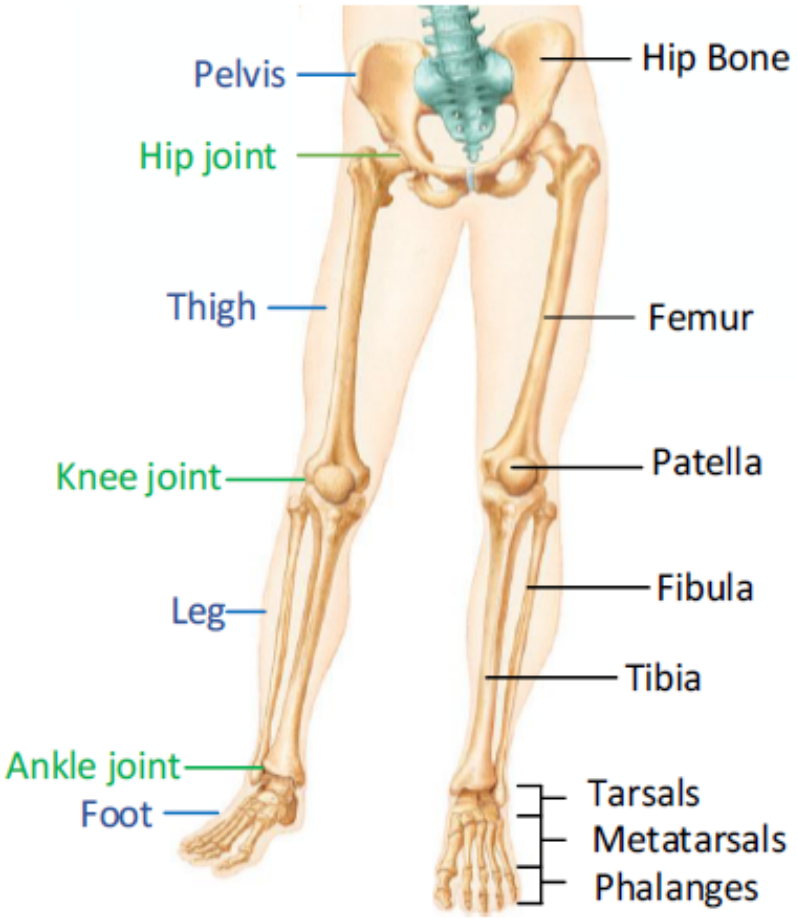

Figure 3.1: Anatomy of the lower limb [2]

The hip joint is a ball-and-socket synovial joint between the femoral head and the acetabulum of the hip bone [36]. This multiaxial joint permits movements in all planes (flexion/extension, abduction/adduction, rotation), yet it is inherently stable due to the deep socket and strong surrounding ligaments needed for weight-bearing. The hip joint provides a secure connection between the lower limb and axial skeleton, supporting the body's weight in standing and transmitting forces during locomotion.

The knee joint is the largest joint in the body and primarily functions as a hinge [36]. It is formed by the articulation of the femur and tibia, with the patella gliding on the femur's anterior surface. The knee allows flexion and extension (and a slight degree of rotation when flexed) to accommodate walking and running. Sturdy ligaments (such as the cruciate and collateral ligaments) and meniscal cartilages help stabilize the knee under the substantial loads of standing and movement. During gait, the knee must both support body weight (particularly in mid-stance) and flex during swing to allow foot clearance.

The ankle joint (talocrural joint) is a hinge joint formed by the distal ends of the tibia and fibula articulating with the talus of the foot [36]. It permits dorsiflexion (raising the foot) and plantarflexion (pointing the foot downward). The dome-shaped superior surface of the talus fits into the mortise formed by the tibia and fibula, creating a stable hinge for forward progression of the body. Strong medial and lateral collateral ligaments support the ankle. Just below the ankle, the interrelated subtalar and midfoot joints allow inversion/eversion and adaptation to uneven surfaces.

Movement relies on the coordinated interaction between the nervous and musculoskeletal systems. The nervous system uses signals from the brain to regulate muscle activity throughout the body. The musculoskeletal system (made up of muscles, tendons, and bones joined by ligaments and joints) then acts as a lever system to convert those signals into force and motion. Both systems must work together to produce coordinated, stable movement. If either one breaks down, motion becomes unstable. In cerebral palsy, impaired muscle-tendon coordination further disrupts this balance and alters day-to-day biomechanics.

There are three types of muscle tissues able to create forces through contractions. These are cardiac, smooth, and skeletal muscles, which are the subject of this thesis. These muscles control voluntary motions and provide structural support. Membrane that connects muscle fiber to a tendon fiber is called sarcolemma, and it holds numerous thin collagen fibers. Fibrous connective tissue is used to create tendon fibers, which are structured bundles. They play a crucial role in linking muscles to bones, allowing the muscle force to pass from muscle into bone to produce movement at the joints . Skeletal muscle is a well-structured tissue consisting of many bundles of muscular fibers known as muscle fascicles. A representation of skeletal muscle structure is illustrated in Figure 3.2.

Muscle fibers typically include numerous myofibrils, often numbering in the hundreds or even thousands. Myofibrils consist of polymerized protein molecules known as actin (thin filaments) and myosin (thick filaments). These protein molecules are responsible for the actual muscle contraction. At the end of each actin filament, there is a Z disk made up of filamentous proteins that are different from actin and myosin. The actin filaments align parallel to the myosin filaments, extending from the Z disks in both directions. A sarcomere is a section of the myofibril that is defined by two Z disks. During sarcomere contraction, actin and myosin undergo sliding filament movement, fully interweaving with each other, resulting in maximum force generation, at the optimum muscle fiber length. The M-band, referred to as the M line in Figure 3.3, functions as a perpendicular structure that secures myosin in the center of the sarcomere. In order to maintain the normal operation of the contractile mechanism, numerous filamentous titin molecules, which are proteins, support the adjacent connection between myosin and actin filaments. Titin, a prominent elastomeric protein, functions as a resilient coil, linking the Z disk to

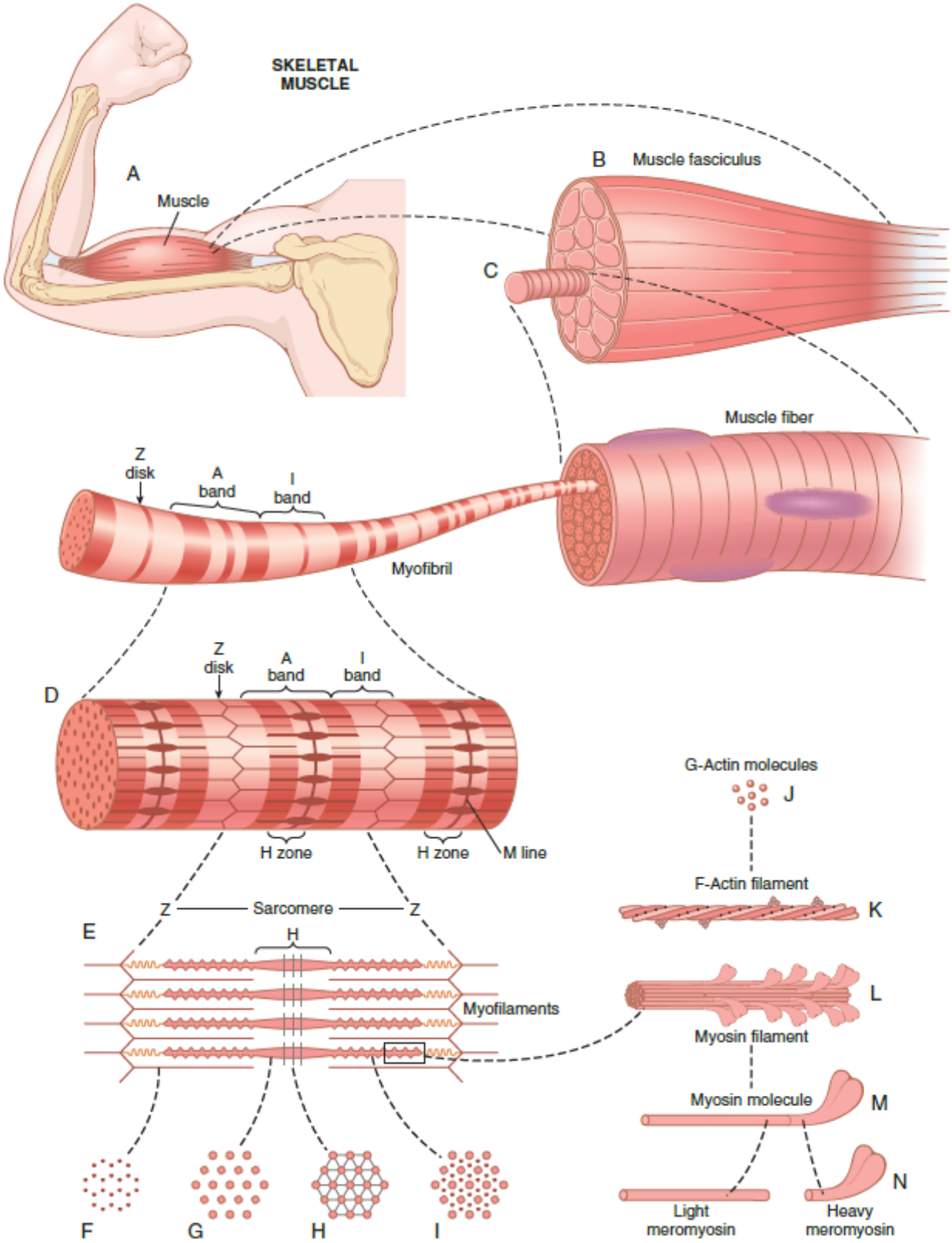

Figure 3.2: Organization of skeletal muscle, from gross to the molecular level [3]

the myosin filament, and possesses the capacity to alter its length during sarcomere contraction [3].

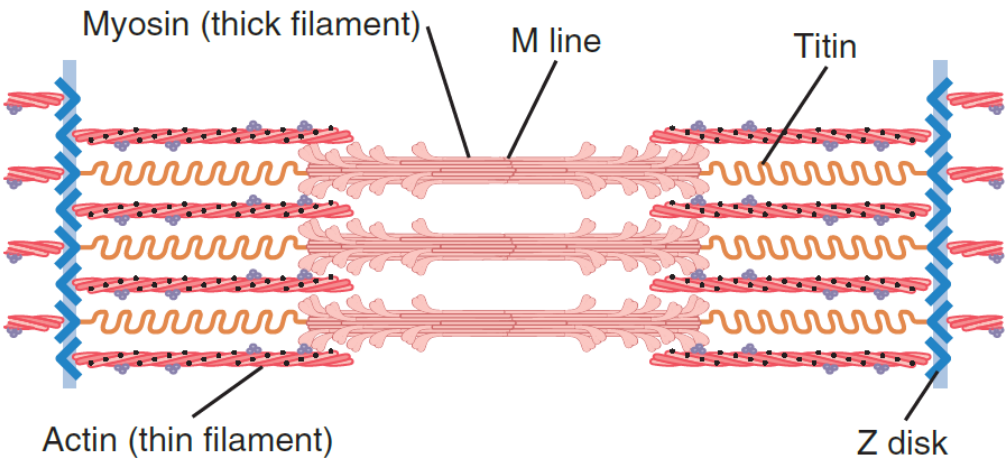

Figure 3.3: Organization of proteins in a sarcomere [3]

Muscles have different architectures depending on their particular roles [37], as their form is intended to improve the effectiveness of specific mechanical tasks. For skeletal muscles, two primary architectures are parallel and pennate. In parallel muscles, fibers are aligned both with the length of the muscle and the direction of force transmission. On the other hand, the pennation angle (α) refers to the angle between the orientation of muscle fibers and the axis of force generation, which is aligned with the tendon. Pennate muscles can produce higher levels of force. The two examples shown in Figure 3.4 illustrate the importance of internal architecture in relation to muscle function. An example of a parallel architecture is the hamstrings. Due to fibers arranged in series and joined by connective tissue, these muscles produce moderate force but have a long range of motion. In contrast, the quadriceps—a pennate muscle—have shorter, angled fibers. With reduced overall excursion, these muscles generate higher forces because of a larger physiological cross-sectional area. This adaptation suits their roles: the hamstrings enable the large shortening needed for running, while the quadriceps generate force for tasks like climbing stairs. An extreme example is the calf's soleus, whose highly pennate structure and abundance of slow, fatigue-resistant fibers allow it to sustain significant force over long periods [4].

Due to its structural ability to generate the electrical stimulation needed for muscle cells to begin contracting, the nervous system is essential for the contraction of muscles. The nerve cells that regulate muscle movement are called motor neurons. The cell bodies of these neurons extend from the spinal cord to facilitate the transmission of electrical signals to the muscle fibers. All of the muscle fibers in a motor unit contract at different rates depending on the electrical activity of a single motor neuron. A motor neuron can get to a very different amount of muscle fibers depending on the size and function of the muscle. A skeletal muscle's voluntary contraction is the result of multiple motor units collaborating.

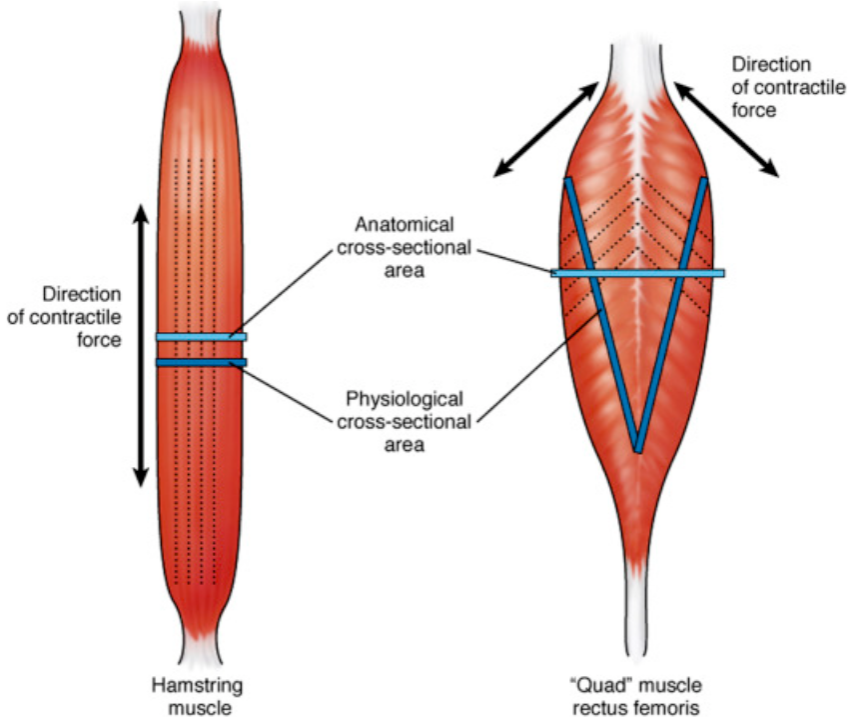

Figure 3.4: Functional architecture of flexor (hamstring) versus extensor (quad) muscles in the human thigh. [4]

The neuromuscular junction is where the electrical signal travels from the motor neuron's terminal end to the muscle fiber, causing the muscle fiber to contract [38].

3.2 Gait cycle and major muscle groups for locomotion

Normal human walking (gait) is a cyclic process divided into repeated gait cycles. A gait cycle initiates with the contact of one foot on the ground and concludes upon the subsequent contact of the same foot with the ground. This cycle can be methodically divided into discrete periods and phases to make it easier to examine normal and aberrant gait patterns. Gait cycles consist of two periods, referred to as gait phases, which are the stance and swing. The entire period of time the foot is on the ground is referred to as the stance. First contact is the beginning of stance. The period of time the foot is in the air for limb progress is referred to as the swing. When the foot is raised off the ground (toe-off), the swing starts [39]. The stance phase usually lasts about 60% of the cycle, the swing phase about 40% and each period of double support about 10%. Figure 3.5 describes terms used to identify major events during one gait cycle. Comprehensive insights are provided by Clinical Gait Analysis, which records four primary types of data simultaneously: spatiotemporal, kinematics, kinetics, and electromyography data.

Movement and stabilisation of the lower limb are generated by several large muscle groups acting across the hip, knee, and ankle. In the hip region, the gluteal muscles (especially gluteus maximus) and

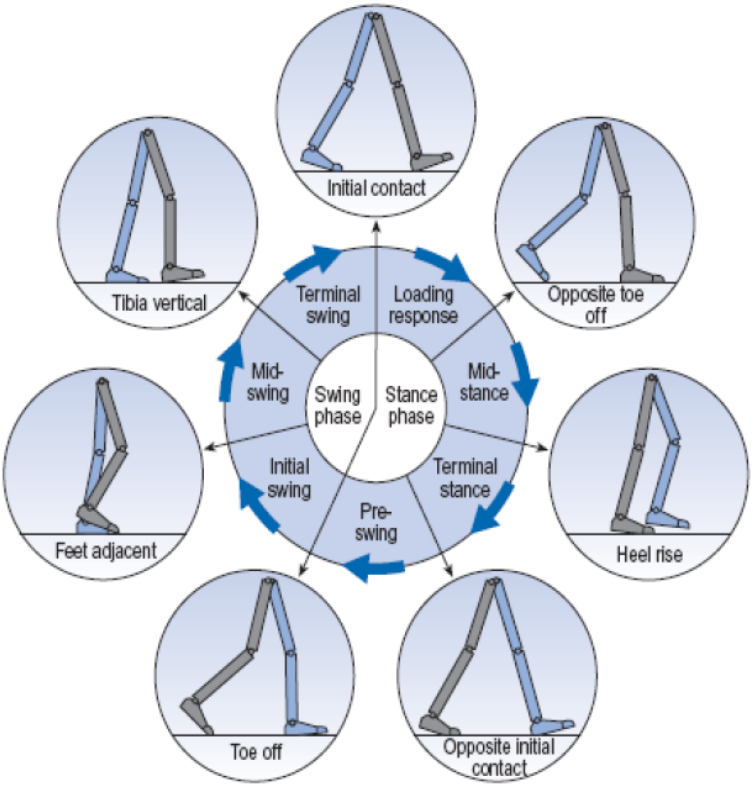

Figure 3.5: Events in a Gait Cycle [5]

the hamstrings (posterior thigh muscles) serve as powerful hip extensors that drive the body forward and upward (for example, during climbing or the push-off phase of gait) [36]. The iliopsoas and rectus femoris (part of the quadriceps) are primary hip flexors, which lift the thigh and swing the limb forward. The hip abductors, mainly gluteus medius and minimus, stabilise the pelvis in the frontal plane; during single-leg stance they contract to prevent the opposite side of the pelvis from dropping. This stabilisation is critical for balanced one-legged support during walking. Conversely, the hip adductor group on the medial thigh helps stabilize the limb and refine lower limb trajectory during the gait cycle.

In the thigh, the quadriceps femoris group is the primary knee extensor [36]. The quadriceps straighten the knee and support the limb during stance – for instance, they contract to absorb shock and stabilize the knee when the foot contacts the ground. The opposing muscle group, the hamstrings (posterior thigh), act as knee flexors and also assist in hip extension. The hamstrings contract during the late swing phase of gait to decelerate the forward motion of the tibia and thigh (preventing the knee from snapping into extension). They also help initiate hip extension in early stance along with gluteus maximus. Surrounding the knee, smaller muscles (e.g., popliteus) and the gastrocnemius (calf muscle, which crosses the knee and ankle) contribute to knee flexion and stability as needed.

In the lower leg, muscle groups acting on the ankle and foot are crucial for effective locomotion. The anterior compartment of the leg (e.g., tibialis anterior and toe extensor muscles) produces dorsiflexion at the ankle, which is vital for lifting the foot during the swing phase of gait and for controlled lowering of the foot at heel contact. Without adequate dorsiflexor action, the toes would drag during swing or the foot would slap down abruptly at initial contact. The posterior compartment of the leg contains the calf muscles, gastrocnemius and soleus, which are powerful plantarflexors of the ankle [36]. These muscles contract to raise the heel off the ground during the terminal stance, propelling the body forward (the "push-off" or third rocker of gait). They also eccentrically control the forward rotation of the leg over the foot during mid-stance (acting as a brake to store elastic energy for push-off). Smaller muscles in the lateral and deep posterior compartments (fibularis/peroneus muscles, tibialis posterior, foot intrinsic muscles, etc.) contribute to balancing the foot, maintaining the arch, and adapting the foot to the walking surface.

3.3 Cerebral Palsy

Cerebral Palsy is a group of neurological disorders affecting posture, balance, and movement development that limit an individual's activities. These conditions are thought to be caused by non-progressive disruptions in the growing fetus or infant brain. Disruptions to the developing brain, manifesting before, during, or after birth, directly influence regions associated with motor control. This connection is explained through the use of the term "Palsy," denoting the loss or impairment of motor function, while "cerebral" refers to the brain. Motor disorders in CP are frequently accompanied by disruptions in sensation, perception, cognition, communication, and behavior, as well as epilepsy and secondary musculoskeletal problems [40].

It was long believed that the primary cause of CP was asphyxia caused by intrapartum factors. However, during the 1980s and 1990s, this notion was reexamined, and it is now believed that 70 - 80% of cases of CP are caused by prenatal causes, with birth asphyxia having a negligible effect. According to a study by Stavsky et al. [41], the primary risk factor for the development of CP is premature birth, particularly before 28 weeks of gestation. When preterm neonates are born between 24 and 27 weeks of gestation, the birth prevalence of CP rises to 15%. This prevalence increases with decreasing gestational age at delivery. The following perinatal conditions have been linked to the development of CP in premature infants: transient hypothyroxinemia (low maternal thyroid hormone levels); hypocapnoea (reduced carbon dioxide levels, which can induce cerebral vasoconstriction) in conjunction with mechanical ventilation; chorioamnionitis (intra-amniotic infection); or other evidence of perinatal inflammation, especially when sustained postnatally. There is uncertainty regarding the causality of some of these relationships, although several are also linked to the risk of white matter damage [6]. Although each

term-born infant has a lower individual risk of CP than preterm or post-term infants, most CP cases still occur in term births simply because the vast majority of babies are born between 37 and 42 weeks. However, the danger is not constant throughout the term. The risk of CP is highest at 37 weeks and 42 weeks or later, and it is lowest at 40 weeks [42].

Additionally, in twin pregnancy, even if one twin dies in utero early in pregnancy, the remaining twin is far more likely to develop CP. This discovery was explained by the theory that the dissolving twin emits thromboplastin and emboli, which may cause brain damage to the surviving twin and the subsequent development of CP [43].

3.3.1 Clinical Classification

There are numerous incomplete categories and an ongoing search for a comprehensive classification since it is still difficult to classify children with CP into clinical groups [14].

3.3.1.A Traditional classifications of CP based on multiple variables

The classification of CP based on multiple variables includes the Swedish classification, Edinburgh classification, and Surveillance for Cerebral Palsy in Europe (SCPE) classification [44]. Among these, the SCPE classification is especially important, being widely recognized and extensively utilised. The SCPE categorizes CP into four subtypes: spastic (bilateral and unilateral), dyskinetic (dystonic and choreoathetotic), ataxic, and mixed.

1. Spastic Cerebral Palsy: Characterized by elevated muscle tone and reflexes. Upper motor neuron symptoms in patients with spastic disorders include extensor plantar response, hyperreflexia, and spasticity. Usually, the arm is more affected than the leg in **spastic hemiplegia**. Children with hemiplegic CP may also experience behavioral issues such as anxiety and particular phobias, in addition to a possible intellectual impairment. While fine motor skills are frequently retained in the upper limbs, children with **spastic diplegia** typically experience severe gross motor difficulties, especially in the lower limbs. Periventricular Hemorrhagic Infarction (PVHI) and Periventricular Leukomalacia (PVL) are frequently connected with it. Conversely, significant motor deficits almost equally impact the upper and lower limbs in those with **spastic quadriplegia**. This syndrome usually manifests in delayed speech and language development, visual impairment, seizures, and feeding issues in children [45].

2. Dyskinetic Cerebral Palsy: Individuals with dyskinetic CP often show a range of involuntary movements, with their limbs getting stiff during movement attempts or emotional moments. A clear sign of extrapyramidal dysfunction is noticeable in athetoid movements, especially in the toes. Dyskinetic CP has two subtypes: **choreo-athetoid CP** and **dystonic CP**. Unlike spastic CP, those with dyskinetic CP

usually do not develop contractures [45].

3. Ataxic Cerebral Palsy: Ataxic CP is quite uncommon and needs careful distinction from progressive neurodegenerative disorders. Children with this form often hit motor and language milestones later than usual. Ataxia tends to get better over time [45].

This classification integrates both physiological and topographic criteria. Although traditional topographic classification involves quadriplegia, triplegia, diplegia, hemiplegia and monoplegia (Figure 3.6), SCPE introduces two new terms. These terms are bilateral and unilateral used to describe the involvement of both sides and one side of the body, respectively. Spastic CP is observed in about 80% of instances of CP, while 10-20% of instances with CP are dyskinetic CP, and 5-10% of CP individuals have ataxic CP. The category of cases that make up 15.4% of all cases is known as mixed CP [46].

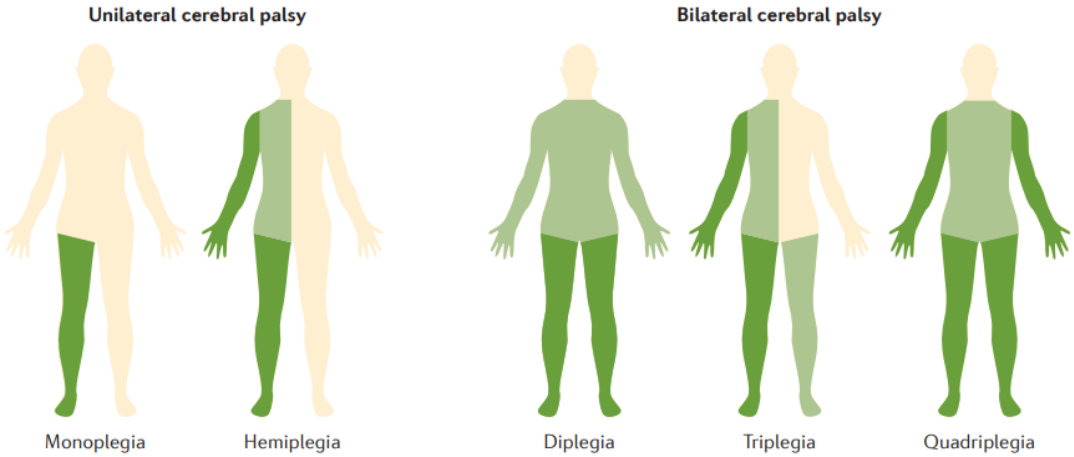

Figure 3.6: Topographical description in cerebral palsy: unilateral and bilateral CP [6]

Currently, the functional classification of each case of CP is internationally advocated due to its important role in management paraphrasing. Functional scales are currently used to classify people with CP based on the many impaired functions, including fine motor, gross motor, oromotor/oropharyngeal, and communication tasks. They are not utilized as outcome measures, examinations, or evaluations; rather, they are essentially ordinal scales for classifying functional skills or the degree of activity limits. When combined, the functional classifications provide a comprehensive description of daily functional activities in CP at the activity or participation level of the International Classification of Functioning, Disability and Health (ICF) [44].

At the activity or participation level of the ICF, the functional classifications are complementary and when combined provide a comprehensive picture of daily functional activities in CP. Among them are:

Gross Motor Function Classification System (GMFCS), Manual Abilities Classification System (MACS), Communication Function Classification System (CFCS), and Eating and Drinking Ability Classification System (EDACS) [44]. GMFCS is the most widely used clinical functional classification of CP, and thus, for the sake of brevity, is the only one further detailed here.

GMFCS is a practical scale categorizing a child's mobility or lower limb function into five levels, ranging from unrestricted walking (Level I) to an inability to maintain antigravity head and trunk postures (Level V) (Table 3.1). Initially introduced by Palisano et al. in 1997 for children under 12 [47], it was later expanded in 2007 to include youths aged 12–18 [48]. This updated version aligns with the ICF. The GMFCS criteria can be summarized as follows:

- Level I: Unrestricted walking.
- Level II: Walking with limitations.
- Level III: Walking using a hand-held mobility device.
- Level IV: Self-mobility with limitations; potential use of powered mobility.
- Level V: Reliance on a wheelchair for transportation.

Table 3.1: Gross Motor Function Classification System (GMFCS) Levels I–V Descriptors [6]

Level	Descriptor
Level I	Children walk at home, school, outdoors and in the community. They can climb stairs without the use of a railing. Children perform gross motor skills such as running and jumping, but speed, balance and coordination are limited.
Level II	Children walk in most settings and climb stairs holding onto a railing. They may experience difficulty walking long distances and balancing on uneven terrain, inclines, in crowded areas or confined spaces. Children may walk with physical assistance, a hand-held mobility device or use wheeled mobility over long distances. Children have only minimal ability to perform gross motor skills such as running and jumping.
Level III	Children walk using a hand-held mobility device in most indoor settings. They may climb stairs holding onto a railing with supervision or assistance. Children use wheeled mobility when travelling long distances and may self-propel for shorter distances.
Level IV	Children use methods of mobility that require physical assistance or powered mobility in most settings. They may walk for short distances at home with physical assistance or use powered mobility or a body support walker when positioned. At school, outdoors and in the community children are transported in a manual wheelchair or use powered mobility.
Level V	Children are transported in a manual wheelchair in all settings. Children are limited in their ability to maintain antigravity head and trunk postures and control leg and arm movements.

Table 3.2: Components of CP classification by Bax et al. [14]

Components	Description
Motor Abnormalities	A. Nature and Typology: Observed tonal abnormalities, diagnosed movement disorders (e.g., spasticity, ataxia, dystonia, athetosis) B. Functional Motor Abilities: Extent of limitations in motor function, including oromotor and speech functions
Associated Impairments	Presence or absence of non-motor neurodevelopmental or sensory problems (seizures, hearing or vision impairments, attentional, behavioral, communicative, cognitive deficits) and interaction among impairments
Anatomic and Radiological Findings	A. Anatomic Distribution: Parts of the body affected by motor impairments or limitations (limbs, trunk, bulbar region) B. Radiological Findings: Neuroanatomic findings on CT or MRI (e.g., ventricular enlargement, white matter loss, brain anomaly)
Causation and Timing	Identification of a clearly identified cause (e.g., meningitis, head injury), and determination of the presumed time frame of the injury

The classifications widely used focus on the nature of motor abnormalities (as seen in SCPE) and functional motor abilities (as seen in GMFCS). However, Bax et al. [14] emphasizes a multi-dimensional approach, considering not only the nature and typology of motor abnormalities and functional motor abilities, but also associated non-motor impairments, anatomical distribution, radiological findings, and the presumed cause and timing of the brain injury. The four major dimensions are represented in Table 3.2.

3.3.1.B Gait Patterns in Cerebral Palsy

Children with CP often show clear musculoskeletal differences compared to TD children. Their muscles tend to be smaller, shorter, stiffer, and weaker - often 30 to 40 % lower in volume [49]. Imaging studies confirm this, revealing that many leg muscles in CP children have a much smaller cross-sectional area than in healthy children [50]. The bone geometry in CP also differs from that in healthy children, largely due to abnormal loading and muscle forces. Excessive femoral anteversion (sometimes paired with a very high neck-shaft angle) and internal tibial torsion are among the most common [51]. These anatomical changes directly shape CP gait patterns. Examining these distinct gait patterns in greater detail is necessary, and this is where clinical gait analysis comes into play. Its main goal is to identify the subtle elements that contribute to each person's unique gait pattern across the range of CP. Walking deviations in people with CP can take many different forms. To make communication easier, classification

techniques are widely used to group common gait pattern variations. However, these classifications are simplifying classification, as the cases are being generalized. Hence, certain combinations or deviations might not be included in these classification schemes. Classifications are different for unilateral spastic CP and bilateral spastic CP. In 1987, Winter et al. [52] proposed the first pattern classification for unilateral spastic CP by observing the kinematic data in the sagittal plane. The four groups proposed by Winter et al. [52] are represented in Figure 3.7. They exhibit increasing impairment severity and a distal to proximal (ankle to pelvis) development of impairments.

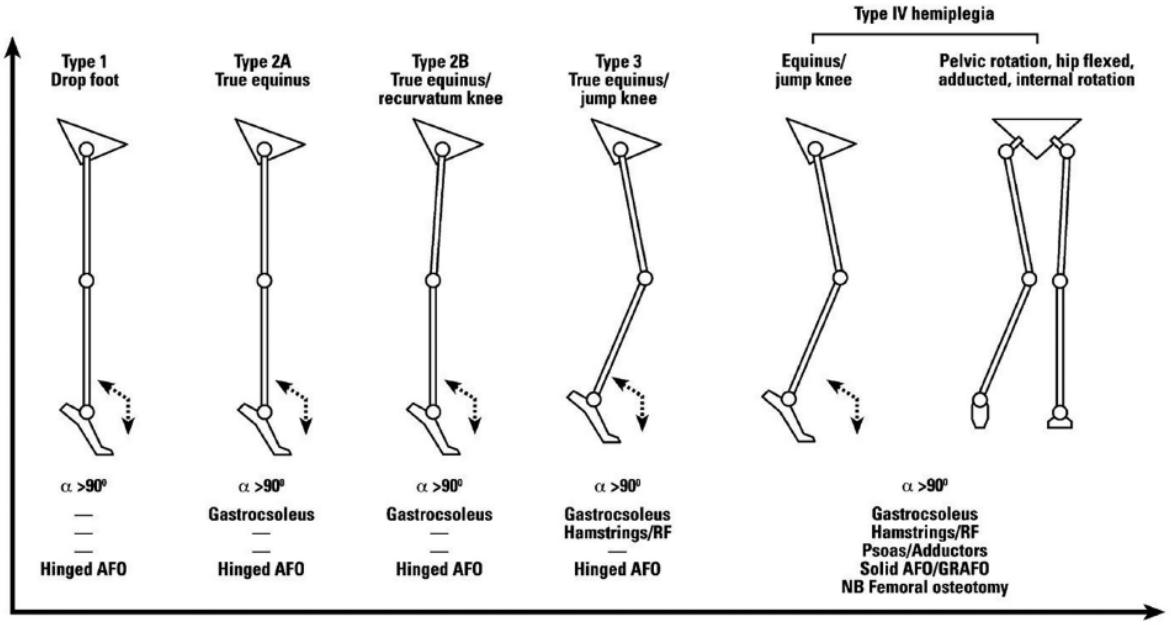

Figure 3.7: Gait patterns and management algorithm for unilateral spastic cerebral palsy [7]

For patients with bilateral spastic CP, Rodda and Graham [7] have suggested a classification scheme based on the sagittal plane kinematics that takes the ankle, knee, hip, and pelvis into account. True equinus, jump gait, apparent equinus, and crouch gait were the four main groups identified, as illustrated in Figure 3.8.

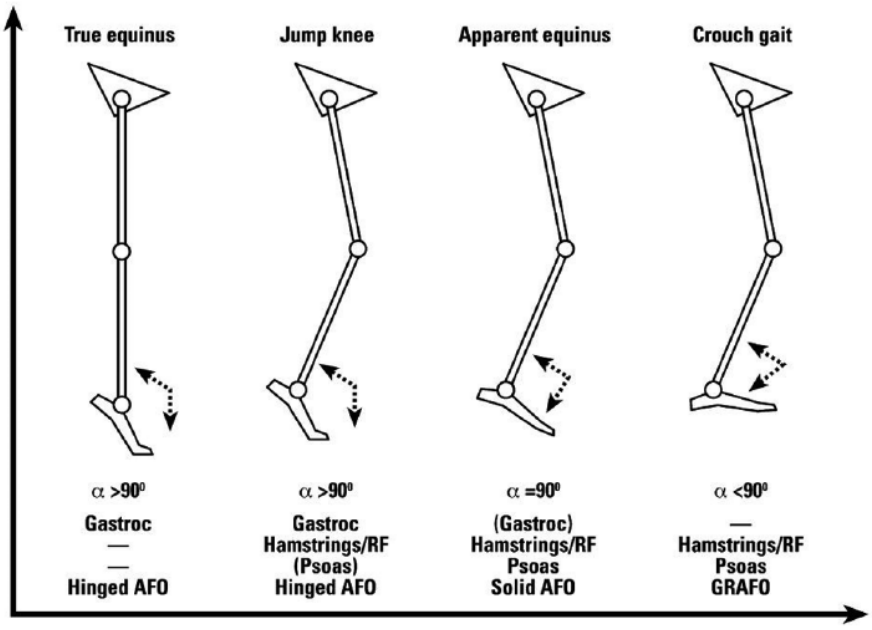

Figure 3.8: Gait patterns and management algorithm for bilateral spastic cerebral palsy [7]

3.3.2 Crouch Gait

Studying crouch gait is particularly important due to its prevalence and the significant impact it has on a child's functional mobility. A severe crouch gait represents the final stage before children face significant mobility challenges, often necessitating surgical intervention. Notably, unsuccessful treatment of other abnormal gaits may eventually result in the development of a crouch gait. Considering these factors, it becomes imperative to prioritize the investigation and understanding of this particular gait pattern.

3.3.2.A Description

Excessive ankle dorsiflexion combined with hip and knee flexion during the stance phase is known as **crouch gait**. Additionally, rotational irregularities in the femurs, tibias, and feet often occur, contributing to a phenomenon known as lever arm dysfunction (crouch). Crouch gait typically emerges during the growth spurt in puberty, often linked to an increase in body mass and an imbalance in the mass-to-strength ratio. This pattern is common in most children with spastic quadriplegia and plays a crucial role in the development of the gait disorder in those with more severe diplegia [7]. There are several factors that contribute to crouch gait, such as weak ankle plantarflexors, problems with lever arms of muscles, hip and knee stiffness, and hamstring constrictions. However, the weakening of the soleus muscle is the most significant one. Selective motor control impairment and the underlying brain dysfunction may be the causes of the soleus muscle weakness. It is also frequently a result of iatrogenic factors, particularly following heel cord lengthening. It is important to mention that crouch gait deviations are not only

related to neurological problems; secondary deviations in the gait are caused by several compensatory mechanisms that react to the abnormal gait [53].

3.3.2.B Treatment Approaches

The crouch gait was once thought to be primarily caused by contractions of the hamstring muscles. Recent studies, however, have demonstrated that many patients with crouch gait have normal hamstring lengths [54, 55]. Although the hamstrings do not directly produce the crouch gait, they do contribute to it by causing the knee to further flex. During stance, the quadriceps (rectus femoris) exert more effort to counteract this flexion. A greater demand is placed on hip extensors, such as the hamstrings, as the quadriceps (rectus femoris) contribute to hip flexion. This creates a cycle in which hip and knee flexion progressively increase [56]. Consequently, this gait pattern has an extremely high energy cost due to the greater demand on the muscles that stabilize the hip and knee joints. If patients do not get appropriate treatment, they may eventually lose their capacity to walk independently as their crouch worsens.

Since there are several contributing factors to crouch gait, each patient's physical deficiencies should be taken into account when designing the treatment plan. While mild crouch gait can be managed conservatively through interventions such as physical therapy, spasticity management, and foot orthoses, surgical treatment becomes a consideration when there is a need to address persistent joint contractures, correct lever arm dysfunctions, and restore optimal muscle length.

Non-surgical treatments

One of the most popular therapies for CP is physiotherapy. Maintaining a range of motion with sufficient muscle length, maintaining or regaining strength, and improving balance and coordination are the main goals [16]. The key strategies that have proven effective in helping individuals with CP are specialized training programs aimed at enhancing motor coordination and performance, along with physical training designed to tackle underlying impairments that might be hindering their ability to engage in desired activities. Intense upper-limb training is the most consistently effective and well-researched therapeutic method for CP, helping children with unilateral involvement improve their hand function. Studies show varying training kinds and forms, but with sufficiently rigorous and regular regimens, success rates are generally consistent. Task-specific procedures in the lower extremities have not shown such robust and sustained benefits [6]. A systematic review with meta-analysis of randomized trials by Scianni et al. [57] found that strengthening interventions had no effect on strength, walking speed, or activity level in children with CP, despite reports that suggest strengthening exercises may help patients with crouch [58, 59]. Therefore, the evidence now available indicates that strengthening therapies are neither desirable nor effective in children and adolescents with CP who are walking, but they are probably not

harmful either. According to Steele et al. [60], some patients may benefit from a progressive resistance strengthening program, but others—like those with spasticity in their hamstrings—may have worsening of their crouch as a result of the therapy.

Spasticity can be reduced either locally-by injecting agents like Botulinum Neurotoxin-A (BoNT-A), phenol, or alcohol directly into muscles-or globally, with drugs like baclofen given orally or intrathecally. Local injections of BoNT-A are designed to be reversible , although the long-term effects of denervation atrophy are still not fully understood. Clinically, BoNT-A is sometimes used as a test injection before surgical muscle-tendon lengthening [16]. For example, Thompson et al. [61] describe how Musgrave Park Hospital in Belfast uses BoNT-A to temporarily stretch small muscles, delaying the need for surgery; spasticity reduction typically begins 12–72 hours after injection and lasts three to six months.

In patients with CP, orthoses are frequently prescribed and used as therapies. Floor reaction Ankle-foot orthoses (AFO) are especially made for crouch gait. AFO can be used to reduce pathological gait in the sagittal plane (Figure 3.9). For instance, AFOs can be used to treat hyperextension of the knee during loading response or mid-stance. Anterior shell or floor reaction AFO designs are two alternate AFO designs that can help limit excessive knee flexion. Saltiel [62] introduced the Ground Response Foot Orthosis (GRAFO) in 1969, with an anterior rigid shell. This shell keeps the knee extended during stance, applies an extension force to the front of the tibia, and maintains the plantar flexion–knee extension pair. Foot deformity, severe tibial torsion, and hip and knee flexion contractures are among the conditions that limit the use of GRAFO [56]. Over time, conservative methods become less acceptable due to the progressive nature of crouch, necessitating surgical treatment.

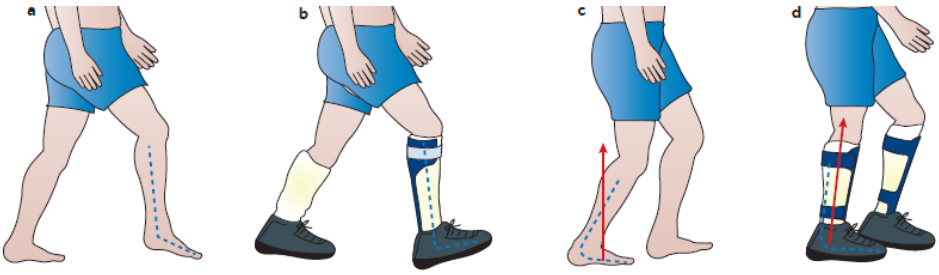

Figure 3.9: (a) Equinus deformity during swing and initial contact, characterised by excessive plantarflexion that increases trip risk. (b) With a floor-reaction AFO, the foot is maintained in dorsiflexion, restoring a normal heel-rocker at initial contact and improving ankle kinematics. (c) In crouch gait, excessive knee flexion and ankle dorsiflexion in late stance shift the ground reaction force posterior to the knee, increasing quadriceps demand and energy expenditure. (d) Bilateral floor-reaction AFOs redirect the ground reaction force anterior to the knee, reducing knee extensor load and promoting a more upright, energy-efficient posture. [6]

Surgical treatments

Surgical treatment for crouch gait focuses on lengthening tight muscles, fixing lever-arm problems, and releasing joint contractures. All of these corrections are usually performed together in a single-event, multilevel surgery, which is the current gold standard for managing ambulatory CP [63, 64].

Flexed knee gait, or excessive knee flexion during the stance phase, is a common anomaly in spastic diplegia. The most common surgical procedure to address this problem is hamstring lengthening, which has been shown in numerous studies to produce good short-term results. However, most studies involve small, varied patient groups, changing surgical techniques, and only short follow-ups, the long-term benefits of hamstring lengthening for flexed-knee gait remain unclear. Only few reports track outcomes beyond three years. In one long-term study by Dreher et al. [65], there has been a noticeable decline in the mean, minimum, and starting knee flexion during stance.

For CP children who have significant bone torsion, a rotational osteotomy is often performed as part of a single-event, multi-level surgery that realigns the bone to a more suitable position. The surgery corrects bone torsion by realigning the femur or tibia in the same session as other required procedures, meaning the child only faces one round of rehabilitation. It typically produces substantial improvements in walking and modest gains in overall motor function. Although it's most common between ages 6 and 12, it can also be beneficial for carefully selected adults [6].

Some research [66] suggests that in CP the rectus femoris may remain active too long, extending from late stance into swing, contributing to a stiff-knee gait. This abnormal activity of this muscle results in a decrease in the maximum knee flexion in the swing phase. One well-established treatment for stiff-kneed gait is rectus femoris transfer surgery [67, 68]. In this surgical intervention, the distal tendon of the rectus femoris is carefully detached from the underlying vasti.

3.4 Electromyography (EMG)

As we explore the field of musculoskeletal modeling, it becomes crucial to recognize the significant importance of EMG. EMG functions as a reliable validation technique, ensuring that modeled muscle activations correspond to actual physiological responses. The use of EMG data in musculoskeletal models provides detailed insights into motor control and coordination. EMG has been a commonly utilized method to evaluate muscular function since muscle activation cannot be measured directly. From the 1960s until the mid-1980s, EMG was the main instrument for practical clinical gait analysis [69]. Nonetheless, the field of clinical gait analysis has changed since the advent of motion capture devices that are sold commercially. Nowadays, kinetics and EMG are viewed as secondary data types, with

kinematic data appearing as the primary data type. EMG data is currently collected in clinical gait analyses to identify incorrect patterns of co-activation, evaluate spasticity, and identify muscles exhibiting excessive activity [70].

Before making relevant comparisons between muscles or subjects, the recording need to be normalized and quantified. The normalization process involves recording the activity during a Maximum Voluntary Contraction (MVC) for each muscle as part of the test procedure. This is determined by giving some sort of task to the person in which they will activate the required muscle to their fullest potential. The most common task is pushing or pulling against an immovable object. It is thus possible to express the signals captured during gait as a percentage of the maximum voluntary contraction (%MVC) [69].

The timing of muscle activity during locomotion can be classified using three reference scales: the gait cycle interval, stance and swing periods, and functional phases. Although determining the gait cycle interval is a straightforward approach, the provided percentage points lack functional value. In order to obtain more significant data, it is important to make a connection between the start and end timing of EMG with the periods of stance and swing. This can be achieved by focusing solely on the signals of initial contact and toe-off. Furthermore, using the seven gait phases as the reference base for the EMG interval provides the most functional significance for the data.

The timing of muscle activity compared to normal function is significantly important when analysing abnormal gait. The classification of abnormal activity consists of seven categories: premature, prolonged, continuous, delayed, curtailed, absent, and out-of-phase (as indicated in Table 3.3). Moreover, abnormal function is characterised as excessive, inadequate, or absent (as illustrated in Table 3.4).

Table 3.3: Table for timing errors of EMG muscle activations [15]

Deviation	Definition
Premature	Action begins before the normal onset
Prolonged	Action continues beyond the normal cessation time
Continous	EMG uninterrupted for 90% or more of the gait cycle
Curtailed	Early termination of the EMG
Delayed	Onset later than normal
Absent	EMG of insufficient amplitude or duration
Out of phase	Swing or stance time reversed

Additionally, the quality of the EMG instrumentation used also affects the signal recorded. In order to guarantee the accuracy of the information, it is important to take into account four levels of instru-

mentation - electrodes, amplification and filtering techniques, signal transmission and recording system.

Table 3.4: Table for relative intensity errors for EMG signals [15]

Deviation	Definition
Excessive	EMG value greater than the normal band
Inadequate	EMG value less than the normal band
Absent	EMG insufficient to identify functional significance

Myoelectric signals can be obtained using three types of electrodes: needles, wires, and surface electrodes. The electrodes are able to collect the signals that extend across the local muscle and adjacent soft tissues. Nevertheless, needles are considered to be impractical and painful for the purpose of gait analysis. The widely employed and endorsed method, following SENIAM criteria [71], utilizes disposable adhesive surface electrodes. The electrodes contain a silver component that provides direct contact with the skin using a silver chloride gel. They are usually used in pairs, with a distance of around 2cm between them. Thin-wire electrodes consist of two fine insulated wires inserted into the muscle, with their exposed tips separated by only a few millimeters, allowing for highly localized signal recording. This approach may be beneficial for smaller muscles, however, it may not capture fully the behaviour of larger muscles. When surface EMG is not feasible, for example, for the tibialis posterior, which lies deep beneath the gastrocnemius and soleus, the only available method for EMG measurement is by the use of small wires. The displacement of the wire electrode is a potential problem that might occur during movement [15]. Wire electrodes are better than surface electrodes in terms of selectivity. However, they are invasive, hence, require special skill and significant preparation time to insert, and may cause the subject discomfort and pain, limiting their utilization. By implementing suitable filtering techniques, it is possible to isolate EMG data specifically from the intended muscle, thereby reducing interference from adjacent muscles. Although it may be difficult to achieve varying levels of muscular activation in connected muscle groups, it is possible for most desired muscles in healthy people. The recordings obtained from these tests are useful resources that are used as references during the process of interpretation.

The efficacy of these tests in individuals with upper motor neuron diseases such as CP is questionable due to the common co-activation of adjacent muscle groups. Distinct muscle activity suggests precise electrode positioning, although differentiating between cross-talk, suboptimal electrode placement, and real co-activation is difficult [69].

Amplification devices are attached to the electrodes. The quality of the connection between the

amplifiers and electrodes is crucial since any noise that enters the system will also be amplified, affecting the EMG signal. Almost all signal processing begins with the application of a low-pass filter to eliminate any remaining low-frequency movement artifacts in the data. The filter's frequency will determine how smooth it is. A filter with a higher frequency will retain more of the original signal's appearance. A filter with a lower frequency tends to blur features.

To obtain reliable surface EMG data, the sensors must be placed suitably. To prevent cross-talk from nearby muscles from affecting the sensors on the muscle belly, the goal is to align them with the underlying fibers [72]. Although the guidelines for positioning the sensors should be followed, like those provided by SENIAM, the exact placement must take into consideration the anatomy of the person. It is crucial to keep in mind that a variety of disorders affecting patients receiving gait analysis can result in varying muscle structures. It is well known that children with CP, for instance, frequently have muscles that are shorter and less bulky. Furthermore, these muscles can also become exaggerated following surgery [73]. Gait analysis services are increasingly including ultrasound, which can provide helpful confirmation of proper sensor placement.

3.5 Musculoskeletal modeling

A musculoskeletal model consists of a mechanical representation of bones, muscles, and joints. Its primary application lies in estimating internal forces, specifically muscle and joint reaction forces, based on data related to movement and external forces. Bones are typically modelled as rigid segments, considering that bone deformations are presumed to have negligible impact on joint articulations or the calculation of muscle forces. Muscles are commonly represented using the Hill phenomenological model, which encompasses the description of the elastic properties of tissues. Depending on the model's focus, joints are portrayed using either kinematic constraint equations to depict fundamental joint movements or more sophisticated joint models that include elastic descriptions of ligaments and cartilage. Withing kinematic constraints, the most common joints are spherical, revolute, and universal joints. The simulation process depends on the available input information. If forces and moments are known, the equations are solved to compute the movement-referred to as forward dynamics. Conversely, if the movements are known, the forces and moments are computed-known as inverse dynamics [9].

3.5.1 Muscle modelling

In order to achieve an accurate representation of muscle activity, computational human modelling has to mimic as well as possible the complex anatomical structures and the relevant physiological and biological functions. This is obtained by using different mathematical formulations. The level of complexity of the model depends on the purpose of the research.

Musculoskeletal modeling offers a noninvasive way to estimate forces and other quantities inside the body [74]. Winters and Stark categorize the muscle models used in these simulations into three groups:

- **Second-order linear models**, which treat the muscle-joint complex as a simple mass-spring-damper arrangement, with no separate tendon element. While this makes the model straightforward to build, it does not capture the subtle dynamics required for realistic gait simulations.

- **Huxley's distributed-parameter models**, which capture the biochemical details of cross-bridge cycling by modeling how myosin heads attach to and detach from actin filaments. These models link a muscle's mechanical output to its metabolic processes, but their computational cost can be prohibitive for large-scale simulations.

- **Hill-type lumped-parameter models**, which strike a balance between realism and efficiency. By representing the muscle–tendon unit with a handful of elements (contractile, series elastic, and parallel elastic), they reproduce the essential behaviors of muscle force generation with far less complexity.

In this work, contraction dynamics are described by the Hill model to capture how muscle activation is converted into force (see Figure 3.10).

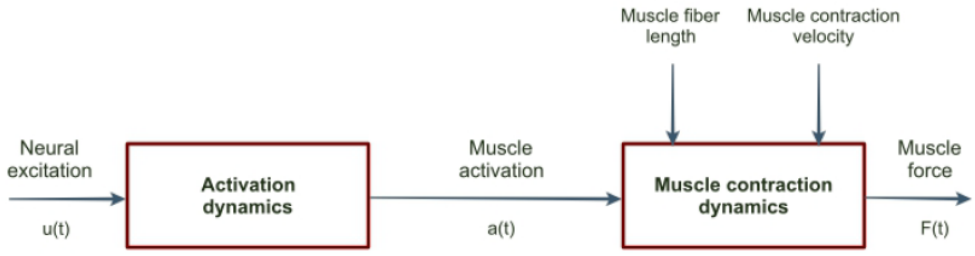

Figure 3.10: The transformation of neural excitation u(t) to muscle force F(t) by means of activation dynamics and muscle contraction dynamics. [8]

3.5.1.A Activation Dynamics

Activation dynamics is the main process that turns neurological excitation signals into activation of the contractile unit. This makes the connection between motor unit excitation and muscle activation.

There exist time lags in neural excitations. Neural signal takes time to reach the muscle fibers and thereby, to produce muscle contraction. Therefore, it is crucial to take them into account when simulating muscle mechanisms.

There are three commonly used models that explain the relationship between neural excitations and muscle force generation. The first model was introduced by Thelen [75], which adopts a first-order differential system with separate activation and deactivation time constants, providing a physiologically plausible approximation of muscle behaviour. In 2013, Millard [76] refined Thelen's approach by introducing damping mechanisms to prevent unrealistic muscle responses during fast changes. The third model was introduced by CEINMS and it processes EMG signals to extract muscle excitations, accounting for the electromechanical delay. To transform neural excitations to muscle activations, CEINMS uses a linear second-order differential system with specific shape factors and coefficients that can be calibrated individually [23].

3.5.1.B Muscle Contraction Dynamics

Activation Dynamics is followed by Contraction Dynamics, which represents the relation between the muscle activation and the force generated by the muscle-tendon actuator. In this stage, the interactions of force-length-velocity properties of the muscle are considered. Additionally, the elastic property of the tendon is taken into account. The Hill model serves as a representation of these characteristics.

Figure 3.11 illustrates the Hill Model and its parts, including a contractile element (CE), a series elastic element (SEE), and a parallel elastic element (PEE). The CE includes the muscle's force-length, and force-velocity properties, and is considered to be the model's main part as it shows the muscle force that comes from its activation. The SEE represents the elasticity of connective tissue, which includes tendons and aponeuroses. Lastly, the PEE is a representation of the passive resistance that the fascia and other surrounding tissue, imposes when the inactive muscle is stretched by external forces. It is important to mention, given that the tissue they are modeling exhibits non-linear elastic behavior, SEE and PEE are represented as non-linear springs. Furthermore, since the orientation of the muscle fibers and the SEE element do not always coincide, this model also takes the pennation angle (α) into account. This angle permits a greater number of muscle fibers per cross-sectional area. Additionally, it influences the muscle's force-length-velocity properties, which characterize how its force production is influenced by changes in muscle length and the rate of contraction [10].

The force–length relationship presents the ability of a muscle to generate force across different ranges of lengths. When there is no neural drive, a muscle produces only passive force against increased stretching. On the other hand, the active force is produced when a muscle is actively contracted. The total force is the sum of passive and active forces [77]. As shown in Figure 3.12, the muscle reaches its peak isometric force at the optimal fiber length (l_0), where cross-bridge overlap is maximal. When the fiber shortens below the optimal fiber length, the total force is equal to the active force, while stretching

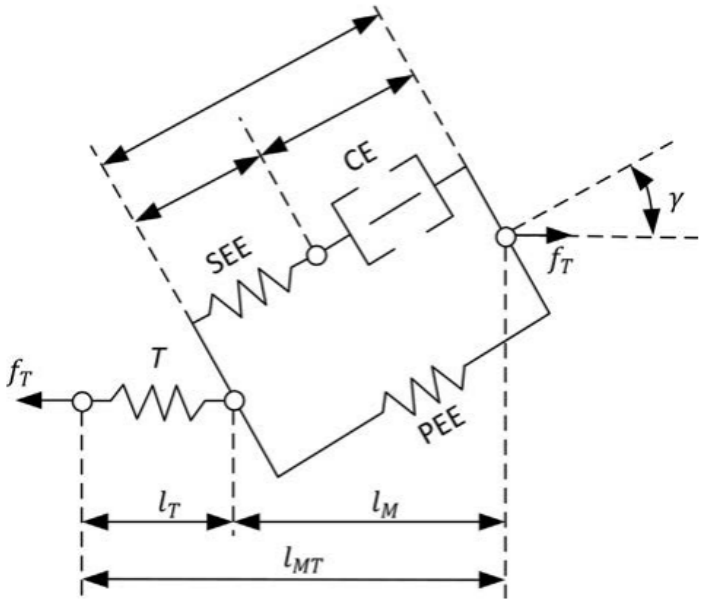

Figure 3.11: Hill muscle model to represent contraction dynamics [9]

beyond the optimal length diminishes the active force, and the passive elements increasingly bear the load.

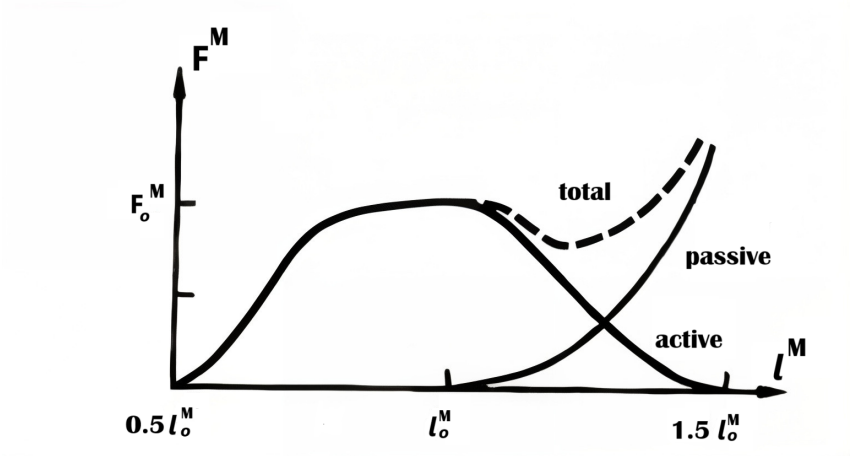

Figure 3.12: Force-length relationship of a muscle.

The force–velocity property of muscle describes the relationship between the magnitude of force a muscle can generate and the velocity at which it contracts. As illustrated in Figure 3.13, an inverse relationship exists between muscle shortening velocity and its capacity to generate force. Specifically, an increase in the velocity of muscle shortening is closely related to a decrease in the potential force output. Conversely, slower shortening velocities allow the generation of greater muscular forces. This relationship is represented by a hyperbolic curve. A key implication of this curve is that the muscle's

capacity to adjust force output is limited at high contraction velocities: during fast concentric contractions, force decreases significantly, while during fast eccentric contractions, force reaches a plateau and does not increase substantially. In contrast, as contraction velocities approach zero (i.e., near-isometric conditions), even slight variations in shortening velocity can correspond to a considerable range of force production. The maximum isometric force (F_0M), which represents the peak force a muscle can produce, is produced when shortening velocity is zero.

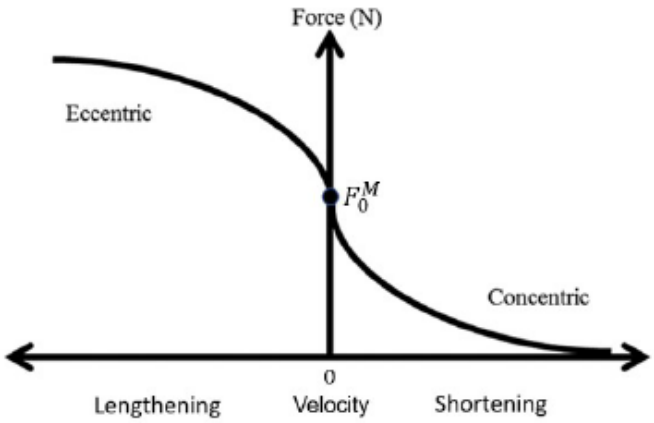

Figure 3.13: Force-velocity relationship of a muscle. Adapted from [10]

3.5.2 OpenSim

Study of movement draws from and contributes to diverse fields, including biology, neuroscience, mechanics, and robotics. OpenSim, a widely recognized platform in the literature [11] for such analyses and one of several available simulation tools, combines techniques from several domains to produce fast and accurate movement simulations. This open-source platform is designed for modeling, simulating, and scrutinizing the neuromusculoskeletal system. The program was initially made available in August 2007 as a movement simulation research tool [78]. Since its inception, numerous new functionalities have been introduced, improving its capabilities and contributing to its ongoing evolution. Because inverse dynamics yields only net moments and not individual muscle contributions, a secondary step is necessary: SO distributes the net joint moments among the available muscles by minimising the sum of squared muscle activations.

Human movement involves the coordinated interplay of the nervous, muscular, skeletal, and sensory systems. OpenSim combines computer models that depict these systems, making it easier to predict and research how people move. Controller models or real – world data, such as electromyography, can be used to anticipate the excitations, or brain impulses, that direct muscles. These excitations are translated into muscular forces using OpenSim's musculotendon models, which take into account the

force – length and force – velocity relationship of the muscles while applying Hill – type concepts, as can be seen in Figure 3.14.

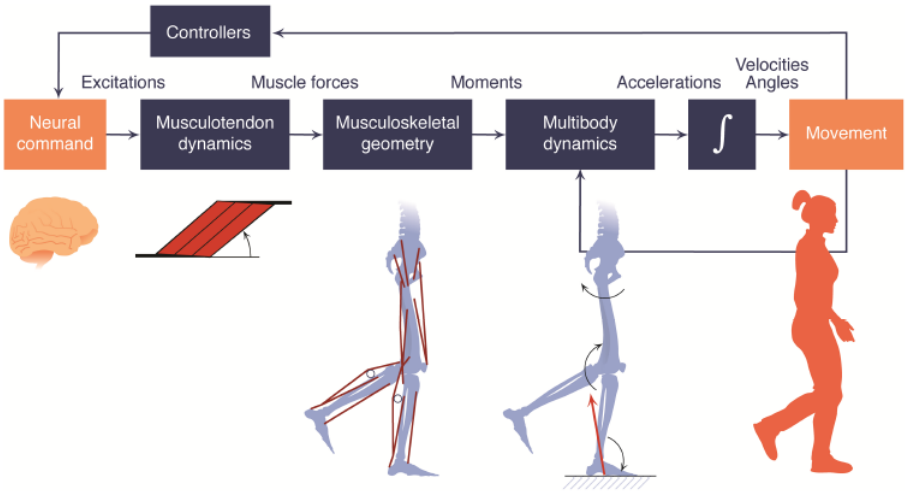

Figure 3.14: Elements of a typical musculoskeletal simulation in OpenSim. [11]

Earlier versions of the software primarily focused on studying human gait and investigating the impacts of different pathologies and treatments. Recent updates have brought in more accurate models, covering aspects such as muscle contraction dynamics, muscle metabolic power, joint kinematics, and assistive devices. Furthermore, users now have the flexibility to go beyond preset workflows and design custom studies by combining various computational tools in innovative ways. For instance, users can directly access muscle-related details, like moment arms, fiber lengths, and passive fiber forces, from a model without having to go through a complex analysis within the OpenSim application [11].

OpenSim has four main functionalities. Initially, users are able to create, modify, and analyze biomechanical models. Secondly, neuromuscular control and musculoskeletal dynamics can be simulated with OpenSim. Thirdly, OpenSim can predict novel movements and adaptations to novel settings without the need for studies, based only on the principles of neuromuscular control and dynamic modeling. Lastly, academics can develop and exchange new computational models, numerical techniques, and simulation tools that expand OpenSim's functionality thanks to its modular and extensible design [11]. These analysis tools compute muscle powers, joint forces, and accelerations caused by muscles, among other factors. For this dissertation, a plug-in tool known as CEINMS was used [23] .

3.5.2.A CEINMS

CEINMS is an OpenSim plugin that enables researchers to predict different neural control outcomes with respect to the same musculoskeletal architecture and recorded motions. Based on the initial electromyography-driven (EMG-driven) techniques [79], Lloyd and associates [24, 80] created software and algorithms to customize EMG-driven neuromusculoskeletal models to individual characteristics. Combining all of these algorithms and software programs resulted in CEINMS.

CEINMS was designed to be flexible and universal software that could function with different anatomical and physiological data, supporting any number of Degrees of Freedom (DOF) and Musculotendon unit (MTU). Because of its modular nature, users can freely choose from a variety of neural control solution algorithms, that are grouped in [81]:

Full-predictive open-loop mode (EMG-driven): Musculotendon force calculations in the neuromusculoskeletal model are driven by empirically recorded EMG signals and 3D joint angles [24, 80].

EMG-informed mode: Uses optimization to estimate excitations for muscles lacking experimental EMG and fine-tune excitations derived from experimentally acquired EMG signals. The neuromusculoskeletal model uses the resulting muscle excitations as inputs along with the three-dimensional joint angles.

Full optimization-driven closed-loop mode (Static optimization mode): Operating independently of experimental EMG data, an optimization algorithm creates all muscle excitations to drive the neuromusculoskeletal model [82].

The use of CEINMS requires three crucial steps: calibration, execution, and validation. The neuromusculoskeletal model parameters (optimal fiber length, tendon slack length, and maximum isometric force) are carefully adjusted during the calibration phase for a specific subject. During execution, inputs include MTU kinematics and external joint moments calculated using OpenSim, along with muscle excitations or primitive muscle excitation data taken from experimental EMG recordings. This combination is used for predicting joint moments and MTU forces. The execution step is integrated into an optimization loop to reduce the error between the estimated and experimental joint moments.

4

Methodology

Contents

This chapter starts by describing participants that took part in this study, then it summarizes the experimental setup used to collect and process data. Next, it explains the OpenSim pipeline, from model scaling to EMG-informed simulation, and it concludes with the normalisation procedures and quantitative metrics used to evaluate the results.

The data used for this dissertation was collected in 2014 in the Biomechanics and Functional Morphology Laboratory of FMH under protocols approved by the Faculty of Human Kinetics Ethics Committee. This research is part of the project 'Development of a simulation platform based on musculoskeletal models to predict recovery of gait following orthopedic interventions in cerebral palsy children', referenced as PTDC/EMD-EMD/5804/2020 [1]. From the larger sample of participants, the CP children included in this dissertation were chosen specifically based on their EMG signal quality. The TD participants were selected based on their ability to simulate the key features of crouch gait - excessive hip and knee flexion combined with excessive ankle dorsiflexion.

4.1 Participants

Four children diagnosed with spastic diplegia CP and six TD children were included in this study.

At the Biomechanics and Functional Morphology Laboratory children underwent a static exam to identify GMFCS level [83]. Two CP children were classified as GMFCS Level III, one as Level II, and the last one was classified as Level I. Some of the problems present in these children are a flexum on the hips, a flexum on both knees, patella alta on both sides, tibial external rotation, and a talus foot position. Subsequently, during the gait analysis performed in the same laboratory, a pronounced crouch pattern was evident, characterized by continuous knee flexion throughout the entire movement cycle. Significantly, both hips consistently exhibited heightened flexion while displaying a reduced overall range of motion. The typically developed children were carefully selected to match the age and height with CP. TD children were instructed to perform both simulated crouch gait and normal walking trials over the force plates.

All TD participants underwent a thorough clinical analysis to confirm the absence of neurological dysfunction. The characteristics of the subjects are presented in Table 4.1. The four children with spastic diplegia ranged in age from 10 to 16 years, whereas the six TD children were younger, between 7 and 9 years old. This age difference is reflected in body size, as CP children, on average, were taller and had higher body weight.

For the analysis of the results, the right leg of all participants was used, except PC006, since the left leg was more affected.

Table 4.1: Participants' Data. GMFCS stands for Gross Motor Function Classification System and it is a five-level scale used to classify children with CP.

SUBJECT	AGE (yrs)	HEIGHT (m)	MASS (kg)	CLINICAL DIAGNOSIS	MORE AFFECTED SIDE	GMFCS
CP002	10	1.22	31.35	Spastic diplegia	both	III
CP003	16	1.57	44.75	Spastic diplegia	both	II
CP006	10	1.34	25.75	Spastic diplegia	left	I
CP013	13	1.69	60.60	Spastic diplegia	both	III
TP006	7	1.32	21.75			
TD013	9	1.32	26.25			
TD017	9	1.31	25.80			
TD021	8	1.32	28.25			
TD023	9	1.30	23.30			
TD026	8	1.32	28.30			

4.2 Data acquisition

All data were collected in the Biomechanics and Functional Morphology Laboratory of FMH-UL by a biomechanist and physiotherapist or orthopedic doctor. The participants were informed about the protocol, including its risks and benefits, and informed consent was obtained.

The session began with a comprehensive physical examination, evaluating lower limb range of motion, muscle strength, tone, and spasticity [84]. As a first step in the gait analysis process, the subjects were asked to stand barefoot to obtain a static trial. Afterwards, the they walked along a 10-meter corridor at their natural walking speed. Dynamic trials were considered valid once the subject successfully completed a minimum of 10 good-quality kinetic walking cycles on each side. A trial was deemed successful only if the participant placed exactly one full foot on each force plate-no part of the foot off the plate and no dual-plate contacts (Figure 4.1).

Participants were equipped with 25 reflective markers and 4 marker clusters placed according to CAST (Calibrated Anatomical Systems Technique) [85] protocol and CODA pelvis [86] (Figure 4.2). The data were captured using Qualisys Track Manager (QTM) software (version 3, Qualisys Inc., Gothenburg, Sweden), with 14 Qualisys cameras (Qualisys Oqus 300, Qualisys AB, Gothenburg, Sweden) operating at a sampling rate of 100 Hz. Ground Reaction Forces (GRF) were collected with three Bertec and one Kistler force plate. Additionally, they were equipped with surface electromyography sensors. EMG data were acquired using the Delsys Trigno Wireless System and were recorded for the gluteus medius, rectus femoris, adductor longus, tibialis anterior, and gastrocnemius medialis. For the hamstring muscles, either semitendinosus or biceps femoris was recorded, depending on the subject.

4.3 Data processing

The raw gait data collected were processed using a combination of QTM software and Visual3D software (C-Motion Inc., Kingston, Canada). QTM was used to digitize and label the markers placed on

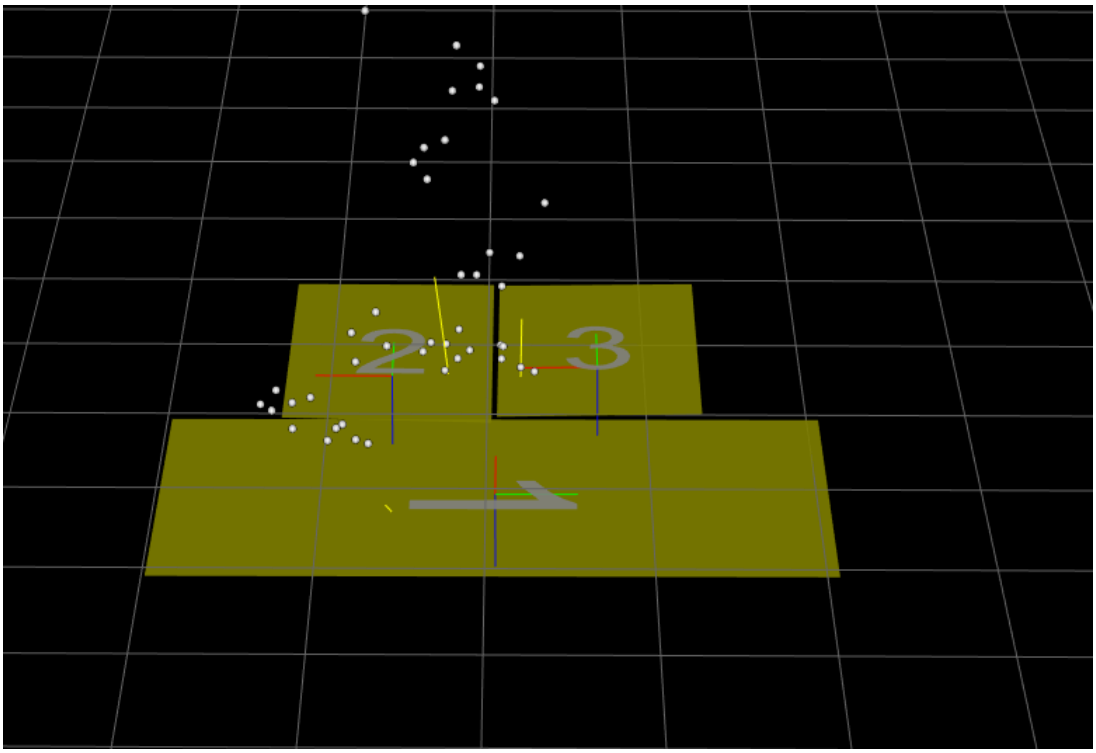

Figure 4.1: An example of an excluded trial: the subject stepped on both force plates. Data inspected and displayed using Mokka software.

anatomical landmarks. Once labeled, the data, which included marker trajectories, GRF, and EMG recordings—were exported in .c3d format to Visual3D. These .c3d files were then imported into Mokka (MOtion Kinematic & Kinetic Analyser) software, provided by The Biomechanical ToolKit [87], where the data inspection was done. Selecting which trial to use for each subject involved careful quality checks. It is important to mention that, since complete double support data were unavailable due to limitations in force plate coverage, the analysis concentrated on the single support phase. Therefore, when choosing the trial, it was essential that the stance foot was fully placed on a single force plate (to avoid mixing signals from both limbs). Furthermore, EMG quality was also a key factor - only signals showing clean activation, minimal noise and physiological amplitude ranges were considered. Finally, after going through all quality checks, the single support phase was defined from the moment the opposite foot lifted off to the moment it contacted the ground again.

To prepare EMG signals for musculoskeletal modeling, a custom Python pipeline was developed [88]. The processing involved four main steps: extracting the raw signals, filtering and cleaning them, generating the activation envelopes, and finally normalizing the amplitude. Raw EMG signals were first extracted directly from the .c3d files. Then, signal cleaning was carried out using the NeuroKit2 library, which offers a set of tools for processing physiological signals [89]. A standard EMG preprocessing

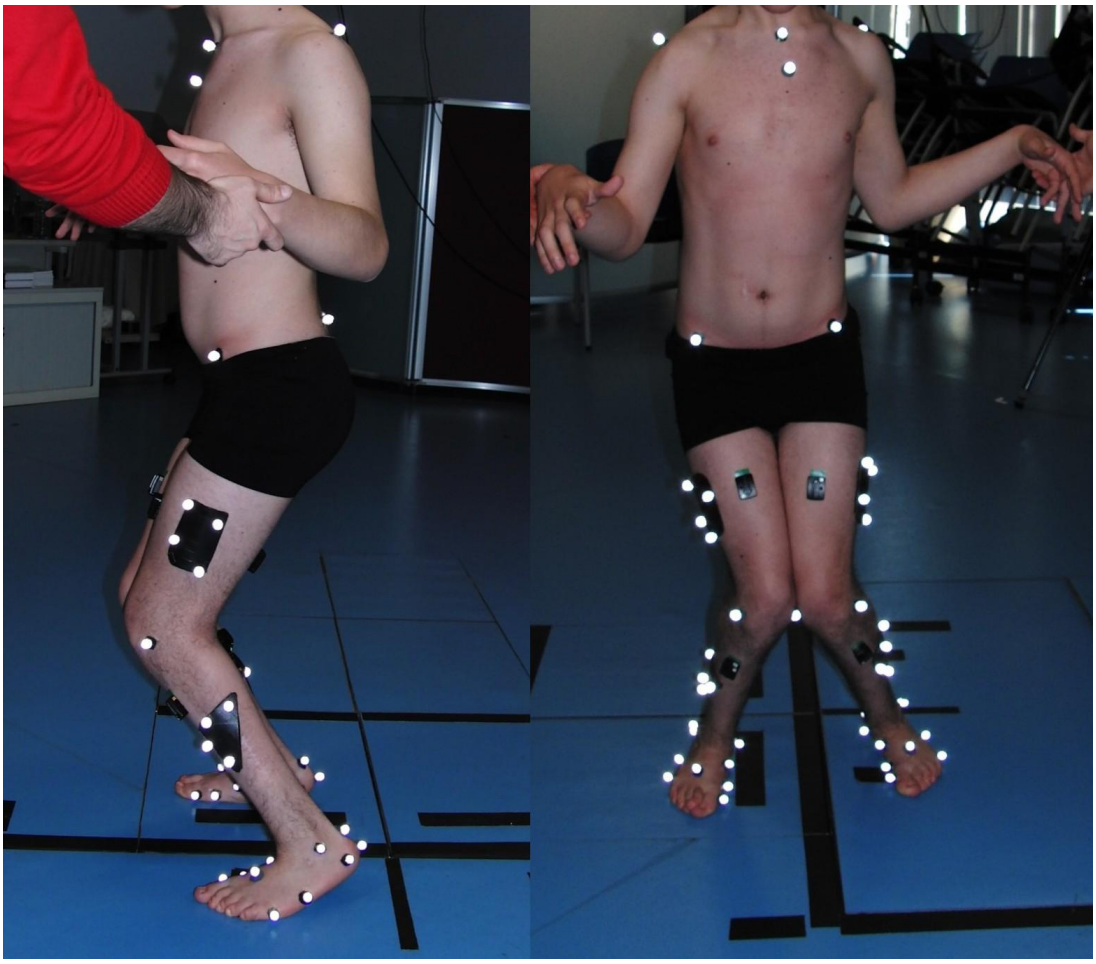

Figure 4.2: Sagittal (left) and frontal (right) views of a subject instrumented for gait analysis. Reflective markers are placed according to CAST (Calibrated Anatomical Systems Technique) protocol and CODA pelvis

pipeline was applied, consisting of a 100 Hz high-pass Butterworth filter (4th order) to remove motion artifacts and a constant detrending step to correct baseline fluctuations. After cleaning, each signal was rectified using NumPy by taking its absolute value [90]. To extract the muscle excitation envelope, a fourth-order low-pass Butterworth filter with a 6 Hz cutoff was applied. This was implemented using SciPy's signal processing module with a dual-pass zero-phase filtering method [91]. Finally, each muscle's envelope was normalised to the peak during the whole stance phase. The processed EMG signals were then visually examined and removed from further analysis if a noise-to-signal ratio was deemed too high or the signal was clipping, as exemplified in Figure 4.3. The EMG signals excluded were left tibialis anterior and right biceps femoris for CP003, right tibialis anterior for TD021 (simulated crouch gait) and right gastrocnemius for TD026 (simulated crouch gait).

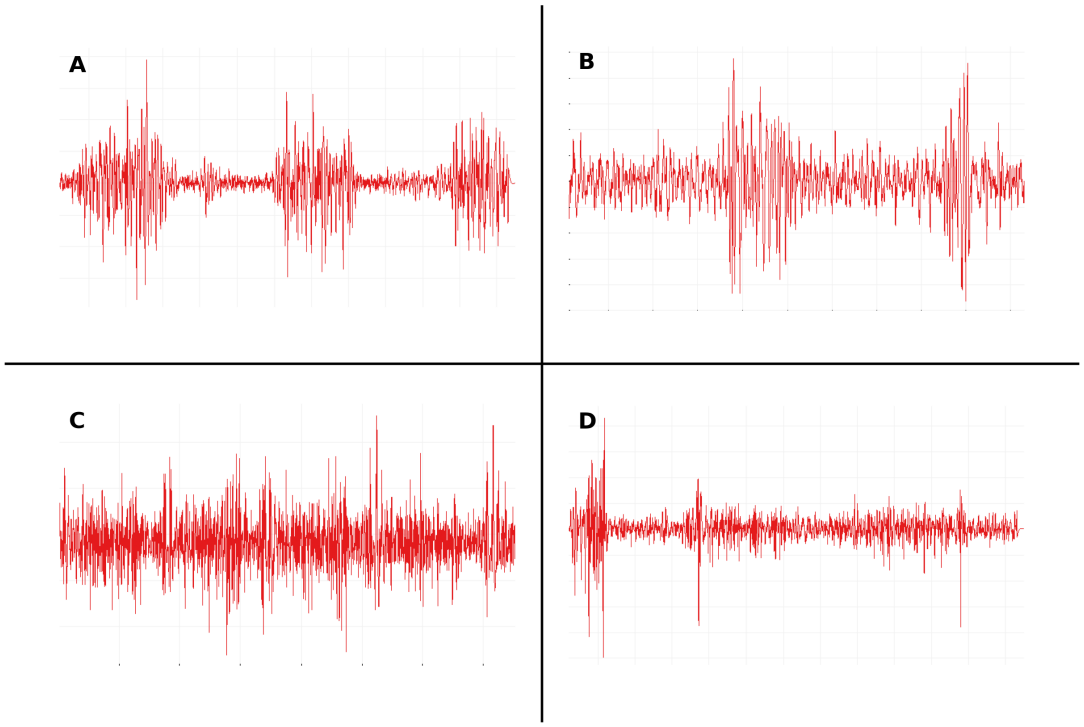

Figure 4.3: Representative EMG recordings: (A) high-quality signal suitable for analysis; (B) acceptable signal with moderate noise; (C) poor-quality signal with excessive noise and artifacts (not usable); and (D) low-quality signal dominated by artifacts (not usable). This layout follows the example in Akhundov et al. [12]

4.4 Visual 3D and OpenSim Implementation

In order to accomplish the objectives of this study, the musculoskeletal analysis was conducted utilizing a combination of Visual 3D, OpenSim, and CEINMS plugin tool for OpenSim.

Visual 3D is software used for data processing and rigid body dynamics (kinematics and kinetics). It has tools for signal processing, filtering, and executing Inverse Kinematics (IK) [92]. Visual 3D exports joint angles and synchronised ground reaction forces that can be imported in OpenSim.

In OpenSim, those same joint trajectories drive the musculoskeletal model, which is made up of rigid body parts connected by frictionless joints and moved by hill-type muscle actuators and perfect torque actuators [78]. These muscles extend across joints and produce both forces and movement.

4.4.1 Generic Musculoskeletal Model

The musculoskeletal model used in this work was the Gait2392 model, based on the models created by Delp et al. [13]. It contains 92 muscle-tendon actuators to represent 76 muscles in the lower extremities and torso. This model represents a subject that is about 1.8 m tall and has a mass of 75.16 kg.

The lower body of the Gait2392 model includes 11 segments: one pelvis, two femurs, two tibias, two taluses, two feet, and two toe bodies. For each leg, the foot segment includes the calcaneus, navicular, cuboid, cuneiforms, and metatarsals. Each of these segments has a fixed reference frame. Figure 4.4 represents the location and orientation of each reference frame.

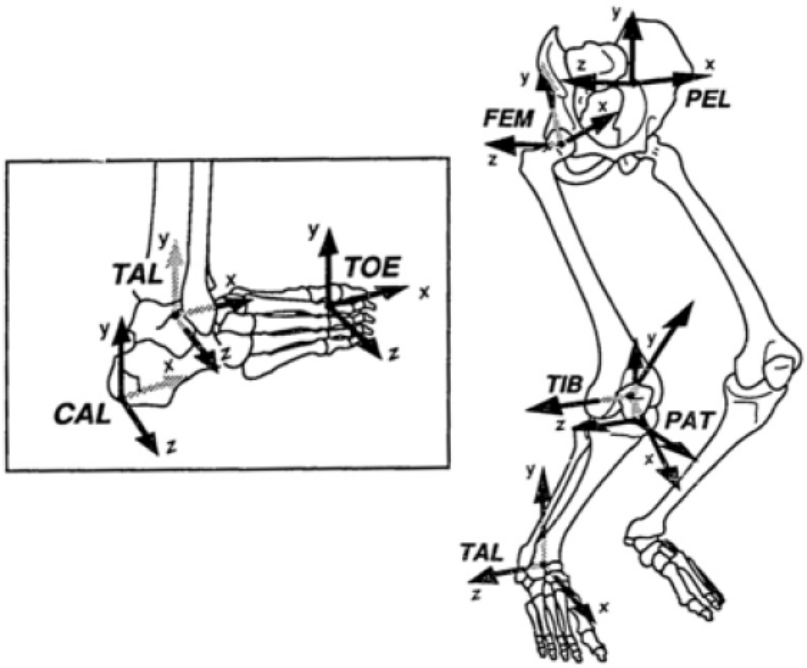

Figure 4.4: Location of the reference frames relative to the body segments. The reference frames are located in the femur (FEM), pelvis (PEL), tibia (TIB), patella (PAT), talus (TAL), toes (TOE), and calcaneus (CAL). Adapted from [13].

The Gait2392 model is one of the most widely used musculoskeletal templates in OpenSim. It comprises 23 kinematic degrees of freedom (DOFs) arranged as presented in Table 4.2.

Table 4.2: Twenty three degrees of freedom in the Gait2392 model

Segment	**Degrees of Freedom**	**DOF**
Pelvis	3 translations + 3 rotations	6
Hips (x2)	flexion/extension, abduction/adduction, internal/external rotation	6
Knees (x2)	flexion/extension only	2
Ankles ($\times$2)	plantarflexion/dorsiflexion, inversion/eversion	4
Subtalar joints ($\times$2)	inversion/eversion	2
Lumbar spine	flexion/extension, lateral bending, axial rotation	3
Total		**23**

The muscle-tendon actuators are defined by a series of line segments and connecting anatomically

defined origin and insertion landmarks. When some of the muscles wrap around bony structures, during the movement, additional wrapping points are inserted to more closely represent the physiological muscle path. However, even with the wrapping, some muscles may still intersect the bone geometry and produce non-physiological moment arms. Nevertheless, these muscle paths and wrapping points are able to accurately simulate walking dynamics, since gait involves only a relatively short range of motion.

4.4.2 Scaling

The first step in the musculoskeletal modeling pipeline was adjusting the generic OpenSim model to match each participant's body dimensions (Figure 4.5).This was done through a process called scaling. This tool allows for modification of the size and mass properties of each segment so that the model better represents the actual anatomy of the subject.

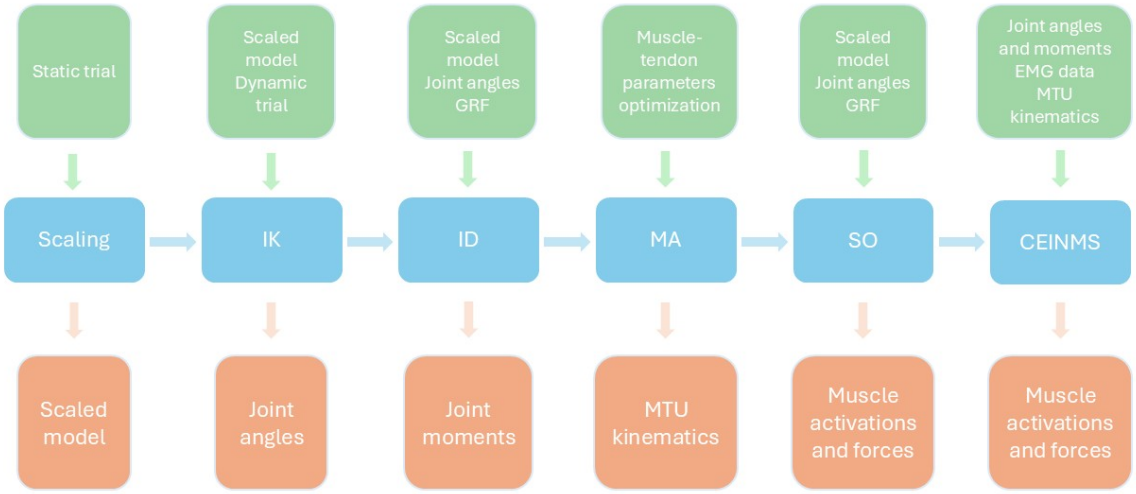

Figure 4.5: OpenSim's pipeline performed in this work, with tools used and their inputs and outputs. The blue color represents each tool used, in order from the first to the last. The green represents inputs necessary for each tool to run, and the orange represents their outputs. IK stands for Inverse Kinematics, ID for Inverse Dynamics, MA for Muscle Analysis, SO for Static Optimisation, while MTU stands for Musle-Tendon Units.

In this study, the manual approach for scaling was used. The scaling factors, defined as the ratios of each segment's measured inter-marker distances to the corresponding distances on the generic model, were obtained from marker data processed in Visual3D, and they were used to resize the model segments (Figure 4.6). Additionally, segment masses, Optimal Fiber Length (OFL) and Tendon Slack Length (TSL) were scaled linearly to participant's body mass and segment lengths.

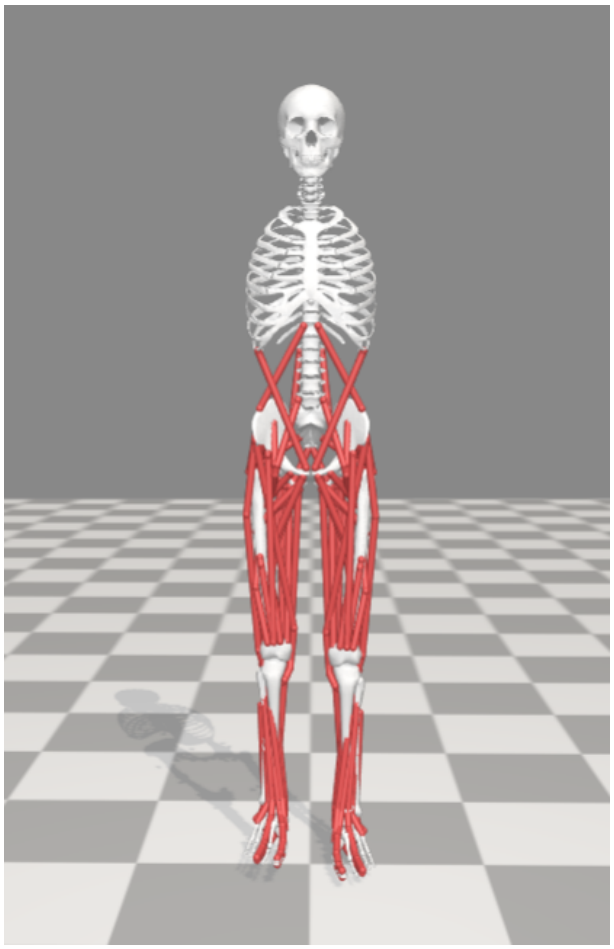

Figure 4.6: Scaled OpenSim Gait2392 model.

The last thing before running the simulations was to lock subtalar (preventing unreliable inversion/eversion) and metatarsophalangeal joints (preventing flexion/extension caused by small marker noise) in a neutral position. This is a common step when modeling gait, since the foot segments are small and light, and standard marker sets do not reliably capture the motion in a static trial. Thus, keeping these joints fixed helps avoid unrealistic forces in the model [93].

4.4.3 Inverse Kinematics and Inverse Dynamics

After scaling the model, joint angles and net internal moments were calculated. Joint angles were calculated using Visual3D. It applies a segment-optimization approach in its inverse kinematics: each body segment's position and orientation is estimated independently as a full six-degree-of-freedom rigid body. Next, joint moments were calculated using Inverse Dynamics (ID) Tool from OpenSim. ID computes net internal joint moments by solving the equations of motion:

$$M(q)\,\ddot{q} \;+\; C(q,\dot{q}) \;+\; G(q) \;=\; \boldsymbol{\tau} \tag{4.1}$$

where $q, \dot{q}, \ddot{q}$ represent the generalized positions, velocities, and accelerations, respectively; M is the mass matrix; C captures Coriolis and centrifugal forces; G represents gravitational loads; and τ are the resulting net joint torques. Before running ID, the joint angle data were filtered using a 6 Hz dual-pass Butterworth filter to reduce potential noise that can lead to unrealistic moments.

In order to evaluate IK results, OpenSim reports the total RMSE and maximum marker errors in the output messages. A general guideline says that the RMSE should be below 2 cm [94]. When it comes to ID results, it is suggested to compare them with the existing literature.

4.4.4 Muscle activation and muscle force calculation

To investigate muscle behaviour during the movement, the Muscle Analysis Tool was used. This tool calculates muscle parameters such as muscle-tendon lengths, moment arms, and muscle-specific variables such as fiber lengths and pennation angles, given a set of joint coordinates. After these parameters were calculated, the next step was to compute muscle activations and forces. This was done with two approaches.

The first approach was running SO. SO tool estimates muscle activations and forces while trying to satisfy joint moments of a given motion. SO calculates muscle forces by minimizing the sum of squared muscle activations. The SO algorithm computes the active force along a muscle's tendon, assuming a rigid tendon and neglecting the contributions of passive muscle forces [95]. In order to compute muscle activations and muscle forces, SO uses as input joint angles, GRF, and a set of actuator forces (where "actuator forces" refers to the set of muscle actuators and reserve actuators, the latter being idealized, low-strength ideal torque generators added to each degree of freedom to supply any small residual moments when muscles alone cannot fully reproduce the required joint loads), which together generate forces to reproduce the joint moments estimated through inverse dynamics. For the SO simulations, the Thelen's muscle model was used [75].

The second approach was using CEINMS in its EMG-informed mode, which proceeds in two main phases: Calibration and Execution [23].

Calibration phase

Firstly, CEINMS calibrates subject-specific muscle–tendon and activation parameters so that it reproduces the desired joint moments [23]. The experimental EMG linear envelopes $e_i(t)$ are mapped onto each model muscle and converted into muscle activations $a_i(t)$ via a two-stage excitation-activation model [24]:

1.

$$u_j(n) = \alpha\, e_j(t-d) - \beta_1\, u_j(n-1) - \beta_2\, u_j(n-2), \tag{4.2}$$

where $u_j(n)$ is neural activation at time index n, $e_j(t)$ is the filtered EMG of muscle j at time t, α is the gain coefficient, β_1 and β_2 are recursive coefficients defined by $\beta_1 = C_1 + C_2$ and $\beta_2 = C_1\, C_2$, with $|C_1| < 1$ and $|C_2| < 1$, and d is the electromechanical delay (0.015 s).

2.

$$a_i(n) = \frac{e^{A_i\, u_i(n)} - 1}{e^{A_i} - 1}, \tag{4.3}$$

with $A_i \in (-3, 0)$ the nonlinear shape factor.

These activations $ai(n)$ then drive a Hill-type muscle–tendon model (force-length, force-velocity, and tendon force-strain relationships) to compute each muscle's force.

Using a simulated-annealing optimizer [96], each muscle's OFL, TSL, maximum isometric force, and EMG gain α_i are adjusted to fit physiological bounds. It varies these parameters within predefined boundaries to minimize the sum of the RMSE between predicted and experimental joint moments. The simulated-annealing optimizer begins with an initial temperature (T) that allows both improvements and occasional degradations. Then, it gradually lowers the temperature so that only improvements are accepted, until it finds the best muscle-tendon and activation values for each subject. In order to find the best T, several different values were tested (see Figures A.3–A.6 in Appendix A). By changing the T value, the muscle forces did not change much, but the muscle activation patterns varied a lot. After comparing all the results by calculating R^2, it was decided to use $T = 2{,}000{,}000$, as it gave the best fit to the EMG data in terms of muscle activations. All the parameters and their ranges allowed are presented in Table 4.3.

Table 4.3: Calibration parameters and imposed bounds in CEINMS

Parameter	Symbol	Lower bound	Upper bound
Activation shape factor	A_i	-2.999	-0.001
EMG–activation gain	C_1	-0.95	-0.05
EMG–activation offset	C_2	-0.95	-0.05
Tendon slack length (TSL)	TSL	$0.85 \times \mathrm{TSL}_{\mathrm{orig}}$	$1.15 \times \mathrm{TSL}_{\mathrm{orig}}$
Optimal fiber length (OFL)	OFL	$0.85 \times \mathrm{OFL}_{\mathrm{orig}}$	$1.15 \times \mathrm{OFL}_{\mathrm{orig}}$
Strength coefficient	γ	$0.8 \times F_{\mathrm{iso,orig}}$	$2.0 \times F_{\mathrm{iso,orig}}$

During the calibration process, the TSL and the OFL were allowed a $\pm$15% variation. CP children have overstretched sarcomeres present in contracted muscles [97]. An increase in sarcomere length leads to fewer sarcomeres in series; thus, a smaller OFL value. Therefore, for all CP participants, the initial OFL values were reduced by 0.7 to simulate the effect of an overstretched sarcomere [33].

Execution phase

Finally, CEINMS finds the best compromise between matching the net joint moments and staying close to the EMG-derived excitations by minimizing the following objective function:

$$F = \alpha\, E^2_{\mathrm{trackMOM}} + \beta\, E^2_{\mathrm{sumEXC}} + \gamma\, E^2_{\mathrm{trackEMG}}, \tag{4.4}$$

where E^2_{trackMOM} is the sum of squared differences between predicted and experimental joint moments; E^2_{sumEXC} is the sum of squared excitations for all musculotendon units and E^2_{trackEMG} is the sum of the squared differences between the experimental excitations (EMG linear envelopes) and the adjusted model excitations. α, β and γ are positive weighting factors. In this study, the values of these weighting factors were set to 1, 10, and 15, respectively, following the results from Sartori et al. [25]. These values were selected based on balancing the trade-off between EMG-excitation tracking error ($E_{\mathrm{trackEMG^2}}$) and joint moment tracking error ($E_{\mathrm{trackMOM^2}}$), as described in their study. Force-length, force-velocity, and tendon force-strain relationships were according to Millard et al. [76]. .

4.5 Data Analysis

All estimates (joint angles, moments, muscle activations and forces) were normalised to the single-leg support phase duration. Additionally, joint moments and muscle forces were amplitude-normalised to the body weight. Joint angles.moments and muscle forces were presented as mean values with 95% confidence intervals. For the validation of muscle activations and joint moments, RMSE, the R^2, and Standard Deviation (SD) were used. The performance of SO and CEINMS in predicting muscle activations was evaluated with EMG data, while joint moment predictions were verified against ID results.

To allow CEINMS outputs to syncronize with EMG recordings, the first three frames of each trial (equivalent to twice the electromechanical delay) were excluded from all activation plots. Figure A.1 in the Appendix A illustrates how including versus excluding those frames affected the results.

5

Results and Discussion

Contents

5.1 Joint kinematics and joint moments

Hip flexion, knee flexion, and ankle dorsiflexion joint angles and moments, which characterize crouch gait in the sagittal plane, are presented in Figures 5.1 and 5.2. The results for the CP children are provided individually, while the simulated crouch and unimpaired gait results are displayed as a shaded SD, due to greater data consistency. All the results were compared to the published reference data for the 10–50% interval of the gait cycle, which represents the single-leg support phase.

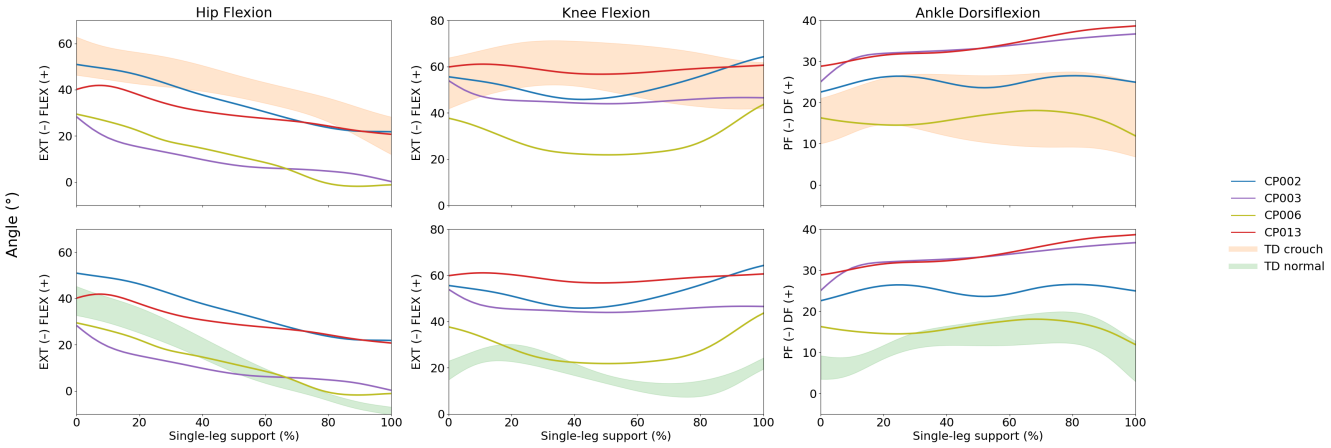

Figure 5.1: Hip, knee, and ankle flexion angles during simulated and real crouch gait, and unimpaired gait. The shaded area represents the SD for the TD groups. The top row compares CP children with TD crouch group, while the bottom row compares the same CP participants against the TD normal group. "TD crouch" represents TD children simulating crouch gait, while "TD normal" represents normal walking of TD children.

All CP subjects show more flexion in all joints during the single-leg support phase than the TD normal group (Figure 5.1). Additionally, Steele [32] observed that the biggest difference between the levels of severity in crouch gait is seen in the knee flexion angles, which was also the case in this study - CP002 and CP013 (severe crouch gait) have higher knee extension angles compared to CP003 and CP006 which have moderate and mild crouch gait, respectively.

Pathological and normal walking patterns are clearly distinguished in the knee flexion plot. Every CP patient has consistent and too much knee flexion. This pattern is typical of spastic diplegic CP and reflects crouch gait [16]. Additionally, they exhibit too much dorsiflexion, which would point to either compensatory mechanisms to keep stability during stance or plantarflexor weakness. The TD crouch group shows that the simulated crouch trials well reproduce the joint mechanics seen in CP children.

Regarding joint moments, CP006 shows moment patterns more like the TD normal gait group (compared with other CP children), suggesting less severe crouch gait. On the other hand, CP013 and CP003 keep high knee extension moments for the majority of the stance phase. This suggests that more quadri-

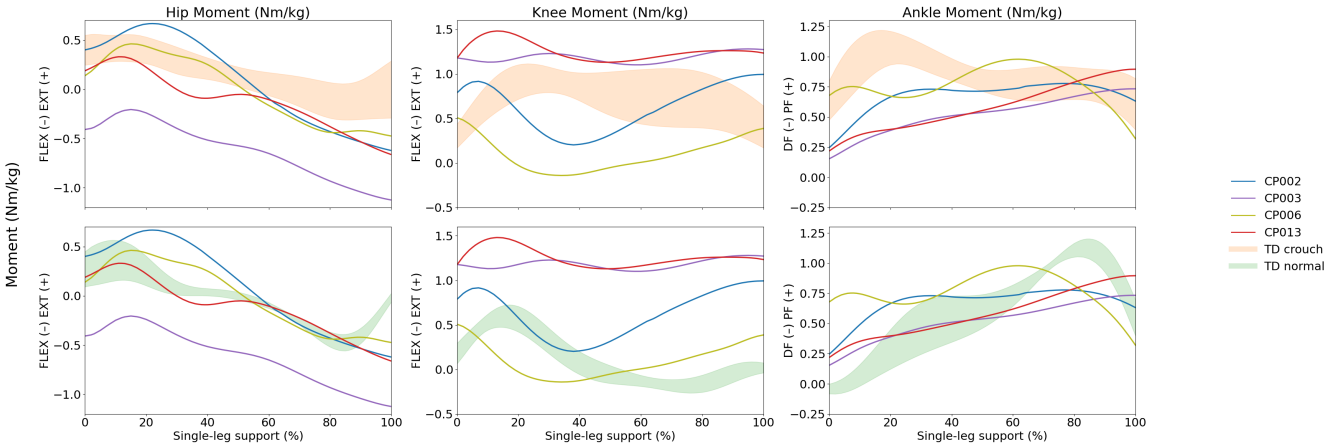

Figure 5.2: Hip, knee, and ankle flexion moments (normalized to body weight) during simulated and real crouch gait, and unimpaired gait. The shaded area represents the SD for the TD groups. The top row compares CP children with TD crouch group, while the bottom row compares the same CP participants against the TD normal group. "TD crouch" represents TD children simulating crouch gait, while "TD normal" represents normal walking of TD children.

ceps action is needed to stabilize the flexed knee posture unique to crouch gait - an outcome Steele et al. [32] also reported for moderate and severe crouch groups. Ankle moments were characterized by a typical plantarflexor moment rise in TD normal participants during late stance, corresponding to the push-off part of stance. The CP children have more flattened profiles and lower peaks, suggesting less ankle power output. Hicks et al. [31] similarly demonstrated that crouch posture reduces and delays peak plantarflexor capacity.

The TD children simulating crouch gait successfully reproduced the primary kinetic characteristics of the crouch pattern: increased hip and knee flexion and ankle dorsiflexion compared to normal gait. These observations align with the previous study conducted by Rezgui et al. [98], who found that healthy adults could voluntarily adopt a crouched gait, by reproducing the main saggital-plane deviations. However, they were not able to simulate it perfectly. Additionally, the greater ankle dorsiflexion was also reported by Balzer et al. [35], who induced a 40° knee flexion contracture in healthy children. She reported that the foot tended to compensate for an artificial knee flexion contracture with an increase in dorsiflexion. Steele et al. [99] noted that in the crouch gait, the same key muscles that give support in normal gait must remain active throughout the single-leg stance, rather than working on and off as they do in healthy children. This finding supports the results obtained as TD crouch group sustained quadriceps activations to prevent knee collapse. Although TD children were not able to mimick spastic co-contractions, they still highlight the differences from natural gait.

5.2 Muscle force verification

To quantify the prediction accuracy of SO and CEINMS across all subjects and groups, the R^2 and RMSE were computed between EMG and predicted activations, and between ID joints moments and estimated joint moments (Fig. 5.3).

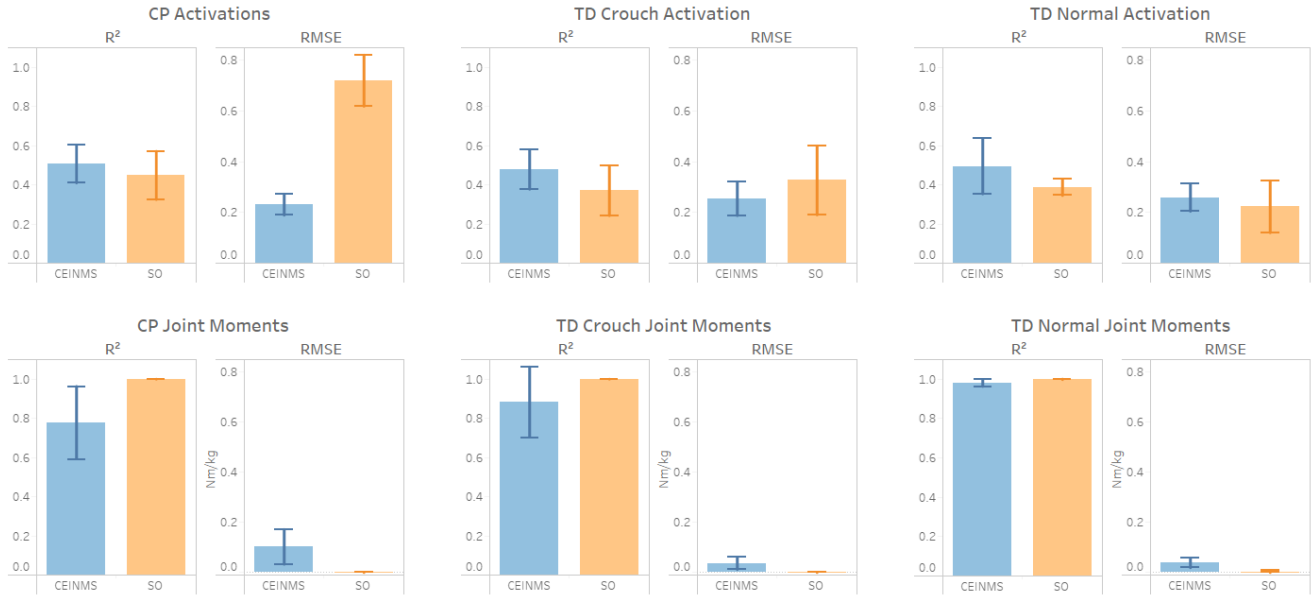

Figure 5.3: Quantitative comparison of SO and CEINMS in predicting muscle activations (top row) and joint moments (bottom row) across CP, TD crouch, and TD normal groups. Bars represent the mean R^2 and RMSE values, with error bars indicating standard deviation across trials. CEINMS is presented in blue colour, while SO is presented in orange colour

In terms of muscle activation tracking, CEINMS consistently outperformed SO across all groups. This was particularly evident in the CP group, where CEINMS improved R^2 values between predicted and measured EMG activation patterns from roughly 0.3–0.4 (SO) to around 0.6, indicating a better fit to the true muscle activation timing. Likewise, the RMSE between predicted and experimental EMG envelopes was about half that of the SO approach (Figure 5.3). These results align with the literature: SO showed poor agreement with EMG-derived activations in CP gait, whereas including EMG data (after model calibration) increased the correlation with experimental EMG [22]. Veerkamp et al. reported that the calibrated EMG-informed approach in CP children achieved significantly higher R^2 with respect to SO. They concluded that SO is not adequate to estimate musculotendon forces in CP" and that calibrated EMG-informed provides a better representation of muscle activations [22]. In TD groups, CEINMS also performed better than SO, although the difference between the two is not as significant as for CP children. It still achieved the higher R^2 values (0.5 vs 0.35), lower RMSE values for TD crouch group, but higher for TD normal group.

Regarding joint moment tracking, both CEINMS and SO demonstrated high performance, with R^2 values approaching 1 and very low RMSE across all groups. In the TD crouch and TD normal groups, both methods achieved almost identical tracking performance; however for CP children, CEINMS achieved slightly lower joint moment agreement - around 0.8. This reduced performance may be linked to the way CEINMS balances minimizing muscle activation costs with tracking experimental data [23]. The model can permit a small amount of joint moment error in exchange for capturing physiologically observed activations.

Figures 5.4 and 5.5 present the predicted muscle activations from CEINMS and SO, together with the corresponding EMG signals, for two subjects: one child with CP (CP013) and one TD child performing crouch gait (TD006). These subjects were chosen to exemplify typical results; data for all participants are available on the GitHub repository [88]. CEINMS performed better in terms of matching EMG data compared to SO, both in the activation timing and magnitude. The high, constantly active muscles in CP013 suggest an increased muscle tone or spastic activity. The SO predictions were less responsive in changes in muscle activity throughout the single-leg support phase. For the TD006, SO tended to produce smooth or minimal muscle activation profiles that often missed the timing of peak muscle activity seen in EMG. In conclusion, these subject-specific examples reinforce the group-level findings, emphasizing that CEINMS is more capable of capturing individual neuromuscular activation, especially in pathological gait [22]. The predicted muscle activations and joint moments for each participant can be found in the GitHub repository [88].

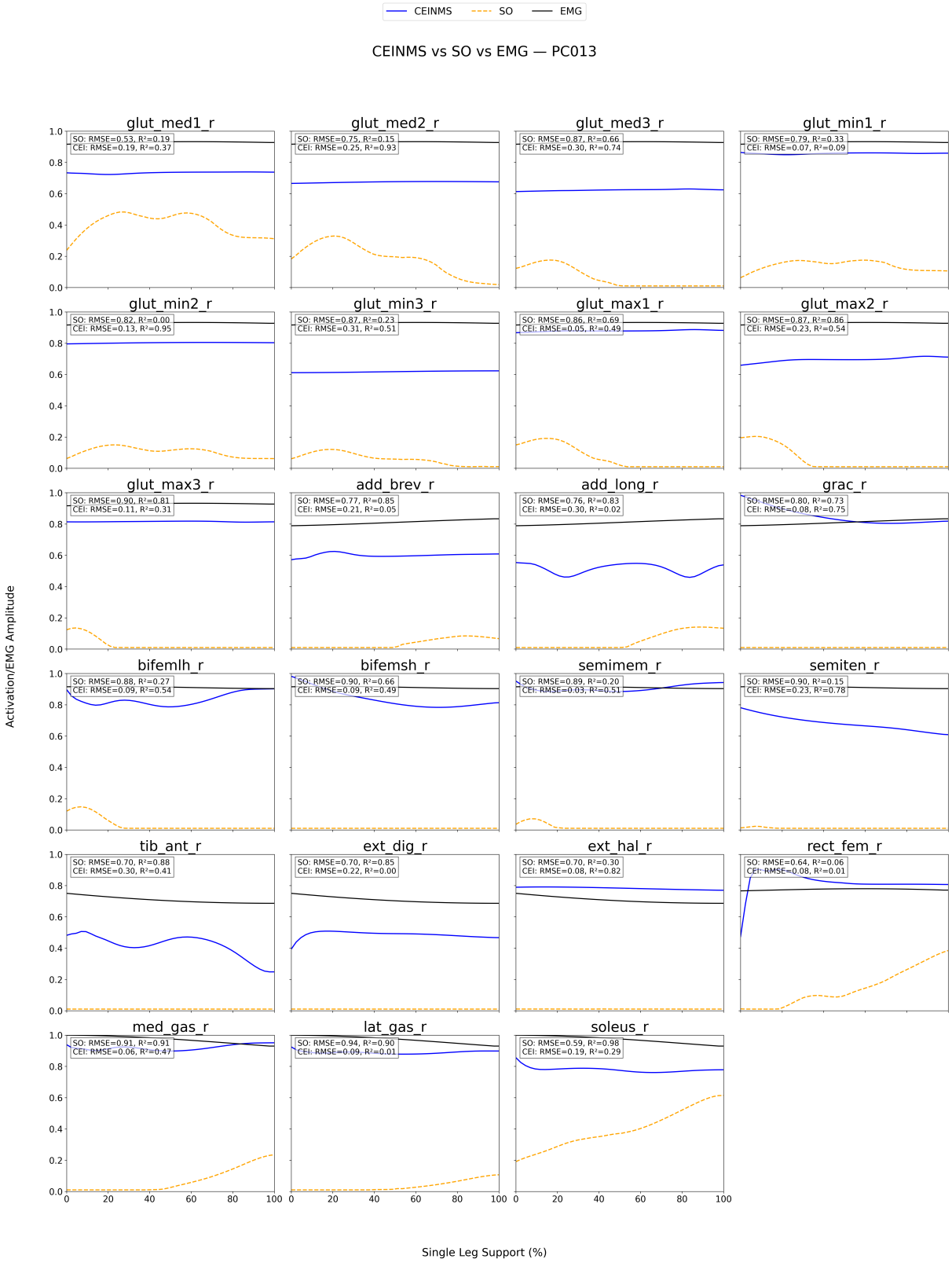

Figure 5.4: Muscle activations for the CP participant (PC013), predicted using Static Optimization (SO) and CEINMS, compared to EMG signals. **Abbreviations:** `glut_med` = gluteus medius; `glut_min` = gluteus minimus; `glut_max` = gluteus maximus; `add_brev`/`add_long` = adductor brevis/longus; `grac` = gracilis; `bifemlh`/`bifemsh` = biceps femoris long/short head; `semi_mem`/`semi_ten` = semimembranosus/tendinosus; `tib_ant` = tibialis anterior; `ext_dig`/`ext_hal` = extensor digitorum/hallucis; `rect_fem` = rectus femoris; `med_gas`/`lat_gas` = medial/lateral gastrocnemius; `soleus` = soleus.

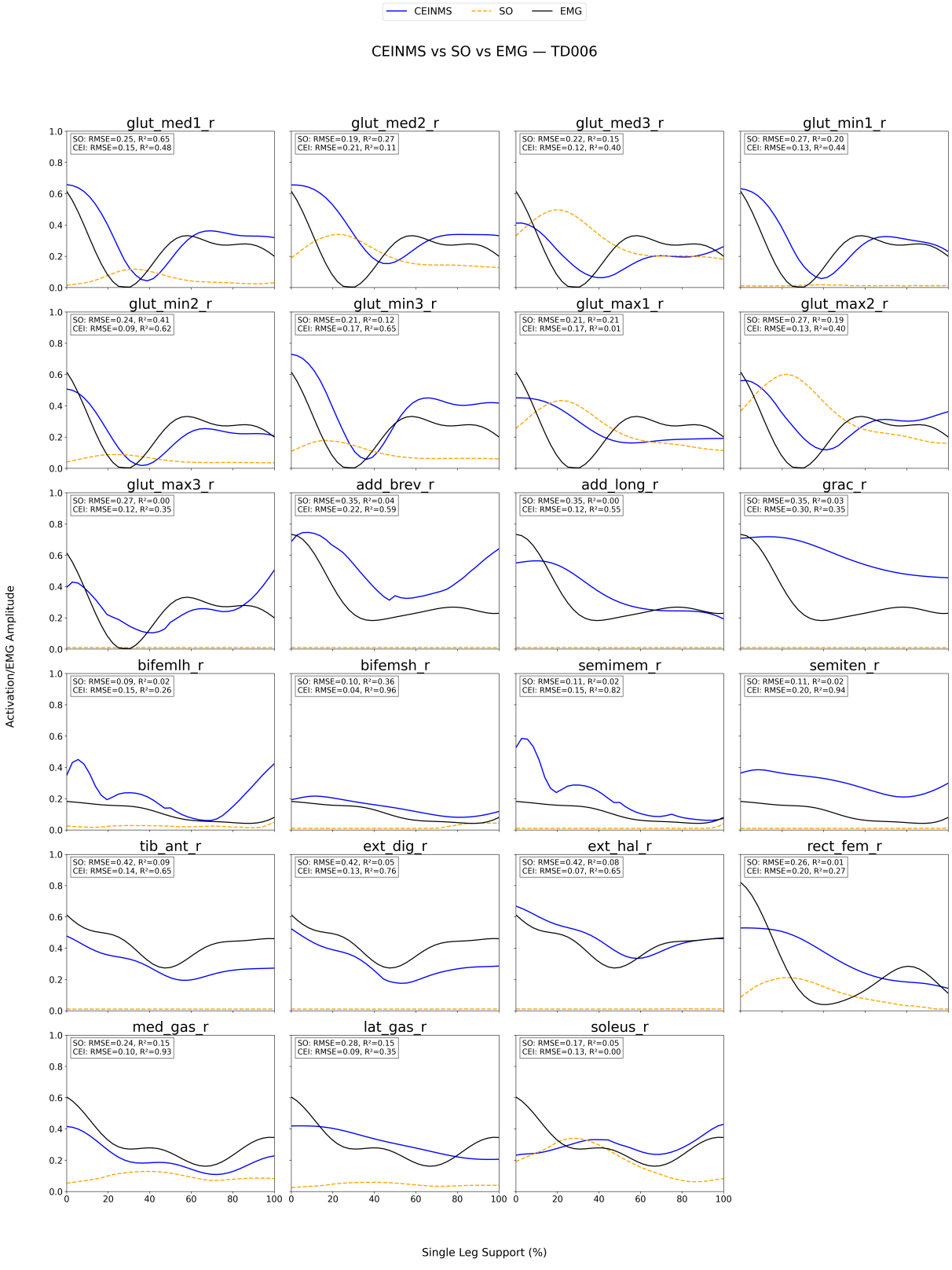

Figure 5.5: Muscle activations for the CP participant (PC013), predicted using Static Optimization (SO) and CEINMS, compared to EMG signals. **Abbreviations:** `glut_med` = gluteus medius; `glut_min` = gluteus minimus; `glut_max` = gluteus maximus; `add_brev`/`add_long` = adductor brevis/longus; `grac` = gracilis; `bifemlh`/`bifemsh` = biceps femoris long/short head; `semi_mem`/`semi_ten` = semimembranosus/tendinosus; `tib_ant` = tibialis anterior; `ext_dig`/`ext_hal` = extensor digitorum/hallucis; `rect_fem` = rectus femoris; `med_gas`/`lat_gas` = medial/lateral gastrocnemius; `soleus` = soleus.

Figure 5.6 represents joint moments calculated by CEINMS and SO, compared to ID, for the subjects shown in Figure 5.4 and Figure 5.5. In terms of the hip and ankle joints both methods show almost perfect fitting, with lower performance from CEINMS for the knee joint, for both subjects. As mentioned before, SO is intended to exactly match the net joint moments generated via ID.

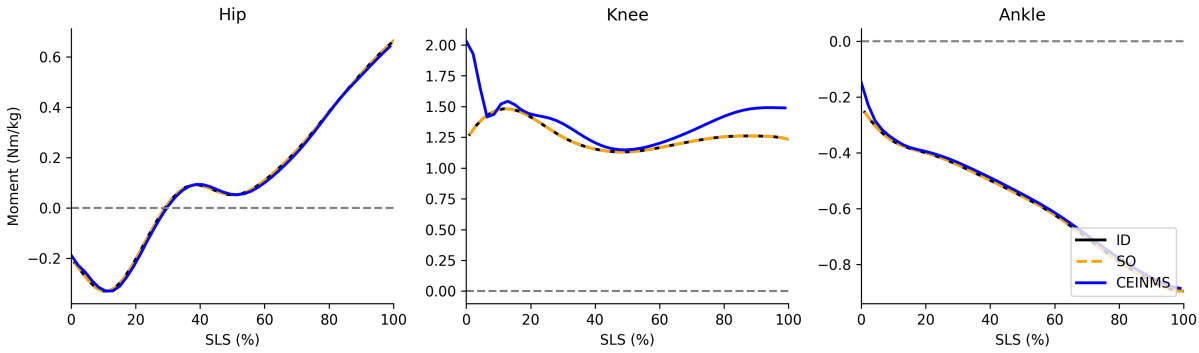

(a) Joint moments – CP013

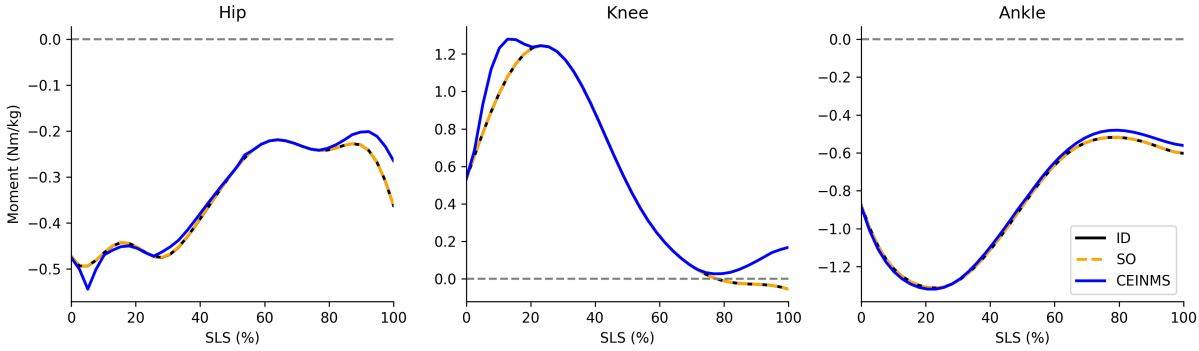

(b) Joint moments – TD006 (crouch)

Figure 5.6: Joint moment predictions using Static Optimization (SO) and CEINMS compared to inverse dynamics for the CP013 and TD006 (crouch gait) subjects.

A standard procedure with EMG is to normalise data with MVC to express activation as a percentage of maximum activation and to enable fair comparison across muscles or subjects. However, due to physical limitations of CP children, EMGs were normalised by the individuals' highest values measured during the trials [22] [33] [25]. EMG is extremely valuable for its timing information and relative magnitude patterns. Normalisation primarily affects the amplitude (y-axis scaling) of EMG signals and not their shape or timing. R^2 is sensitive mostly to the pattern of the signal over the gait cycle, not its absolute value. Thus, the higher R^2 observed for CEINMS vs EMG (compared to SO vs EMG) is indicative of better temporal agreement and pattern matching. This is something unaffected by whether the EMG was normalized to MVC or simply to its own peak.

A common concern with EMG-informed models is that by adding EMG data into the simulation CEINMS is simply reproducing the input signals. However, in the EMG-informed mode used here, EMG signals are converted into muscle excitations via equation 4.2, excitations are converted to activations via equation 4.3, and final activations are adjusted by a weighting factor in equation 4.4. Furthermore, the model must satisfy the activation dynamics and muscle properties, such as force-length and force-velocity relationships. As a result, the output is influenced by EMG but also by the model's constraints [23]. On the other hand, SO tries to simply minimise muscle effort by minimising the sum of activations squared, which for CP children is hardly the case. In conclusion, SO can ignore co-contractions present in CP children, while EMG-informed model is more likely to take them into account [22, 33].

5.3 Muscle force comparison between the groups

Since CEINMS provided better agreement with experimental EMG data and produced more physiologically plausible muscle activations, all muscle force analyses were based on CEINMS-derived estimates. These forces were standardized to body mass and averaged across the groups.

Figure 5.7 shows the mean muscle force profiles, with SD shaded area, during the single-leg support phase for three participant groups. Forces are grouped functionally into six categories: hip extensors and flexors, knee extensors and flexors, and ankle plantarflexors and dorsiflexors. The classification was based on anatomical function and follows the grouping of individual muscles provided by the OpenSim musculoskeletal model Gait2392 (Table 5.1).

Table 5.1: Functional grouping of muscles based on anatomical role and OpenSim Gait2392 model

Muscle Group	Included Muscles
Hip extensors	Adductor longus, adductor magnus (1–3 segments), biceps femoris long head, gluteus maximus (1–3), gluteus medius (posterior part), gluteus minimus (posterior part), semimembranosus, semitendinosus
Hip flexors	Adductor brevis, adductor longus, gluteus medius (anterior part), gluteus minimus (anterior part), gracilis, iliacus, pectineus, psoas, rectus femoris, sartorius, tensor fasciae latae
Knee extensors	Rectus femoris, vastus intermedius, vastus lateralis, vastus medialis
Knee flexors	Biceps femoris long head, biceps femoris short head, gracilis, gastrocnemius (medial and lateral heads), sartorius, semimembranosus, semitendinosus
Ankle plantarflexors	Flexor digitorum longus, flexor hallucis longus, gastrocnemius (medial and lateral), peroneus brevis, peroneus longus, soleus, tibialis posterior
Ankle dorsiflexors	Extensor digitorum longus, extensor hallucis longus, peroneus tertius, tibialis anterior

Across all muscle groups, CP children generated significantly higher muscle forces compared to both TD groups. This trend was especially evident in the knee extensors, where CP subjects showed peak forces surpassing 30 N/kg, while both TD groups remained below 15 N/kg. The estimated muscle forces indicate higher muscle demand or co-contractions in CP children, which aligns with findings reported in previous studies [31, 32].

When it comes to TD crouch group, it generally showed values higher than TD normal group, but lower than CP. This indicates an increased effort which is required to sustain crouch posture. Furthermore, the ankle plantarflexors in TD crouch group was almost double of the TD normal group, which is consistent with the increased ankle demand in crouch gait. For the other muscle groups, TD crouch values were slightly higher from TD normal group.

These results suggest that CP children experience significantly higher muscle forces during single leg support, likely due to the altered motor control strategies, compensation for joint instability, or due to spasticity. Although TD crouch group showed higher loading forces compared to TD normal, they adopted crouch gait with preserved motor coordination, while CP children often rely on simultaneous activations of antagonistic muscle groups to maintain joint stability and compensate for poor motor control. Steele et al. [100] found soleus and vasti are the primary contributors to supporting body weight in crouch gait, but because of this posture, they end up working simultaneously rather than sequentially. It can be seen in Figure 5.7 that knee extensors and ankle plantarflexors remain highly active throughout the entire single-leg support phase in CP children. In contrast, in the TD normal group, knee extensors are primarily active during the initial part of the phase, while ankle plantarflexors show greater activation toward the end, contributing to a more efficient gait pattern. While TD crouch group had higher muscle forces compared with TD normal, they still had similar patterns to TD normal group (muscles turning on and off appropriately), which is consistent with Rezgui et al. [98] findings that healthy subjects cannot capture pathological activation patterns.

Given that the CP group exhibited considerably wider variability compared to TD children, particularly in knee extensors, Figure 5.8 was plotted to investigate further the individual differences among the CP children. The TD crouch group was included for reference.

The CP subjects with higher functional impairment (GMFCS III) showed the largest, most prolonged hip extensor forces, suggesting a compensatory strategy to use the gluteus maximus and hamstrings continuously for stability. This finding is consistent with the study by Steele et al. [99]. Additionally, subject CP013 generated the highest forces across knee muscle groups, with knee extensor forces exceeding 30 N/kg throughout the single-leg support phase, approximately double the peak forces ob-

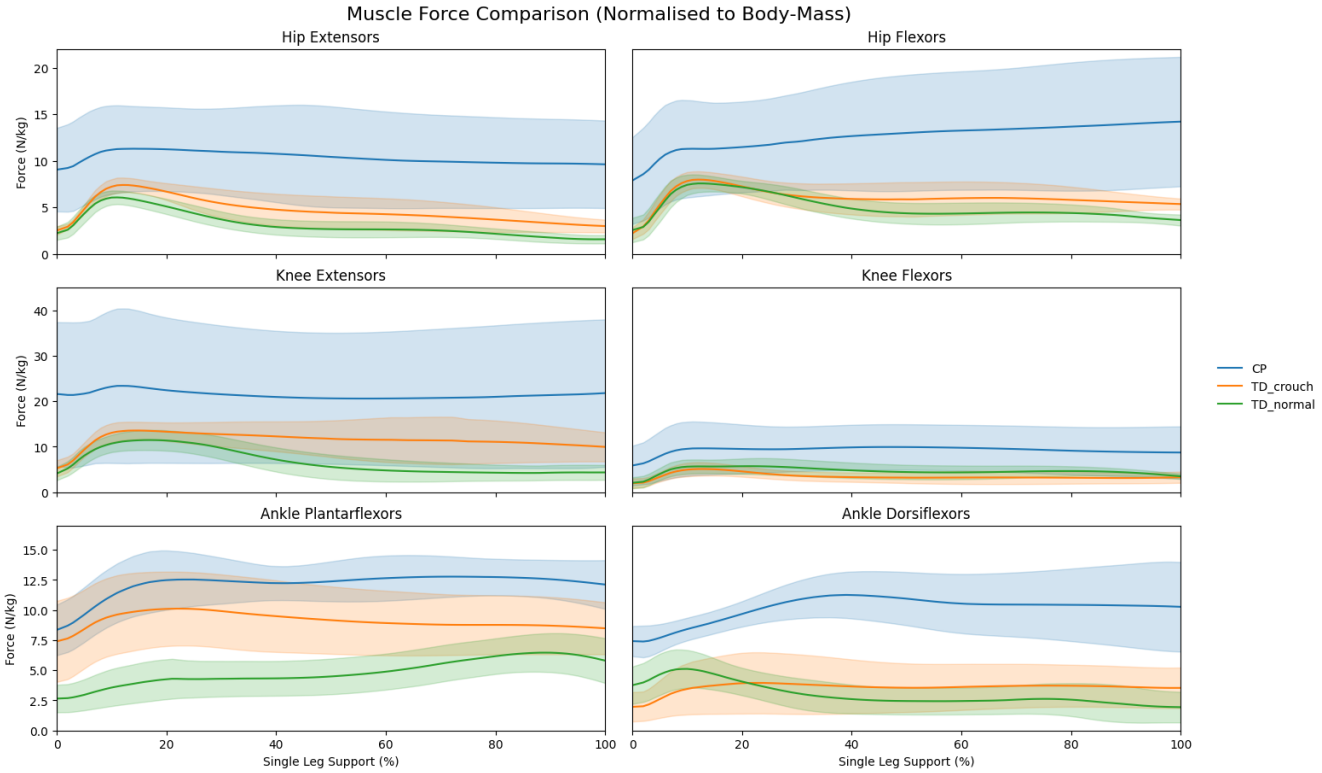

Figure 5.7: The mean muscle force profiles, normalized to body mass, for the CP children (CP group), TD simulating crouch gait (TD crouch group), and TD walking normally (TD normal group) across the single-leg support phase. Forces are organized by functional groups: hip extensors/flexors, knee extensors/flexors, and ankle plantarflexors/dorsiflexors.

served in both the TD crouch group and CP006. This difference in force magnitude between CP006 and CP013 is consistent with their respective GMFCS levels (I and III), reflecting differences in motor function severity [32]. On the other hand, CP006 demonstrated the highest forces in the ankle dorsiflexor and plantarflexor groups, while CP013 remained within the same range as those observed in the TD crouch group. This likely emphasizes co-contractions present in the ankle muscles of CP006 (The muscle activations for this subject can be seen in the Appendix A). Looking at CP002 and CP003, it can be noticed that they exhibit intermediate force profiles between CP006 and CP013 in most muscle groups, with CP002 having a slightly higher force profile to CP003. This pattern supports a graded relationship between clinical severity and biomechanical demands experienced during gait. Another difference can be noted in the timing of peak muscle forces. While the TD crouch group has early peaks, the CP participants tend to maintain high forces throughout the single-leg support phase with flatter peaks. This can be a consequence of the compensatory strategies to stabilize posture.

Although Figure 5.7 shows that ankle forces in CP were higher than in TD crouch, it can be seen in Figure 5.8 that CP013 had lower ankle plantarflexor forces than TD crouch group. The literature confirms

that the weakness of the calf muscles is the major contributor to crouch gait. When the calf muscles are weak, they cannot properly help extend the knee through plantarflexion, so the knee tends to collapse into a bent position even if the person tries to remain upright [101].

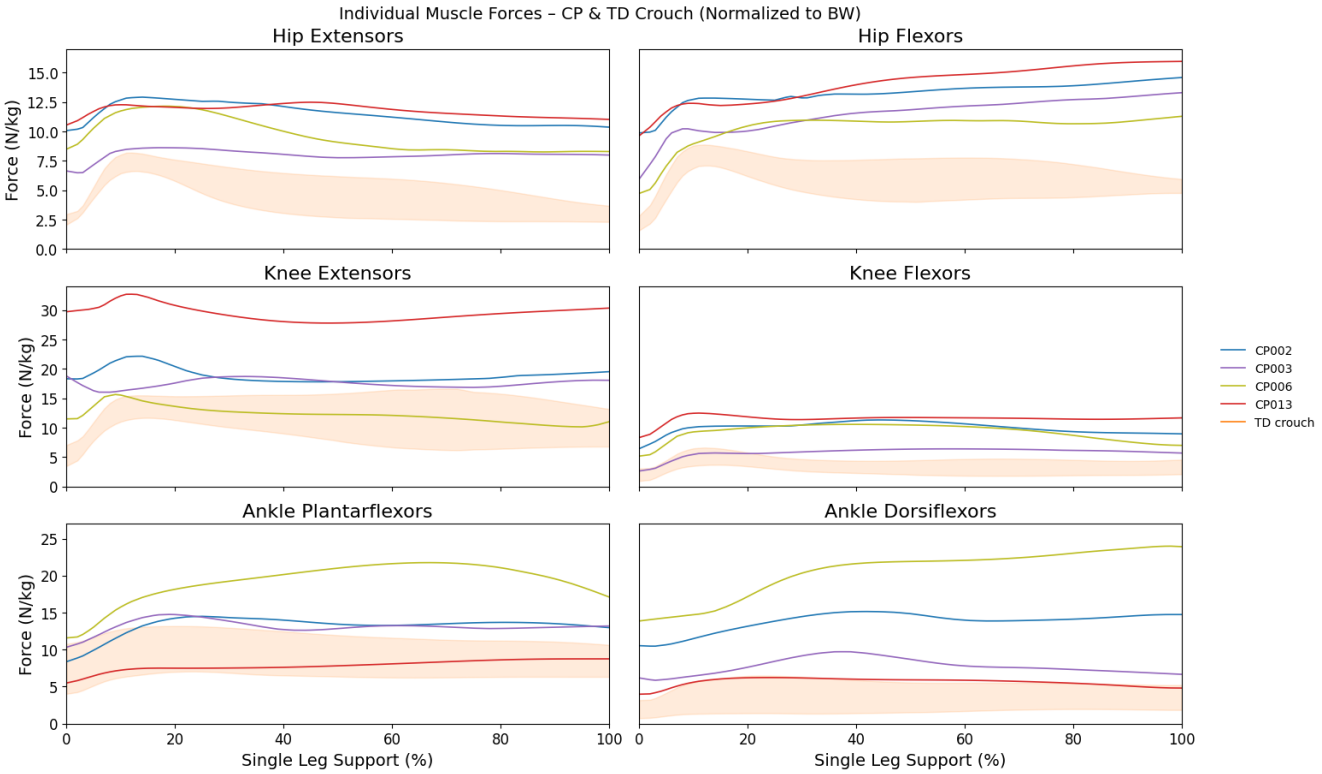

Figure 5.8: The individual muscle force profiles for each CP subject alongside the group mean of the TD children simulating crouch gait (TD crouch), normalized to body mass. GMFCS levels for children with cerebral palsy: CP002 – Level III, CP003 – Level II, CP006 – Level I, and CP013 – Level III.

To better visualize and compare the overall magnitude of muscle forces across the groups, Figure 5.9 represents the mean forces for TD groups, with the SD, and individual forces for CP children. CP children exhibit higher forces across all muscle groups compared to both TD groups. The knee extensors show the largest difference. The TD crouch group showed higher muscle forces compared to TD normal in hip extensors, knee extensors, and ankle plantarflexors. Furthermore, this bar chart can help to identify how different muscle groups are affected in children with CP. For example, CP006 shows higher forces in the ankle muscles, which may suggest strong distal compensation. On the other hand, CP013 (GMFCS Level III) shows much higher forces in the hip and knee muscles, suggesting a greater dependence on proximal muscles to support walking. These observations can help in improving rehabilitation strategies.

Although increased hip flexion and knee extensor activity, characteristics of crouch gait, were observed in this study, ankle plantarflexor forces were higher than expected. This contrasts with previous

literature, which typically reports a reduced contribution from the plantarflexors in crouch gait [101]. Nevertheless, the TD crouch trials managed to demonstrate the pure biomechanical effect of walking with flexed hips and knees with an otherwise normal neuromuscular system. The differences observed between TD normal and TD crouch groups reflect the consequences of adopting a crouched gait posture. On the other hand, the differences between TD crouch and CP children reflect the impact of neurological impairments due to cerebral palsy, such as spasticity, compensatory movements, or poor selective motor control, as their muscle patterns went well beyond a simple crouch compensation. Together, these comparisons aid in the differentiation between primary gait deviations associated with neurological disorders and secondary deviations resulting from compensatory body mechanisms.

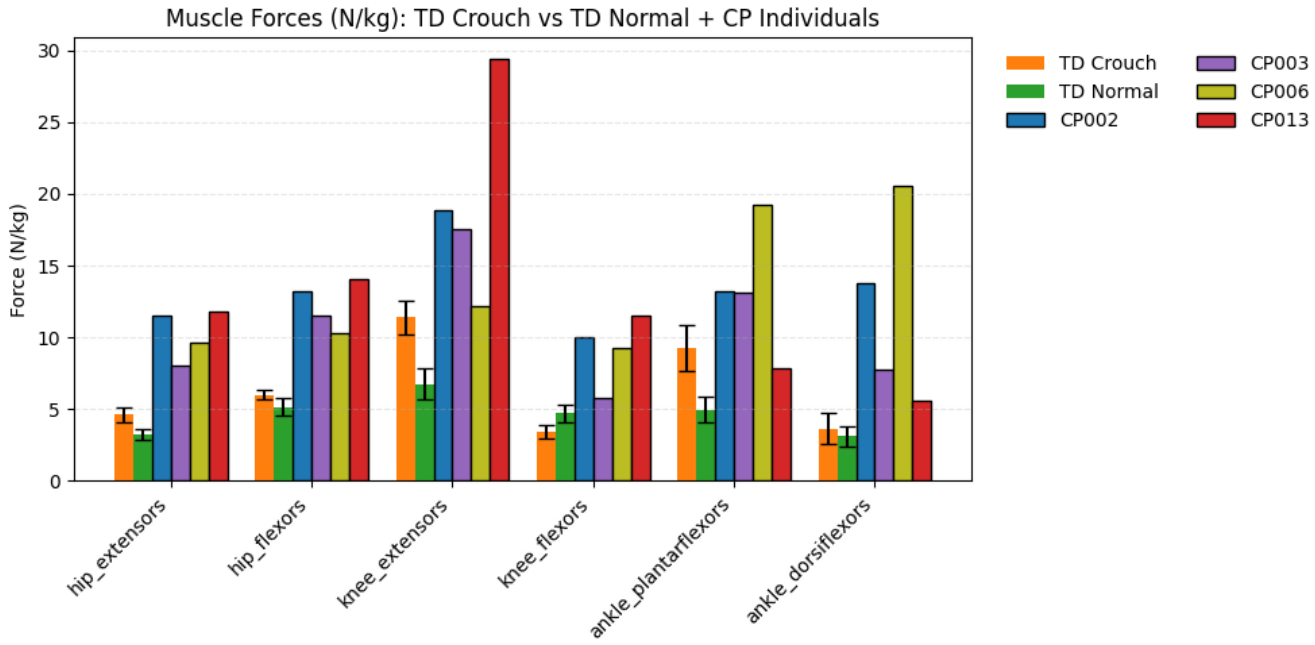

Figure 5.9: Mean muscle forces during single-leg support for each muscle group. Bars for TD children simulating crouch gait (TD crouch) and TD walking normally (TD Normal) represent group averages with standard deviation, while CP subjects are shown individually. The chart highlights the differences in muscle loading due to crouch gait posture (TD crouch vs. TD normal) and the additional neuromuscular burden observed in children with cerebral palsy. GMFCS levels for children with cerebral palsy: CP002 – Level III, CP003 – Level II, CP006 – Level I, and CP013 – Level III.

6

Conclusion and Future work

Contents

6.1 Conclusion

The main goals of this dissertation were to determine whether an EMG-informed neuromusculoskeletal model could outperform traditional SO in predicting individual muscle activations and joint moments, and to use these tools to distinguish between primary deviations caused by neurological disease and secondary deviations caused by the crouch posture.

Firstly, by comparing CEINMS and SO across CP and TD groups, it was demonstrated that including EMG data improves muscle activation predictions, while still maintaining good joint moments results. CEINMS achieved substantially higher R^2 and lower RMSE against EMG envelopes in both healthy and CP children, while closely matching ID moments. This confirms that EMG-informed models capture co-contractions, which SO's minimal-effort assumptions fail to identify.

Secondly, muscle force produced varied across normal gait, simulated crouch by TD children, and pathological crouch gait in CP. TD children adopted the mechanical demands of crouch gait - higher muscle forces, especially quadriceps forces, and prolongated muscle activity. However, they retained muscle activations patterns similar to the normal gait. On the other hand, CP children exhibit high co-contractions, spasticity, motor control limitations, together with the mechanical challenges of a crouch gait. Consequently, their muscle forces were even higher than in the TD crouch group. These inter-group differences in muscle forces can serve as indicators of primary and secondary causes, as healthy children cannot mimic the neurological deficits seen in CP.

6.2 Limitations

Although the findings of this study are consistent with previous studies, there are limitations that need consideration.

First, only four CP children were included in this study, whose individual variability was pronounced. This limits the generalizability of the findings to the broader CP population. Furthermore, none of the data used were collected for this work. Instead, existing datasets were provided for the simulations. This may have introduced inconsistencies beyond our control.

Second, the EMG data was recorded only from six muscles. While the EMG-informed model accounts for muscles without EMG data, collecting EMG from a larger set of muscles would enable a more comprehensive and accurate EMG mapping. Furthermore, surface EMG is limited to superficial muscles and can be affected by crosstalk and noise. Additionally, EMG envelopes were normalised to the maximum value observed during the trial rather than to MVC, which is the recommended approach,

as it expresses activations as a percentage of true maximum effort. Nevertheless, CP children cannot produce reliable and isolated MVCs due to the impaired selective motor control.

Third, while this does not necessarily have to be a limitation, it is important to acknowledge that Visual 3D and OpenSim may compute different joint angle results due to the use of different optimization approaches. Recent work has shown that pelvis and hip angle estimates can differ by several degrees between these two solvers, which may affect muscle–tendon lengths, moment arms, and force predictions [102].

Fourth, although the OpenSim model was scaled to match each child's marker-based anthropometry, the model was derived from a healthy adult. Children have different limb proportions and joint alignments than adults. Furthermore, CP patients often exhibit bony deformities, such as tibial torsion that the simple Gait2392 scaled model cannot capture.

Fifth, the force-plate set up did not cover the entire gait cycle. Consequently, the analysis was restricted to the single-support phase, and it was not possible to draw a conclusion about the loading response. Comparison with the literature was only possible for the 10-50% of the stance phase.

Lastly, CEINMS calibration requires multiple trials to predict more accurately muscle-tendon and activation-dynamics parameters. In this study, each subject's parameters were calibrated on a single representative gait trial. While the simulated-annealing optimizer produced a good accuracy with experimental data, using more trials would improve the model parameters.

6.3 Future work

The values of the CEINMS model's cost function weights (α,β,γ) were selected from the study reported by Sartori et al. [25]. While this was a reasonable starting point, future studies should consider calculating these factors for the specific application by following the optimization approach provided in [25].

Another important improvement is to obtain more accurate OFL values. In this study, OFL values for CP children were scaled to 0.7 (70%) of the generic model values based on the literature reports that CP muscles often have shorter OFL lengths compared to healthy muscles. Future work could utilise advanced imaging techniques to directly measure muscle length. Furthermore, the OpenSim Torsion Tool can be used to introduce subject-specific bone torsions—such as femoral anteversion and tibial torsion—directly into the scaled model [103].

Future implementations should obtain the scaled model and joint angles directly from OpenSim,

instead of using external software. This would ensure consistency and improve accuracy of simulations. Moreover, multiple trials should be used in the calibration and execution steps of CEINMS.

One of the possible solutions for the challenge of limited EMG data in paediatric groups can be the use of muscle synergy–informed neuromusculoskeletal modelling [104]. This approach can reconstruct a full set of muscle excitations from only three to four recorded channels. It uses just a few recorded EMG signals and combines them according to the synergy basis derived from a database of TD children's gait, filling in the missing activations. Rabbi et al. [104] demonstrated that this approach produces knee contact-forces nearly as accurate as full-EMG models.

The non-MVC calibration technique developed by Dufour et al. [105] replaces the traditional MVC normalisation by introducing a "gain ratio" parameter. This single parameter combines MVC and muscle gain in one property, which is estimated directly during the model calibration. The results obtained using this approach for spinal-load predictions match the fidelity of MVC-normalised models. This approach eliminates the need for subjects to perform maximum contractions, which can be especially valuable for subjects that have neurological impairments, such as CP.

Bibliography

[1] FMH-UL Biomechanics and Functional Morphology Laboratory, "Development of a simulation platform based in musculoskeletal models to predict recovery of gait following orthopaedic interventions in cerebral palsy children," Project PTDC/EMD-EMD/5804/2020, 2020. [Online]. Available: https://doi.org/10.54499/PTDC/EMD-EMD/5804/2020

[2] E. N. Marieb, P. B. Wilhelm, and J. B. Mallatt, *Human Anatomy, Media Update, Books a la Carte Edition*. Benjamin-Cummings Publishing Company, 2011.

[3] J. E. Hall, *Guyton and Hall Textbook of Medical Physiology*, 13th ed. Elsevier Health Sciences, 2016. [Online]. Available: https://doi.org/10.4103/sni.sni_327_17

[4] B. M. Carlson, *The Human Body: Linking Structure and Function*. Academic Press, Oct. 2018.

[5] M. W. Whittle, *Gait Analysis: An Introduction*, 4th ed. Edinburgh ; New York: Butterworth-Heinemann, 2007.

[6] H. K. Graham, P. Rosenbaum, N. Paneth, B. Dan, J.-P. Lin, D. L. Damiano, and R. L. Lieber, "Cerebral palsy," *Nature Reviews Disease Primers*, vol. 1, p. 15082, 2016. [Online]. Available: https://doi.org/10.1038/nrdp.2015.82

[7] J. Rodda and H. K. Graham, "Classification of gait patterns in spastic hemiplegia and spastic diplegia: A basis for a management algorithm," *European Journal of Neurology*, vol. 8, no. s5, pp. 98–108, 2001. [Online]. Available: https://doi.org/10.1046/j.1468-1331.2001.00042.x

[8] M. Harrach, "Modeling of the semg/force relationship by data analysis of high resolution sensor network," Ph.D. dissertation, PhD Thesis, Institution Not Specified, Sep 2016. [Online]. Available: https://doi.org/10.13140/RG.2.2.31448.49922

[9] M. S. Andersen, "Introduction to musculoskeletal modelling," *Computational Modelling of Biomechanics and Biotribology in the Musculoskeletal System*, 2021. [Online]. Available: https://doi.org/10.1016/B978-0-12-819531-4.00004-3

[10] F. Heinen *et al.*, "Muscle-tendon unit scaling methods of hill-type musculoskeletal models: An overview," *Proceedings of the Institution of Mechanical Engineers, Part H: Journal of Engineering in Medicine*, vol. 230, no. 10, 2016. [Online]. Available: https://doi.org/10.1177/0954411916659894

[11] A. Seth, J. L. Hicks, T. K. Uchida, A. Habib, C. L. Dembia, J. J. Dunne, and S. L. Delp, "Opensim: Simulating musculoskeletal dynamics and neuromuscular control to study human and animal movement," *PLOS Computational Biology*, vol. 14, no. 7, p. e1006223, 2018. [Online]. Available: https://doi.org/10.1371/journal.pcbi.1006223

[12] R. Akhundov, D. J. Saxby, S. Edwards, S. Snodgrass, P. Clausen, and L. E. Diamond, "Development of a deep neural network for automated electromyographic pattern classification," *The Journal of Experimental Biology*, 2019. [Online]. Available: https://doi.org/10.1242/jeb.198101

[13] S. L. Delp, J. P. Loan, M. G. Hoy, F. E. Zajac, E. L. Topp, and J. M. Rosen, "An interactive graphics-based model of the lower extremity to study orthopaedic surgical procedures," *IEEE Transactions on Biomedical Engineering*, vol. 37, no. 8, pp. 757–767, 1990. [Online]. Available: https://doi.org/10.1109/10.102791

[14] M. Bax, M. Goldstein, P. Rosenbaum, A. Leviton, N. Paneth, B. Dan, and D. Damiano, "Proposed definition and classification of cerebral palsy," *Developmental Medicine and Child Neurology*, vol. 47, no. 8, pp. 571–576, apr 2005. [Online]. Available: https://doi.org/10.1017/S001216220500112X

[15] J. Perry, *Gait Analysis: Normal and Pathological Function*. Slack Incorporated, 1992.

[16] S. Armand, G. Decoulon, and A. Bonnefoy-Mazure, "Gait analysis in children with cerebral palsy," *EFORT Open Reviews*, vol. 1, no. 12, pp. 448–460, 2016. [Online]. Available: https://doi.org/10.1302/2058-5241.1.000052

[17] M. M. Van der Krogt, L. Bar-On, T. Kindt, K. Desloovere, and J. Harlaar, "Neuro-musculoskeletal simulation of instrumented contracture and spasticity assessment in children with cerebral palsy," *Journal of NeuroEngineering and Rehabilitation*, vol. 13, no. 1, 2016. [Online]. Available: https://doi.org/10.1186/s12984-016-0170-5

[18] SCPE Working Group, "Surveillance of cerebral palsy in europe: A collaboration of cerebral palsy surveys and registers," *Developmental Medicine and Child Neurology*, vol. 42, pp. 816–824, 2000.

[19] S. A. Galey, Z. F. Lerner, T. C. Bulea, S. Zimbler, and D. L. Damiano, "Effectiveness of surgical and non-surgical management of crouch gait in cerebral palsy: A systematic review," *Gait & Posture*, vol. 54, pp. 93–105, 2017. [Online]. Available: https://doi.org/10.1016/j.gaitpost.2017.02.02

[20] N. M. Mirza, A. Ali, and M. K. Ishak, "Interactive software-based modeling for gait analysis of musculoskeletal structures," *Makara Journal of Technology*, vol. 26, no. 2, p. Article 5, 2022. [Online]. Available: https://doi.org/10.7454/mst.v26i2.1542

[21] L. Pitto, S. van Rossom, K. Desloovere, G. Molenaers, C. Huenaerts, F. De Groote, and I. Jonkers, "Pre-treatment emg can be used to model post-treatment muscle coordination during walking in children with cerebral palsy," *PLOS ONE*, vol. 15, no. 2, p. e0228851, 2020. [Online]. Available: https://doi.org/10.1371/journal.pone.0228851

[22] K. Veerkamp, W. Schallig, J. Harlaar, C. Pizzolato, C. P. Carty, D. G. Lloyd, and M. M. van der Krogt, “The effects of electromyography-assisted modelling in estimating musculotendon forces during gait in children with cerebral palsy,” *Journal of Biomechanics*, vol. 92, pp. 45–53, 2019. [Online]. Available: https://doi.org/10.1016/j.jbiomech.2019.05.026

[23] C. Pizzolato, D. G. Lloyd, M. Sartori, E. Ceseracciu, T. F. Besier, B. J. Fregly, and M. Reggiani, “Ceinms: A toolbox to investigate the influence of different neural control solutions on the prediction of muscle excitation and joint moments during dynamic motor tasks,” *Journal of Biomechanics*, 2015. [Online]. Available: https://doi.org/10.1016/j.jbiomech.2015.09.002

[24] D. G. Lloyd and T. F. Besier, “An emg-driven musculoskeletal model to estimate muscle forces and knee joint moments in vivo,” *Journal of Biomechanics*, vol. 36, no. 6, pp. 765–776, 2003. [Online]. Available: https://doi.org/10.1016/S0021-9290(03)00010-1

[25] M. Sartori, D. Farina, and D. G. Lloyd, “Hybrid neuromusculoskeletal modeling to best track joint moments using a balance between muscle excitations derived from electromyograms and optimization,” *Journal of Biomechanics*, 2014. [Online]. Available: https://doi.org/10.1016/j.jbiomech.2014.10.000

[26] D. Levine, J. Richards, and M. W. Whittle, *Whittle’s Gait Analysis*. Elsevier Health Sciences, 2012.

[27] R. Baker, “The history of gait analysis before the advent of modern computers,” *Gait & Posture*, vol. 26, no. 3, pp. 331–342, 2007. [Online]. Available: https://doi.org/10.1016/j.gaitpost.2006.10.01

[28] E. Surer and A. Kose, “Methods and technologies for gait analysis,” in *Computer Analysis of Human Behavior*, 2011, pp. 105–123. [Online]. Available: https://doi.org/10.1007/978-0-85729-994-9_5

[29] M. G. Pandy, “Computer modeling and simulation of human movement,” *Annual Review of Biomedical Engineering*, vol. 3, no. 1, pp. 245–273, 2001. [Online]. Available: https://doi.org/10.1146/annurev.bioeng.3.1.24

[30] U. Trinler, K. Hollands, R. Jones, and R. Baker, “A systematic review of approaches to modelling lower limb muscle forces during gait: Applicability to clinical gait analyses,” *Gait & Posture*, vol. 61, pp. 353–361, 2018. [Online]. Available: https://doi.org/10.1016/j.gaitpost.2018.02.00

[31] J. L. Hicks, M. H. Schwartz, A. S. Arnold, and S. L. Delp, “Crouched postures reduce the capacity of muscles to extend the hip and knee during the single-limb stance phase of gait,” *Journal of Biomechanics*, vol. 41, no. 5, pp. 960–967, 2008. [Online]. Available: https://doi.org/10.1016/j.jbiomech.2008.01.00

[32] K. M. Steele, M. M. van der Krogt, M. H. Schwartz, and S. L. Delp, "How much muscle strength is required to walk in a crouch gait?" *Journal of Biomechanics*, vol. 45, no. 15, pp. 2564–2569, 2012. [Online]. Available: https://doi.org/10.1016/j.jbiomech.2012.07.02

[33] G. Davico, C. Pizzolato, D. G. Lloyd, S. J. Obst, H. P. J. Walsh, and C. P. Carty, "Increasing level of neuromusculoskeletal model personalisation to investigate joint contact forces in cerebral palsy: A twin case study," *Clinical Biomechanics*, vol. 72, pp. 141–149, 2020. [Online]. Available: https://doi.org/10.1016/j.clinbiomech.2019.12.011

[34] Z. Matjačić and A. Olenšek, "Biomechanical characterization and clinical implications of artificially induced crouch walking: Differences between pure iliopsoas, pure hamstrings and combination of iliopsoas and hamstrings contractures," *Journal of Biomechanics*, vol. 40, no. 3, pp. 491–501, 2007. [Online]. Available: https://doi.org/10.1016/j.jbiomech.2006.02.018

[35] J. Balzer, S. Schelldorfer, C. Bauer, and M. L. van der Linden, "Effects of simulated crouch gait on foot kinematics and kinetics in healthy children," *Gait & Posture*, vol. 38, no. 4, pp. 619–624, 2013. [Online]. Available: https://doi.org/10.1016/j.gaitpost.2013.02.009

[36] J. G. Betts, K. A. Young, J. A. Wise, E. Johnson, B. Poe, D. H. Kruse, O. Korol, J. E. Johnson, M. Womble, and P. DeSaix, *Anatomy and Physiology 2e*, 2nd ed. Houston, TX: OpenStax, 2022, [Online]. Available: https://openstax.org/details/books/anatomy-and-physiology-2e.

[37] A. Wilson and G. A. Lichtwark, "The anatomical arrangement of muscle and tendon enhances limb versatility and locomotor performance," *Philosophical Transactions of the Royal Society B: Biological Sciences*, vol. 366, no. 1570, 2011.

[38] V. M. Zatsiorsky and B. I. Prilutsky, "Biomechanics of skeletal muscles," *Human Kinetics*, 2012.

[39] A. Kharb, V. Saini, Y. Jain, S. Dhiman, M. Tech, and Scholar, "A review of gait cycle and its parameters," *IJCEM: International Journal of Computer Engineering and Management*, vol. 13, 2011.

[40] P. Morgan and J. L. McGinley, "Cerebral palsy," *Balance, Gait, and Falls*, pp. 323–336, 2018. [Online]. Available: https://doi.org/10.1016/b978-0-444-63916-5.00020-3

[41] M. Stavsky, O. Mor, S. A. Mastrolia, S. Greenbaum, N. G. Than, and O. Erez, "Cerebral palsy-trends in epidemiology and recent development in prenatal mechanisms of disease, treatment, and prevention," *Frontiers in Pediatrics*, vol. 5, 2017. [Online]. Available: https://doi.org/10.3389/fped.2017.00021

[42] D. Moster, "Cerebral palsy among term and postterm births," *JAMA*, vol. 304, no. 9, p. 976, 2010. [Online]. Available: https://doi.org/10.1001/jama.2010.1271

[43] A. I. Scher, B. Petterson, E. Blair, J. H. Ellenberg, J. K. Grether, E. Haan, and K. B. Nelson, "The risk of mortality or cerebral palsy in twins: A collaborative population-based study," *Pediatric Research*, vol. 52, no. 5, pp. 671–681, 2002. [Online]. Available: https://doi.org/10.1203/00006450-200211000-00011

[44] C. C. Ogoke, "Clinical classification of cerebral palsy," *International Journal of Molecular Sciences*, 2018. [Online]. Available: https://doi.org/10.5772/intechopen.79246

[45] S. Gulati and V. Sondhi, "Cerebral palsy: An overview," *The Indian Journal of Pediatrics*, 2017. [Online]. Available: https://doi.org/:10.1007/s12098-017-2475-1

[46] S. Paul, A. Nahar, M. Bhagawati, and A. J. Kunwar, "A review on recent advances of cerebral palsy," *Oxidative Medicine and Cellular Longevity*, vol. 2022, p. 2622310, 2022. [Online]. Available: https://doi.org/10.1155/2022/2622310

[47] R. Palisano, P. Rosenbaum, S. Walter, D. Russell, E. Wood, and B. Galuppi, "Development and reliability of a system to classify gross motor function in children with cerebral palsy," *Developmental Medicine and Child Neurology*, vol. 39, pp. 214–223, 1997. [Online]. Available: https://doi.org/10.1111/j.1469-8749.1997.tb07414.x

[48] R. J. Palisano, P. Rosenbaum, D. Bartlett, and M. H. Livingston, "Gmfcs—expanded & revised," *Can Child Centre for Childhood Disability Research, McMaster University*, 2007.

[49] G. G. Handsfield, S. Williams, S. Khuu, G. Lichtwark, and N. S. Stott, "Muscle architecture, growth, and biological remodelling in cerebral palsy: a narrative review," *BMC Musculoskeletal Disorders*, vol. 23, no. 1, p. 233, mar 2022.

[50] N. G. Moreau, S. A. Teefey, and D. L. Damiano, "In vivo muscle architecture and size of the rectus femoris and vastus lateralis in children and adolescents with cerebral palsy," *Developmental Medicine & Child Neurology*, vol. 51, no. 10, pp. 800–806, 2009.

[51] A. Aroojis, N. Mantri, and A. N. Johari, "Hip displacement in cerebral palsy: The role of surveillance," *Indian Journal of Orthopaedics*, vol. 55, no. 1, pp. 5–19, jun 2020.

[52] T. F. J. Winters, J. R. Gage, and R. Hicks, "Gait patterns in spastic hemiplegia in children and young adults," *Journal of Bone and Joint Surgery: American Volume*, vol. 69, pp. 437–441, 1987.

[53] J. R. Gage and T. F. Novacheck, "An update on the treatment of gait problems in cerebral palsy," *Journal of Pediatric Orthopaedics Part B*, vol. 10, no. 4, pp. 265–274, 2001. [Online]. Available: https://doi.org/10.1097/01202412-200110000-00001

[54] J. L. Hicks, A. S. Arnold, F. C. Anderson, and S. L. Delp, “The effect of excessive tibial torsion on the capacity of muscles to extend the hip and knee during single-limb stance,” *Gait & Posture*, vol. 26, pp. 546–552, 2007.

[55] A. S. Arnold, M. Q. Liu, M. H. Schwartz, and S. L. Delp, “The role of estimating muscle-tendon lengths and velocities of the hamstrings in the evaluation and treatment of crouch gait,” *Gait & Posture*, vol. 23, pp. 273–281, 2006.

[56] P. Kedem and D. M. Scher, “Evaluation and management of crouch gait,” *Current Opinion in Pediatrics*, vol. 28, no. 1, pp. 55–59, 2016. [Online]. Available: https://doi.org/10.1097/MOP.0000000000000316

[57] A. Scianni, J. M. Butler, L. Ada, and L. F. Teixeira-Salmela, “Muscle strengthening is not effective in children and adolescents with cerebral palsy: a systematic review,” *Aust J Physiother*, vol. 55, pp. 81–87, 2009.

[58] D. L. Damiano, L. E. Kelly, and C. L. Vaughn, “Effects of quadriceps femoris muscle strengthening on crouch gait in children with spastic diplegia,” *Phys Ther*, vol. 75, pp. 658–667, 1995.

[59] D. L. Damiano, A. S. Arnold, K. M. Steele, and S. L. Delp, “Can strength training predictably improve gait kinematics? a pilot study on the effects of hip and knee extensor strengthening on lower-extremity alignment in cerebral palsy,” *Phys Ther*, vol. 90, pp. 269–279, 2010.

[60] K. M. Steele, D. L. Damiano, M. N. Eek *et al.*, “Characteristics associated with improved knee extension after strength training for individuals with cerebral palsy and crouch gait,” *Pediatr Rehabil Med*, vol. 5, pp. 99–106, 2012.

[61] N. Thompson, R. Baker, A. Cosgrove, I. Corry, and H. Graham, “Musculoskeletal modelling in determining the effect of botulinum toxin on the hamstrings of patients with crouch gait,” *Developmental Medicine & Child Neurology*, vol. 40, no. 9, pp. 622–625, 2008. [Online]. Available: https://doi.org/10.1111/j.1469-8749.1998.tb15428.x

[62] J. Saltiel, “A one-piece laminated knee locking short leg brace,” *Orthotics & Prosthetics*, vol. 23, pp. 68–75, 1969.

[63] P. Thomason, P. Selber, and H. K. Graham, “Single event multilevel surgery in children with bilateral spastic cerebral palsy: A 5-year prospective cohort study,” *Gait & Posture*, vol. 37, pp. 23–28, 2013.

[64] J. L. McGginley, F. Dobson, and R. Ganeshalingam, “Single event multilevel surgery for children with cerebral palsy: A systematic review,” *Developmental Medicine and Child Neurology*, vol. 54, pp. 117–128, 2012.

[65] T. Dreher, D. Vegvari, S. I. Wolf, A. Geisbüsch, S. Gantz, W. Wenz, and F. Braatz, "Development of knee function after hamstring lengthening as a part of multilevel surgery in children with spastic diplegia," *The Journal of Bone and Joint Surgery – American Volume*, vol. 94, no. 2, pp. 121–130, 2012. [Online]. Available: https://doi.org/10.2106/JBJS.J.00890

[66] A. I. Cruz, S. Õunpuu, and P. A. DeLuca, "Distal rectus femoris intramuscular lengthening for the correction of stiff-knee gait in children with cerebral palsy," *Journal of Pediatric Orthopaedics*, vol. 31, no. 5, pp. 541–547, 2011. [Online]. Available: https://doi.org/10.1097/BPO.0b013e31821f818d

[67] N. Moreau, S. Tinsley, and L. Li, "Progression of knee joint kinematics in children with cerebral palsy with and without rectus femoris transfers: A long-term follow-up," *Gait & Posture*, vol. 22, no. 2, pp. 132–137, 2005. [Online]. Available: https://doi.org/10.1016/j.gaitpost.2004.08.001

[68] A. Saw, P. A. Smith, Y. Sirirungruangsarn, S. Chen, S. Hassani, G. Harris, and K. N. Kuo, "Rectus femoris transfer for children with cerebral palsy: Long-term outcome," *Journal of Pediatric Orthopaedics*, vol. 23, pp. 672–678, 2003. [Online]. Available: https://doi.org/10.1097/00004694-200309000-00020

[69] R. W. Baker, *Measuring Walking: A Handbook of Clinical Gait Analysis*. Mac Keith Press, May 2013.

[70] K. M. Steele, M. E. Munger, K. M. Peters, B. R. Shuman, and M. H. Schwartz, "Repeatability of electromyography recordings and muscle synergies during gait among children with cerebral palsy," *Gait & Posture*, 2018. [Online]. Available: https://doi.org/10.1016/j.gaitpost.2018.10.00

[71] H. J. Hermens, B. Freriks, C. Disselhorst-Klug, and G. Rau, "Seniam 8: European recommendations for surface electromyography," Roessingh Research and Development, Tech. Rep., 1999.

[72] F. Zaheer, S. H. Roy, and C. J. De Luca, "Preferred sensor sites for surface emg signal decomposition," *Physiological Measurement*, vol. 33, no. 2, pp. 195–206, 2012. [Online]. Available: https://doi.org/10.1088/0967-3334/33/2/195

[73] R. S. Barrett and G. A. Lichtwark, "Gross muscle morphology and structure in spastic cerebral palsy: A systematic review," *Developmental Medicine & Child Neurology*, vol. 52, no. 9, pp. 794–804, 2010. [Online]. Available: https://doi.org/10.1111/j.1469-8749.2010.03686.x

[74] J. M. Winters and L. Stark, "Muscle models: What is gained and what is lost by varying model complexity," *Biological Cybernetics*, vol. 55, no. 6, 1987.

[75] D. G. Thelen, “Adjustment of muscle mechanics model parameters to simulate dynamic contractions in older adults,” *Journal of Biomechanical Engineering*, 2003. [Online]. Available: https://doi.org/10.1115/1.1531112

[76] M. Millard, T. Uchida, A. Seth, and S. L. Delp, “Flexing computational muscle: Modeling and simulation of musculotendon dynamics,” *Journal of Biomechanical Engineering*, 2013. [Online]. Available: https://doi.org/10.1115/1.4023390

[77] D., M. Glueck, A. Khan, E. Fiume, and K. Jackson, “Modeling and simulation of skeletal muscle for computer graphics: A survey,” *Foundations and Trends in Computer Graphics and Vision*, vol. 7, no. 4, 2011. [Online]. Available: https://doi.org/10.1561/0600000036

[78] S. L. Delp, F. C. Anderson, A. S. Arnold, P. Loan, A. Habib, C. T. John, E. Guendelman, and D. G. Thelen, “Opensim: Open-source software to create and analyze dynamic simulations of movement,” *IEEE Transactions on Biomedical Engineering*, vol. 54, no. 11, pp. 1940–1950, 2007. [Online]. Available: https://doi.org/10.1109/TBME.2007.901024

[79] S. M. McGill, “A myoelectrically based dynamic three-dimensional model to predict loads on lumbar spine tissues during lateral bending,” *Journal of Biomechanics*, vol. 25, no. 4, pp. 395–414, 1992. [Online]. Available: https://doi.org/10.1016/0021-9290(92)90259-4

[80] D. G. Lloyd and T. S. Buchanan, “Strategies of muscular support of varus and valgus isometric loads at the human knee,” *Journal of Biomechanics*, vol. 34, no. 10, pp. 1257–1267, 2001. [Online]. Available: https://doi.org/10.1016/S0021-9290(01)00095-1

[81] CEINMS GitHub Repository, “Introduction to ceinms,” https://github.com/CEINMS/CEINMS/blob/master/help/introduction/CEINMS.rst, data accessed: 2024-01-14.

[82] A. Erdemir, S. McLean, W. Herzog, and A. J. van den Bogert, “Model[U+2010]based estimation of muscle forces exerted during movements,” *Clinical Biomechanics*, vol. 22, no. 2, pp. 131–154, 2007. [Online]. Available: https://doi.org/10.1016/j.clinbiomech.2006.09

[83] R. J. Palisano, P. Rosenbaum, D. Bartlett, and M. H. Livingston, “Content validity of the expanded and revised gross motor function classification system,” *Developmental Medicine and Child Neurology*, vol. 50, no. 10, pp. 744–750, oct 2008. [Online]. Available: https://doi.org/10.1111/j.1469-8749.2008.03089

[84] K. Sarathy, C. Doshi, and A. Aroojis, “Clinical examination of children with cerebral palsy,” *Indian Journal of Orthopaedics*, vol. 53, no. 1, pp. 35–44, 2019.

[85] A. Cappozzo, F. Catani, U. Della Croce, and A. Leardini, “Position and orientation in space of bones during movement: Anatomical frame definition and determination,” *Clinical Biomechanics*, 1995. [Online]. Available: https://doi.org/10.1016/0268-0033(95)91394-T

[86] L. Bell, R. Pedersen, and R. Brand, “A comparison of the accuracy of several hip center location prediction methods,” *Journal of Biomechanics*, vol. 23, pp. 617–621, 1990.

[87] A. Barre and S. Armand, “Biomechanical toolkit: Open-source framework to visualize and process biomechanical data,” *Elsevier*, 2013.

[88] Vasilisa98, “Cerebral-Palsy-Project,” GitHub repository, 2025, [Accessed: 2025-05-31]. [Online]. Available: https://github.com/Vasilisa98/Cerebral-Palsy-Project

[89] D. Makowski, T. Pham, Z. J. Lau, J. C. Brammer, F. Lespinasse, H. Pham, C. Schölzel, and S. H. A. Chen, “NeuroKit2: A python toolbox for neurophysiological signal processing,” *Behavior Research Methods*, vol. 53, no. 4, pp. 1689–1696, 2021. [Online]. Available: https://doi.org/10.3758/s13428-020-01516-y

[90] C. R. Harris, K. J. Millman, S. J. van der Walt, R. Gommers, P. Virtanen, D. Cournapeau, E. Wieser, J. Taylor, S. Berg, N. J. Smith, R. Kern, M. Picus, S. Hoyer, M. H. van Kerkwijk, M. Brett, A. Haldane, J. F. del Río, M. Wiebe, P. Peterson, P. Gérard-Marchant, K. Sheppard, T. Reddy, W. Weckesser, H. Abbasi, C. Gohlke, and T. E. Oliphant, “Array programming with NumPy,” *Nature*, vol. 585, no. 7825, pp. 357–362, 2020. [Online]. Available: https://numpy.org/

[91] P. Virtanen, R. Gommers, T. E. Oliphant, M. Haberland, T. Reddy, D. Cournapeau, E. Burovski, P. Peterson, W. Weckesser, J. Bright, S. J. van der Walt, M. Brett, J. Wilson, K. J. Millman, N. Mayorov, A. R. J. Nelson, E. Jones, R. Kern, E. Larson, C. J. Carey, İ. Polat, Y. Feng, E. W. Moore, J. VanderPlas, D. Laxalde, J. Perktold, R. Cimrman, I. Henriksen, E. A. Quintero, C. R. Harris, A. M. Archibald, A. H. Ribeiro, F. Pedregosa, P. van Mulbregt, and SciPy 1.0 Contributors, “Scipy 1.0: Fundamental algorithms for scientific computing in python,” *Nature Methods*, vol. 17, no. 3, pp. 261–272, 2020. [Online]. Available: https://scipy.org/

[92] HAS-Motion, “Has-motion wiki,” https://wiki.has-motion.com/doku.php?id=main_page, accessed: 2025-05-09.

[93] OpenSim Development Team, “Guide to opensim workflow and tools,” https://opensimconfluence.atlassian.net/wiki/spaces/OpenSim24/pages/54001688/Guide+to+OpenSim+Workflow+and+Tools, 2025, accessed: 2025-05-20.

[94] J. L. Hicks, T. K. Uchida, A. Seth, A. Rajagopal, and S. L. Delp, “Is my model good enough? best practices for verification and validation of musculoskeletal models and

simulations of movement," *Journal of Biomechanical Engineering*, 2015. [Online]. Available: https://doi.org/10.1115/1.4029304

[95] S. A. Roelker, E. J. Caruthers, R. K. Hall, N. C. Pelz, A. M. W. Chaudhari, and R. A. Siston, "Effects of optimization technique on simulated muscle activations and forces," *Journal of Applied Biomechanics*, 2020. [Online]. Available: https://doi.org/10.1123/jab.2018-0332

[96] A. Corana, M. Marchesi, C. Martini, and S. Ridella, "Minimizing multimodal functions of continuous variables with the "simulated annealing algorithm"," *ACM Transactions on Mathematical Software*, pp. 262–280, 1987.

[97] M. A. Mathewson and R. L. Lieber, "Pathophysiology of muscle contractures in cerebral palsy," *Physical Medicine and Rehabilitation Clinics of North America*, 2015. [Online]. Available: https://doi.org/10.1016/j.pmr.2014.09.005

[98] T. Rezgui, F. Megrot, L. Fradet, and F. Marin, "On the imitation of cp gait patterns by healthy subjects," *Gait & Posture*, vol. 38, no. 4, pp. 576–581, 2013. [Online]. Available: https://doi.org/10.1016/j.gaitpost.2013.01.022

[99] K. M. Steele, A. Seth, J. L. Hicks, M. S. Schwartz, and S. L. Delp, "Muscle contributions to support and progression during single-limb stance in crouch gait," *Journal of Biomechanics*, vol. 43, no. 11, pp. 2099–2105, 2010. [Online]. Available: https://doi.org/10.1016/j.jbiomech.2010.04.003

[100] K. M. Steele, A. Seth, J. L. Hicks, M. H. Schwartz, and S. L. Delp, "Muscle contributions to vertical and fore-aft accelerations are altered in subjects with crouch gait," *Gait & Posture*, vol. 38, no. 1, pp. 86–91, 2013. [Online]. Available: https://doi.org/10.1016/j.gaitpost.2012.10.019

[101] R. A. Pandey, A. N. Johari, and T. Shetty, "Crouch gait in cerebral palsy: Current concepts review," *Indian Journal of Orthopaedics*, vol. 57, no. 12, pp. 1913–1926, September 2023.

[102] B. Eng Wan Xuan, S. S. Chan, H. Johan, L. S. Lim, B. Zuo, and W. T. Ang, "Investigation of modeling differences between opensim and visual3d for gait analysis of healthy gait," in *Proceedings of the 16th International Convention on Rehabilitation Engineering and Assistive Technology (i-CREATe 2023)*. Pathum Thani, Thailand: ACM, Aug. 2023, pp. 1–8. [Online]. Available: https://doi.org/10.1145/3628228.3628492

[103] K. Veerkamp *et al.*, "Torsion tool: An automated tool for personalising femoral and tibial geometries in opensim musculoskeletal models," *Journal of Biomechanics*, vol. 125, 2021. [Online]. Available: https://doi.org/10.1016/j.jbiomech.2021.110589

[104] M. F. Rabbi, G. Davico, D. G. Lloyd, C. P. Carty, L. E. Diamond, and C. Pizzolato, "Muscle synergy-informed neuromusculoskeletal modelling to estimate knee contact forces in children with

cerebral palsy," *Biomechanics and Modeling in Mechanobiology*, vol. 23, no. 3, pp. 1077–1090, 2024, epub 2024 Mar 9. [Online]. Available: https://pubmed.ncbi.nlm.nih.gov/38459157/

[105] J. S. Dufour, W. S. Marras, and G. G. Knapik, "An emg-assisted model calibration technique that does not require mvcs," *Journal of Electromyography and Kinesiology*, vol. 23, no. 3, pp. 608–613, 2013, epub 2013 Feb 14. [Online]. Available: https://pubmed.ncbi.nlm.nih.gov/23415699/

Appendix A

A.1 Effect of Dropping Initial Frames in CEINMS

In Figure A.1, maintaining the first three frames in CEINMS produces a solver-induced spike at the beginning of the single-leg support phase, leading to non-physiological early peaks. After removing those frames (Figure A.2), the timing and magnitude of muscle activations align more closely with expected EMG patterns throughout the single-leg support phase.

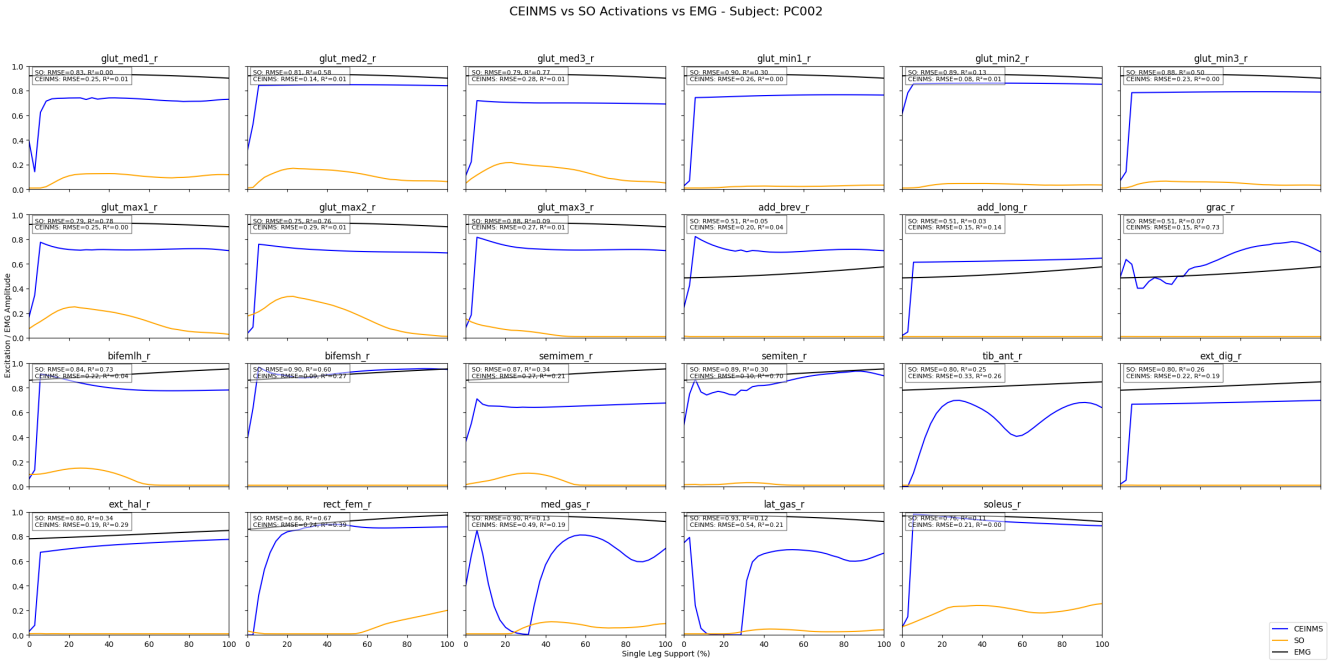

Figure A.1: CEINMS output without removing the first 3 frames

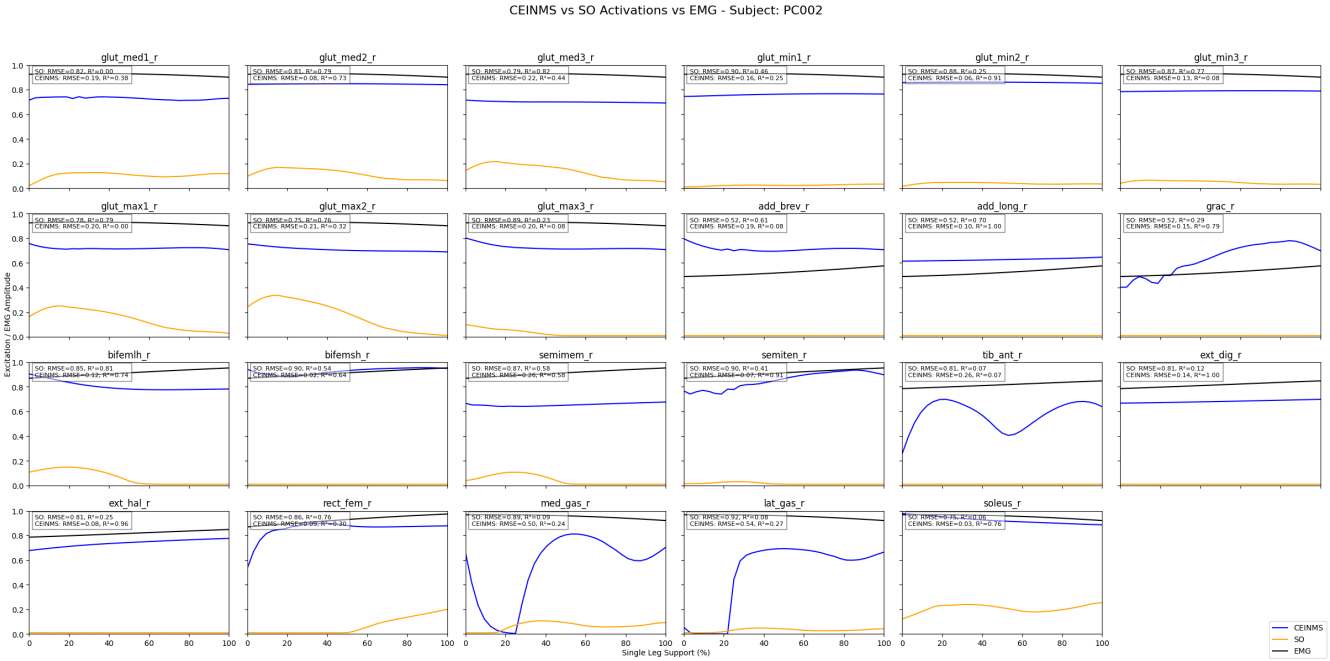

Figure A.2: CEINMS output with the first 3 frames removed

A.2 Different T values

Figures Fig. A.3 - Fig. A.6 illustrate how varying the CEINMS time-constant T alters activation dynamics. Among the four, the model with T = 2 000 000 (Figure A.6) provided the best overall fit to the EMG in both timing and magnitude.

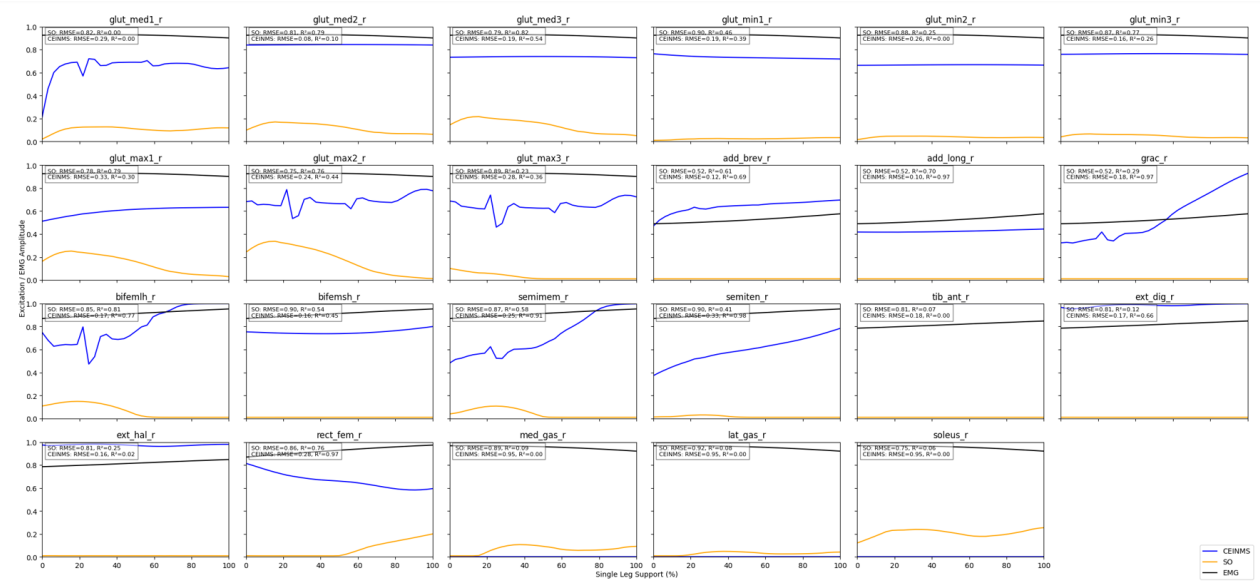

Figure A.3: Muscle activations estimated using CEINMS with T = 2,000.

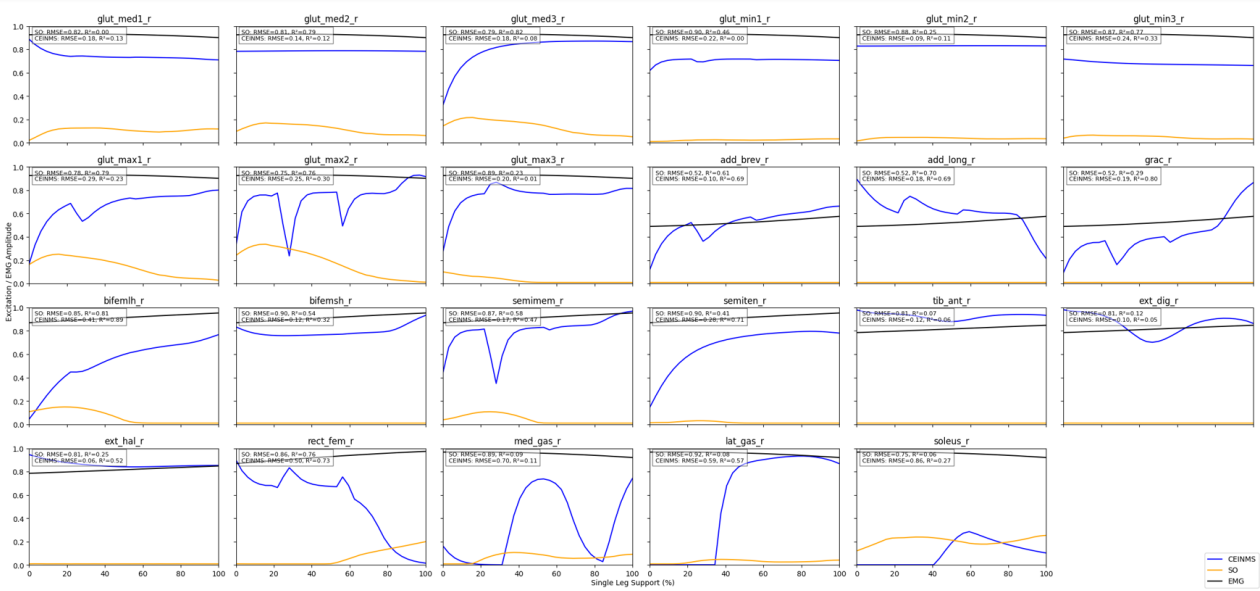

Figure A.4: Muscle activations estimated using CEINMS with T = 20,000.

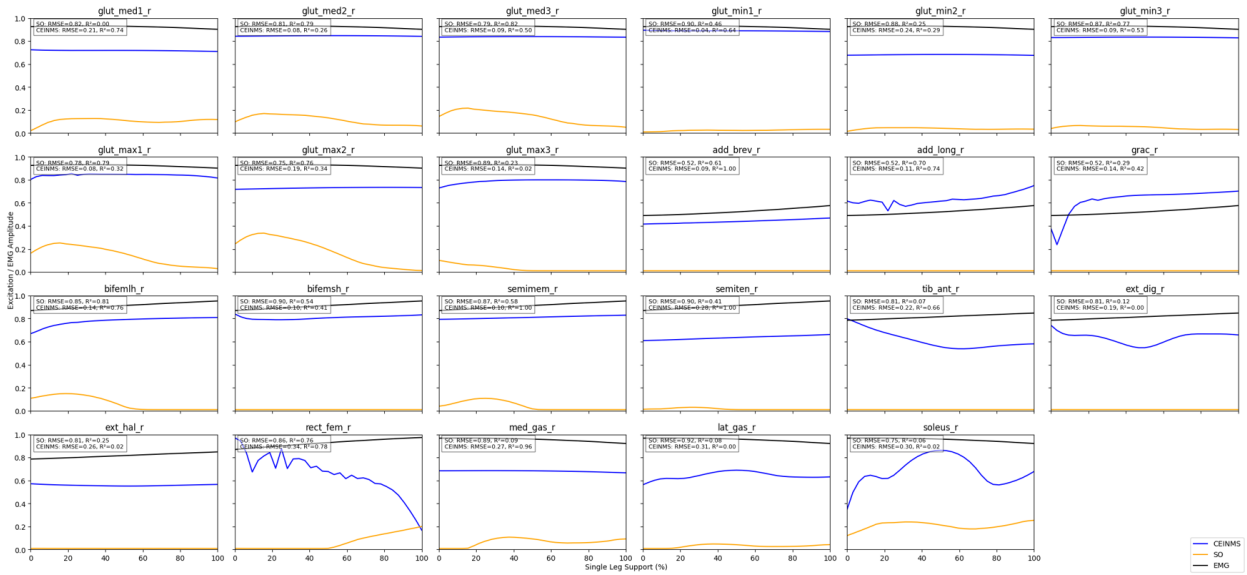

Figure A.5: Muscle activations estimated using CEINMS with T = 200,000.

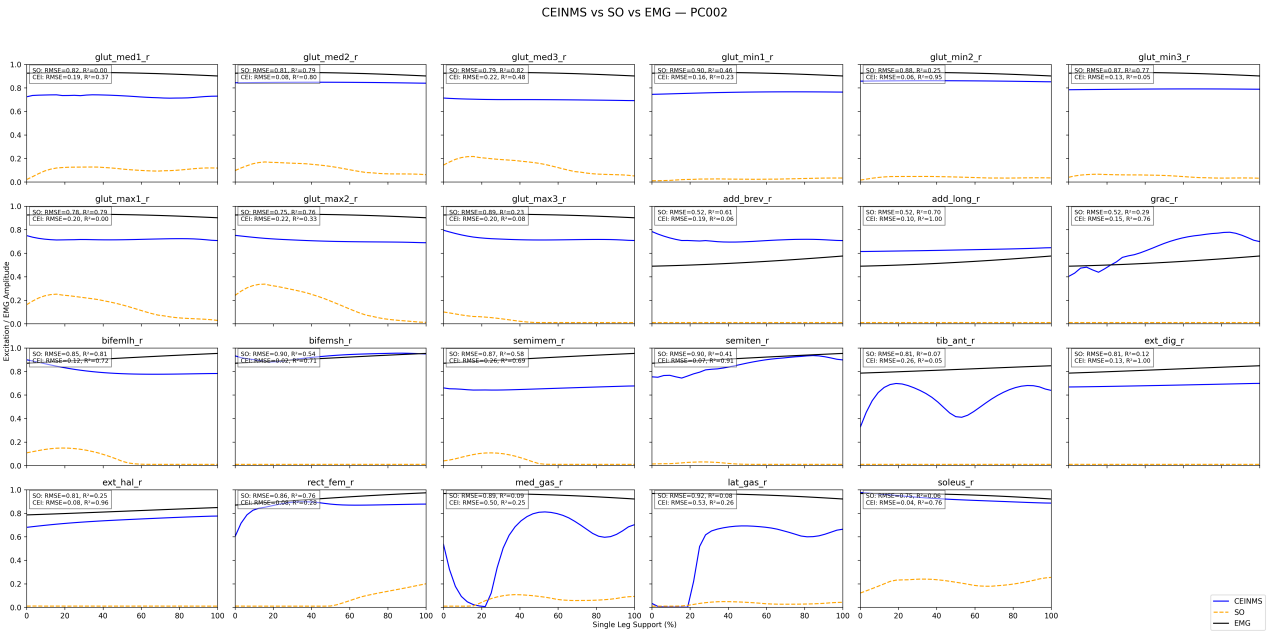

Figure A.6: Muscle activations estimated using CEINMS with T = 2,000,000.